Colored optic filters on c-Si IBC solar cells for building integrated photovoltaic applications

Ortiz Lizcano, Juan Camilo; Procel, Paul; Calcabrini, Andres; Yang, Guangtao; Ingenito, Andrea; Santbergen, Rudi; Zeman, Miro; Isabella, Olindo

DOI
10.1002/pip.3504

Publication date
2021

Document Version
Final published version

Published in
Progress in Photovoltaics: research and applications

Citation (APA)
Ortiz Lizcano, J. C., Procel, P., Calcabrini, A., Yang, G., Ingenito, A., Santbergen, R., Zeman, M., & Isabella, O. (2021). Colored optic filters on c-Si IBC solar cells for building integrated photovoltaic applications. *Progress in Photovoltaics: research and applications*, *30*(4), 401-435. https://doi.org/10.1002/pip.3504

Received: 20 March 2021 | Revised: 5 October 2021 | Accepted: 12 October 2021
DOI: 10.1002/pip.3504

RESEARCH ARTICLE

PROGRESS IN PHOTOVOLTAICS WILEY

Colored optic filters on c-Si IBC solar cells for building integrated photovoltaic applications

Juan Camilo Ortiz Lizcano[1] | **Paul Procel**[1,2] | **Andres Calcabrini**[1] | **Guangtao Yang**[1] | **Andrea Ingenito**[3] | **Rudi Santbergen**[1] | **Miro Zeman**[1] | **Olindo Isabella**[1]

[1]Photovoltaic Materials and Devices group, Delft University of Technology, Delft, Netherlands

[2]Instituto de Micro y Nanoelectrónica, Universidad San Francisco de Quito, Quito, Ecuador

[3]Centre Suisse d'électronique et de Microtechnique (CSEM), PV-Center, Neuchâtel, Switzerland

Correspondence
Juan Camilo Ortiz Lizcano, Photovoltaic Materials and Devices group, Delft University of Technology, Mekelweg 4, 2628 CD Delft, Netherlands.
Email: j.c.ortizlizcano@tudelft.nl

Abstract

Building Integrated Photovoltaic systems can produce a significant portion of the energy demand of urban areas. Despite their potential, they remain a niche technology that architects and project engineers still find esthetically limited. The dark blue or black color of standard photovoltaic panels is considered inappropriate for restoration projects of historic buildings and represents a major constraint on the development of new projects. This work will provide insight into how the use of optic filters can offer new pathways for architectural acceptance of photovoltaic panels. Optic filters selectively reflect or transmit light by interference and can be designed and fabricated using cost-effective and industrially compatible processes. By using in-house developed ray tracing software coupled with TCAD Sentaurus, more than 400 colors were obtained, and their impact on the opto-electrical performance of interdigitated back-contacted solar cells was studied. Results show a maximum efficiency loss of 1.6% absolute at the perpendicular incidence of light on the range of obtained colors when compared with a standard dark blue solar cell. Simulations for different angles of incidence showed that the current reduction on the standard device could be modeled using a cosine relationship. The colored cells, however, deviated significantly from this relationship. We propose that the angular behavior of any cell (colored or standard) could be simulated by modifying the effective irradiance with scaling factors equal to the ratios of the photogenerated current at any angle with respect to the value at normal incidence. We demonstrate that this approach accurately models the effect of the color filter and allows for an easy transition from a bare cell to an encapsulated one. Due to the spectral effect of the filter, we developed both a spectrally resolved optical model and a two-dimensional finite volume transient thermal model. In case of the optical model, we demonstrate an accuracy in the prediction of the reflectance produced by the color with values of mean bias error (MBE) between 2.0% and 3.9%. As for the thermal model, it was validated by first analyzing a standard model under conditions of nominal operating cell temperature and then comparing its results with published scientific literature. Later, we compare its prediction against 2 weeks of measurements. In both cases the thermal model proves an adequate accuracy, yielding differences below 1.5°C with respect to other scientific works and an MBE value of 0.89°C as well as a root-mean-square error value of 2.10°C for the entire measurement period. With the validated models, we studied the effect of the encapsulation on the color perception. We present two options of color filters. The first one produces relatively low reflectance losses and presents relative annual direct current (DC) energy losses of up to 6.4% for Delft, in the Netherlands, and up to 5.9% for Alice Springs in Australia. However, this first option has very poor color brightness. The second studied filter produces highly saturated bright colors. Improving brightness can increase the annual DC relative losses up to 13.7% and 13.5% for Delft and Alice Springs, respectively. Overall, we demonstrate that colored filters based on multilayer optical stacks are a versatile option for coloring cells that allow a good compromise between esthetics and performance.

KEYWORDS

BIPV, c-Si Solar Cells, colored modules, color perception, performance assessment, solar energy

1 | INTRODUCTION

Urban areas are among the largest contributor of CO_2 emissions,[1] and this trend will significantly increase in the coming years.[2,3] To reduce the carbon footprint of cities and towns, most of the countries are making efforts to produce carbon-neutral buildings in next decades.[4] In the United States, for example, the Department of Energy (DoE) seeks to halve the energy consumption of buildings by 2030. To this end, the DoE is focusing its efforts on solar water heating and Building Integrated Photovoltaic (BIPV) systems.[5] The latter can replace a standard roof or façade as they generate electrical energy and provide protection from environmental condition.[6] In the Europe Union too, the directive related to the energy performance of buildings (2018/844/EU) establishes that member estates must create roadmaps to reduce the greenhouse gasses emissions by 80%–95% compared with 1990 by creating an energy efficient building stock either via new project developments or effective renovation of existing structures.[7] To achieve these objectives, the International Energy Agency (IEA) argues that BIPV implementation must be a priority.[8]

BIPV systems deployed in available areas can substantially contribute to urban energy needs. In the United States, 58% of the residential electrical energy demand could be supplied by BIPV systems. For Germany, United Kingdom, and the Netherlands this figure is around 30%.[9] Yet, despite this potential, BIPV systems remain a niche technology with less than 2% of market share.[10] Several barriers hinder BIPV market growth, such as the lack of standards, little synergies among stakeholders, performance issues, elevated costs, no specific governmental incentives, and esthetic limitations.[11,12] Architects and project engineers have expressed that color and shape of modules are a limiting factor for BIPV implementation.[13] Among several technical requirement that these new products must have, color versatility is one of those. Several techniques have been introduced to change the esthetics of standard photovoltaic (PV) modules. With respect to color, the use of automotive paints on the front side glass[14] has been proposed. Additionally, implementation of ceramic inks on glass can also produce incredibly versatile esthetics.[15,16] Some solutions are focused on coloring the polymer used as encapsulant,[17] while other solutions focus on coloring the cells, like implementing dielectric resonant nano scatterers[18] or the use of textured structures on the Glass/EVA interface.[19] One technology, however, that can be applied both on cells and the glass is optic color filters (hence referred as Color filters). Among all the available technologies, color filters have shown great potential in terms of color saturation and reduced performance losses, albeit with an increased cost.[17] Given its marked technical advantages, this last technique was selected as the focus of this work.

This research seeks to provide insight on how color filters can be used to provide esthetic flexibility to BIPV systems based on crystalline silicon (c-Si) modules. The selected architecture is based on interdigitated back-contacted (IBC) c-Si solar cells. Such technology currently holds the highest conversion efficiency (η) not only at cell level at laboratory scale[20,21] but also at module level among all commercially available technologies.[22] Moreover, as both metallic contacts are at the back side of the cells, modules based on such architecture result in a pleasant and homogeneous esthetic. Combining our in-house developed ray tracing software coupled with device's physics modeling platform, optical cell-to-module (CTM) losses model and energy yield model, we can predict not only the appearance of colored IBC c-Si modules, but also their angular- and location-dependent energy yield performance for BIPV applications.

2 | BASIC THEORY OF OPTICAL FILTERS

2.1 | Fundamentals of multilayer optical systems

Optic filters (OF) are multilayered systems designed to deliver a desired wavelength-dependent reflection or transmission of light. With proper design, these optical devices can provide very high values of transmittance/reflectance (reaching 99%) at a given wavelength,[23] the so-called Bragg wavelength (λ_B), and exhibit a so-called photonic bandgap (Δ_g).[24] This is the width of the reflectance peak produced by the design of the filter. The working principle of an OF is based on light interference. As shown in Figure 1A, when a thin layer of a material with given refractive index (n_L) and thickness d_L is deposited between an incident medium and a substrate (with refractive indexes of n_0 and n_s, respectively), such that $n_0 < n_L < n_S$, the rays reflected at point A of the first interface defined by the media n_0 and n_L can interact with the one reflected at point B of the second interface, at point C. Depending on the phase shift of the ray which is related to the refractive index and the thickness of the medium, either constructive or destructive interferences can occur leading to an increase or decrease of the reflected ray, respectively.[25]

Mathematically, to produce destructive interference of a photon of wavelength λ at normal incidence ($\theta = 0^\circ$) in Figure 1A), the thin layer with a refractive index of n_L should have a thickness equal to: $= \lambda / 4n_L$. This design is commonly known as a Quarter Wavelength Optical Thickness (QWOT) layer. In this work, we have modeled OFs based on two materials with a refractive index mismatch. Both the high refractive index (n_H) and the low refractive index (n_L) materials constituting the OF can be intersperse and deposited on the surface (see Figure 1B). To achieve a desired reflectance (R) profile, the pattern of the two-media constituting the OF can be varied in different ways (thicknesses and position of n_L and n_H). Each pattern defines the so-called period (p), as indicated in Figure 1B. For example, an OF which delivers high reflectance in a narrow wavelength range can be obtained by using many periods in the multilayer stack. An OF with a period based on two materials (n_L, n_H) can provide high reflectance either by deposition of an even number of layers on a n_L/n_H sequence or an odd number of layers for a n_H/n_L one.[23] For these setups, their reflectance is given by[23]:

$$R = \left(\frac{1 - \left(\frac{n_H}{n_L}\right)^{2p} \cdot \frac{n_H^2}{n_s}}{1 + \left(\frac{n_H}{n_L}\right)^{2p} \cdot \frac{n_H^2}{n_s}} \right)^2 \tag{1}$$

while their photonic band gap Δ_g can be estimated as follows.[26]

$$\Delta_g = \frac{4}{\pi} \cdot \sin^{-1}\left(\frac{n_H - n_L}{n_H + n_L}\right) \tag{2}$$

Since the purpose of the OF is to provide esthetic flexibility with minimum optical losses, the following design guidelines were considered for this study:

1. Materials composing the filter must have an energy bandgap equal or higher than 2.75 eV (i.e., wavelength shorter than 450 nm) to mitigate parasitic losses due to photon absorption. Furthermore, as expressed in Equation 2, we consider two potential design options in this study. **Option 1** is a filter with a low refractive index difference ($n_H - n_L$) and **Option 2** with a higher value of this same difference. We selected these two options to analyze how color saturation and brightness can be tuned by slight modifications of the optical properties of a given material.
2. The filter design should provide flexibility on installation. It could be deposited on the encapsulating glass of a PV module or on

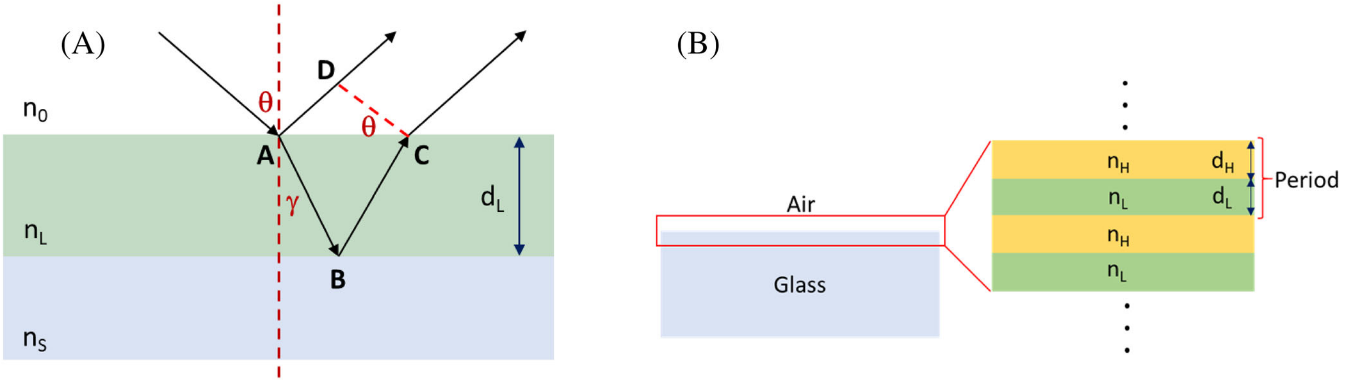

FIGURE 1 (A) Optical system comprising a thin film layer (n = nL) of thickness dL in between an incident medium (n = n0) and a substrate (n = ns). A ray of a given wavelength (black line) is reflected both on the surface of the layer (A) and the surface of the substrate (B), their optical paths AD and ABC, respectively, are dependent of the layer thickness dL. For a given thickness dL both rays interact producing constructive (bolstering reflectance) or destructive (bolstering transmittance) interference. (B) The reflectance or transmittance of any surface can be tuned by using multilayer optic filters. This is done by tuning the thickness of the layers, the optical properties of the materials used, and how they are arranged in the filter [Colour figure can be viewed at wileyonlinelibrary.com]

the cell itself. For the former application, fabrication, and installation of the filter need to be decoupled. See Appendix A for more details.

The color tuning OF used in this work was designed based on two dielectric layers: silicon dioxide (SiO_2) and silicon nitride (SiN_X). The first reason for selecting these materials is related to the deposition method. Deploying Plasma Enhanced Chemical Vapor Deposition (PE-CVD), both materials can be quickly deposited. Deposition rates for the SiO_2 and SiN_x on this study were 26.4 and 18.2 nm/min, respectively, for the case of **Option 1**. More information of the manufacturing process can be found in Appendix A. The second reason is that SiO_2/SiN_X layers significantly improve color purity and brightness and exhibit low parasitic losses.[27] On a potential upscale scenario, a single-sided, low-CAPEX and high throughput[28] physical vapor deposition technique, such as sputtering,[29] could be suitable to manufacture these devices.

By tuning the bandgap of SiO_2 and SiN_x, achieved by adjusting the deposition parameters during fabrication, the first abovementioned guideline is met (See Appendix A). Filter **Option 1** deployed a refractive index value of SiN_x of $n_H = 1.73$. Whereas **Option 2** used a SiN_x with a refractive index value $n_H = 2.10$). To produce bright colors, a stack of *10 pairs* of SiO_2/SiN_X was used for both filter options.

2.2 | General behavior of OFs at different angles of incidence

The reflectance profile of a multistack OF is not independent from the angle of incidence of light, as Figure 2A shows. Increasing the angle of incidence, the high reflectance region of an OF applied to a polished surface tends to shift towards shorter wavelengths compared with the one designed for normal incidence. This effect is related to the change of the optical light path through the layers of the filter which was designed only considering normal incidence. This leads to a wavelength shift of the constructive interference.[23]

For textured surfaces, the angular behavior of the OF is different compared with flat surfaces. As Figure 2B depicts, when the angle of incidence increases, the Δ_g width expands. The wavelength at which the R has a peak remains constant at least for angles between 0° and 40°. At larger angles of incidence, the peak of R shifts slightly towards longer wavelengths. This behavior is highly dependent on the type of texturing the device has. Figure 2B reports the simulated reflectance change for a OF-coated and pyramidally textured c-Si wafer (slope of 54.7°). This is the reason why, as the angle of incidence approaches this value, the reflectance spectra present a larger photonic bandgap and reflectance peak.

Given their ability to modify the way a surface reflects light, OFs have been studied for various applications on PV devices. For example, studies have been performed to assess their suitability as metal-free back reflectors.[30–32] Also, other works focus on their use to produce colored cells.[33] Color filters, however, require a specific modeling approach to reasonably assess their impact on the performance of colored cells, particularly considering their spectral nature.

3 | MODELING FRAMEWORK—CELL LEVEL

The modeling framework presented in this investigation is divided in two parts. First, a study on how the implementation of an OF affects the performance of a c-Si solar cell. It is important to highlight that we do not consider any potential effect that the *manufacturing* process might have on the cell when the color filter is deposited. From the study, we investigate how the behavior can be modeled using standard electrical models. We latter extrapolate this method towards fully encapsulated cells and examine the effect that the color filter deposited on cells has on the direct current (DC) energy yield and operational temperature of PV modules installed in two different locations.

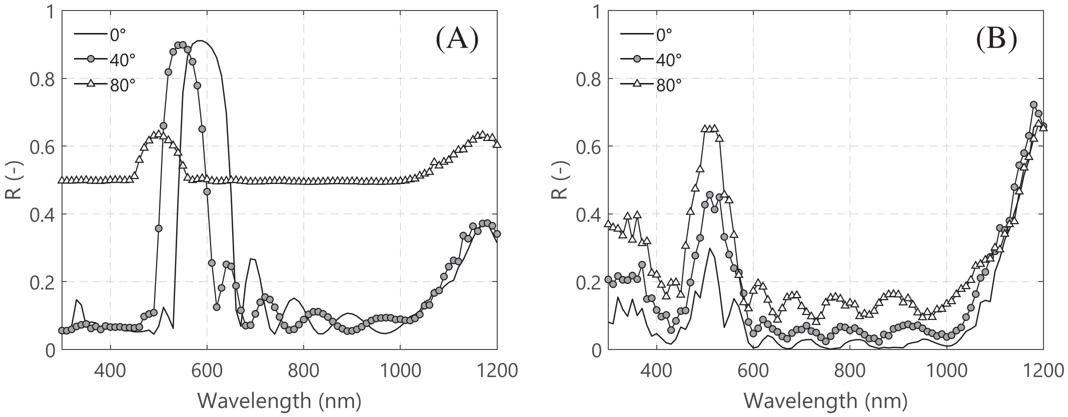

FIGURE 2 (A) Simulated effect of increasing the angle of incidence on the reflectance profile of a color filter deposited on a flat glass surface. Such a filter is formed by 10 pairs of SiN_X/SiO_2 (90 and 110 nm, respectively). (B) Simulated effect of increasing the angle of incidence on the reflectance profile for the same filter layout as in (A) but deposited on a pyramidally textured solar cell surface. The wavelength at which R is maximum remains within a small range up until 40°; then the reflectance across all wavelengths starts to increase

We begin with the optical effect that the OF has on the appearance of surfaces. To this end, GenPro4[34] is used to calculate the reflectance produced by a color filter. A color perception model provides an estimation of the color produced by a given combination of thickness values of the materials used on the filter.

Given a certain color, we are interested in simulating the impact of the color tuning OF on the conversion efficiency of our selected structure (an IBC c-Si solar cell) not only when the OF covers the cell itself but also for different angles of incidence (AOI). To this end, we deploy TCAD Sentaurus to study the effect of the filter on the electrical quality of the cell. From this knowledge, we demonstrate that by calculating color-specific and angle-dependent modifying factors, the optical losses introduced by the OF can be modeled by using these factors to scale the effective irradiance reaching the cell. The open circuit voltage (V_{OC}) and the fill factor (FF) of the colored cells are instead mostly independent from the OF in place, something that we shall show in the following section. Furthermore, we corroborate that these angular scaling factors are the same whether calculated from Sentaurus or from GenPro4. This allows the direct use of a two-diode electrical model, simplifying the modeling process, particularly the extrapolation to module level.

3.1 | Selected solar cell structure

The inset of Figure 3A depicts an IBC architecture based on poly-Si carrier-selective passivating contacts.[35] This device, designed, manufactured, and characterized at our facilities,[36] was used as the reference case for the performance assessment. Measured external quantum efficiency (EQE) spectrum and current density-voltage (J-V) curve of the selected device are reported in Figure 3A,B, respectively. The conversion efficiency of this device is 21.36%.

The opto-electrical performance of the reference cell is the starting point for assessing how the implementation of a colored filter affects device performance. To this end, 10 pairs of SiO_2/SiN_X (Option 1) with different thickness combinations were modeled onto the reference cell architecture by means of TCAD Sentaurus.[37,38] Device considerations include a random pyramidal texturing at the front side. Pyramids present a maximum height of 5.6 μm and a fixed based angle of 54.7°. The thickness of the wafer is 280 μm. The simulation considered a 650-μm-wide rear pitch. Further details of the complete modeling, simulation, and optimization study of this structure can be found elsewhere.[37,38]

3.2 | Optical model

The optical model consists of the following steps: (1) determination of the reflectance, absorptance and transmittance spectra of a colored solar cell (bare and encapsulated) and (2) application of a color perception model to predict the color produced by the filter. The backbone of both steps is the in-house developed MATLAB®-based ray tracing software named GenPro4.[34]

3.2.1 | GenPro4 simulations

GenPro4 (GP4) combines ray tracing and wave optics in a single package. The core of the software is the extended net-radiation method. On incoherent layers, GP4 uses the Lambert–Beer and Fresnel law equations. On multistack optical systems with coherent layers, GP4 deploys a different algorithm based on the characteristic matrix method described by Mcleod.[23] The outputs of the software are the wavelength dependent absorptance, the reflectance and the transmittance of the optical system modeled. Additionally, GP4 uses the AM1.5 spectrum to estimate a photogenerated current density (mA/cm^2) by assuming that every photon effectively absorbed on the cell yields an electron–hole pair. In this work, this implied photocurrent density will be defined as J_{ph}.

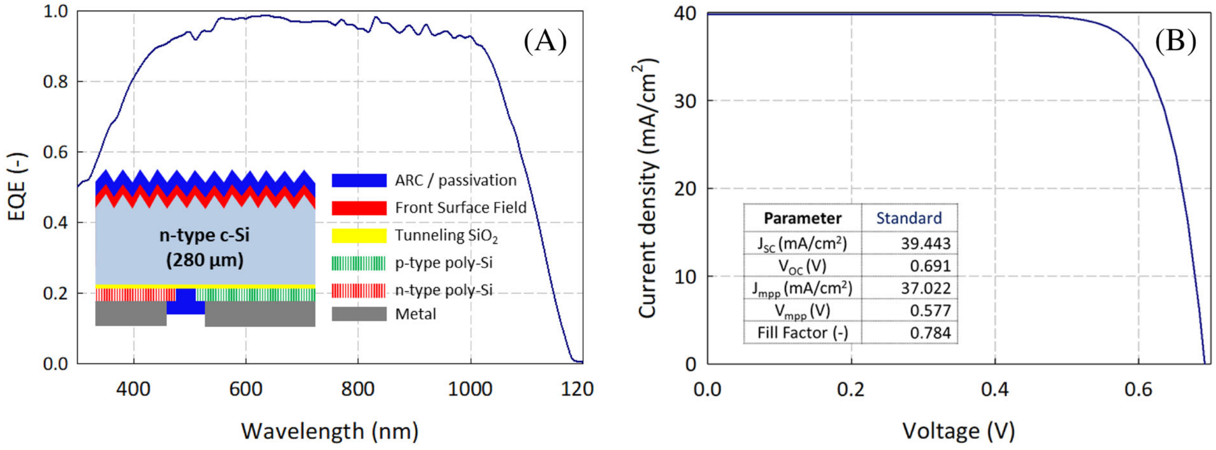

Parameter	Standard
J_{SC} (mA/cm^2)	39.443
V_{OC} (V)	0.691
J_{mpp} (mA/cm^2)	37.022
V_{mpp} (V)	0.577
Fill Factor (-)	0.784

FIGURE 3 (A) External quantum efficiency (EQE) spectrum and (B) current density-voltage (J-V) curve of the selected reference interdigitated back-contacted (IBC) solar cell. Insets: (A) solar cell sketch, (B) external parameters of the reference solar cell [Colour figure can be viewed at wileyonlinelibrary.com]

3.2.2 | Color perception model

Colors perceived by humans from nonluminous objects depends on how they are illuminated and how they *reflect* light.[39] The way to model this phenomenon has been heavily studied during the last century.[40–42] GP4 is used to design the pattern of the OF required to deliver a desired R spectrum. The model then converts such generated spectrum into Red, Green, and Blue [R_{RGB}, G_{RGB}, B_{RGB}] color coordinates to render the color as perceived by humans on a computer screen. A common standard for evaluating color perception is given by the *Comission Internationale de l'Eclairage* (CIE) system.[42] An example the application of color perception models on solar cells and modules can be found also on.[43] Details of this model, the mathematics involved, and how R spectrum can be converted to a perceived color can be found in Appendix B.

3.3 | Electrical model

As stated earlier, the selected model to assess the electrical performance of a colored cell is the two-diode model.[44,45] As inputs, this model requires in first place the effective irradiance reaching the c-Si solar cell, after considering all the optical effects. These effects include the reflectance, transmittance, and absorptance of all the incoherent and coherent layers (glass, EVA, OF, antireflective coating, etc.). In second place, this model also needs the operational temperature of the c-Si solar cell.

First, the parameters of a standard device were found by using the J-V curve obtained for normal incidence as shown in Figure 3B. The cell area was assumed equal to 153 cm^2, which is the area of the commercial IBC cell from SunPower, the Maxeon generation III.[46] The geometry of the cell can be found in Appendix B.

The fitting method used to find these values was the calculator devised by[47] assuming a cell temperature of 298.15 K. The result from this fitting can be found oin Appendix B.6. With these parameters, we applied the two-diode equivalent electrical circuit to calculate the I-V curve of a solar cell for a vast combination of irradiances and temperatures. Curves were obtained for irradiances ranging from 1 W/m^2 to 1200 W/m^2 with a resolution of 1 W/m^2, combined with cell temperatures ranging from $-10^\circ C$ to $120^\circ C$ every $2^\circ C$. In total, 77,935 different IV curves were produced. In the calculation, both the series and shunt resistances were considered temperature independent.

4 | MODELING FRAMEWORK—MODULE LEVEL

4.1 | Optical effects of encapsulation on color saturation and angular behavior

For the case of a module, the effective irradiance reaching the solar cell is now also determined by the reflectance and absorptance spectra of the glass, the encapsulant ethylene vinyl acetate (EVA), the colored filter, and the antireflective coating. We used GenPro4 simulations to calculate the transmittance τ_0 for normal incidence. This parameter is defined as the ratio between the light intensity that reaches the silicon (I_{cell}) and the light intensity reaching the front surface of the module (I_{POA}).

$$\tau_0 = \frac{I_{cell}}{I_{POA}} \tag{3}$$

We performed the calculations by considering the properties of the encapsulant glass and EVA shown in Table 1. For the case of a module without filter (standard case), τ_0 was found to be equal to 0.903.

To calculate the plane of array irradiance G_{POA}, we use the Perez simplified diffuse irradiance model.[50] Typical meteorological year data obtained from Meteonorm,[51] with a 10-min resolution, are utilized to obtain the following irradiance components: direct (G_{dir}), circumsolar (G_c), horizon brightening (G_{hb}), isotropic diffuse (G_{id}), and ground reflected (G_{gr}). The sum of these components produces the value of G_{POA}. To account for the sensible dependence of the colored modules on the angle of incidence, three different values are calculated for each time instant.

$$AOI_{(dir,c)} = \cos^{-1}[\cos\theta_z \cos\theta_M + \sin\theta_z \sin\theta_M \cos(\theta_A - \theta_{AM})] \tag{4}$$

$$AOI_{(id,hb)} = 59.7 - 0.1388\theta_M + 0.001497\theta_M \tag{5}$$

$$AOI_{(gr)} = 90 - 0.5788\theta_M + 0.002693\theta_M \tag{6}$$

where θ_z and θ_A are the solar zenith and azimuth, respectively. θ_M and θ_{AM} are the module tilt and azimuth, respectively. Equations 5 and 6 where extracted from the work of Gilman et al[52]

4.2 | Thermal model

The spectral nature of the color filter demands a specific modeling approach for the estimation of the operational temperature. An important contribution to the temperature of a solar cell comes from the thermalization of highly energetic photons. The additional reflectance of light within the visible spectrum produced by the color filter

TABLE 1 Physical and optical properties of the layers that contribute to front side optical losses

Material	Thickness	Optical properties
Glass	3.20 cm	See Vogt et al.[48]
EVA	0.58 cm	See Vogt et al.[49]
SiN_X layer	Variable (0–200 nm)	See Appendix A for both options
SiO_2 layer	Variable (0–200 nm)	See Appendix A for both options
Antireflective coating-SiN_X	78 nm	See Procel et al.[38]

can result in lower operational temperatures when compared with a standard solar cell. Moreover, different colors generate different effects on the cell temperature, depending on the wavelength range in which they reflect. To assess this effect, we have developed a two-dimensional finite volume transient thermal model based on the work of Aly et al.[53]

From GenPro4, we calculate the spectral absorptance at each layer of the PV module for a wavelength range from 300 to 1800 nm. We estimate the spectral irradiance by calculating, at every time instant, the value of air mass. We then used SMARTS[54] to obtain a spectral direct normal incidence irradiance and a spectral diffuse horizontal irradiance. With these, alongside the Perez transposition model,[50] we obtain the spectral plane of array irradiance. We finally estimate the volumetric heat generation at each layer of the PV module by multiplying the spectral absorptance at each layer with the irradiance that reaches it and integrate over the whole wavelength range.

We divide the module into finite volumes, each represented by a node (see Figure 4). At each node, we carried out an energy balance equation, which depends on the node location within the module. A surface node, for example, has three different heat transfer mechanisms: convection and radiation from the front surface with the ambient and conduction with the nodes inside the material (see nodes 2 and 11 in Figure 4.) and conduction from the nodes that depict the layers above or below the surface node. In general, the thermal balance equation is defined as follows:

$$\dot{E}_{in} + \dot{E}_{gen} = \dot{E}_{st} \tag{7}$$

where $\dot{E}_{in}$ represents the energy flow entering (or exiting) a node; $\dot{E}_{gen}$ is the generated energy flow, which in this case, is produced by light absorption of the different layers on the PV module; and $\dot{E}_{st}$ is the energy stored in each node.

All the equations deployed for this thermal model can be found in Appendix B. Overall, our thermal model has the following assumptions:

1. The space between cells is not considered. The solar cell is modeled as a continuous layer over the entire module geometry.
2. Radiation and convection on the sides are neglected. Aly et al. demonstrated that this assumption leads to very low error.[53]
3. The frame of the module is not considered in this calculation.
4. The thermalization losses are calculated considering an energy bandgap that is temperature independent. More details on the calculation of the thermalization losses and on the thermal properties used for these calculations are reported in Appendix B.

5 | SIMULATION WORK AND VALIDATION

5.1 | Color perception results

We established that variation of the thicknesses of the layers inside an optical stack changed the wavelength value at which the reflectance reached a maximum value. With an OF Option 1 as base, the thickness values of both the SiO_2 and the SiN_X were varied from 0 to 200 nm in steps of 10 nm. The color perception model was used to build color matrices, which depict the predicted color appearance at *normal incidence*. Two matrices were considered, one for the case of a color filter deposited on glass (as in Figure 5A), another for the case of the filter deposited on a bare cell. Figure 5 shows the different colors obtained for all thickness combinations. The matrices show that the deposition of the filter on the textured surface of a bare solar cell produces colors with lower brightness compared with the case of a color filter deposited on flat glass.

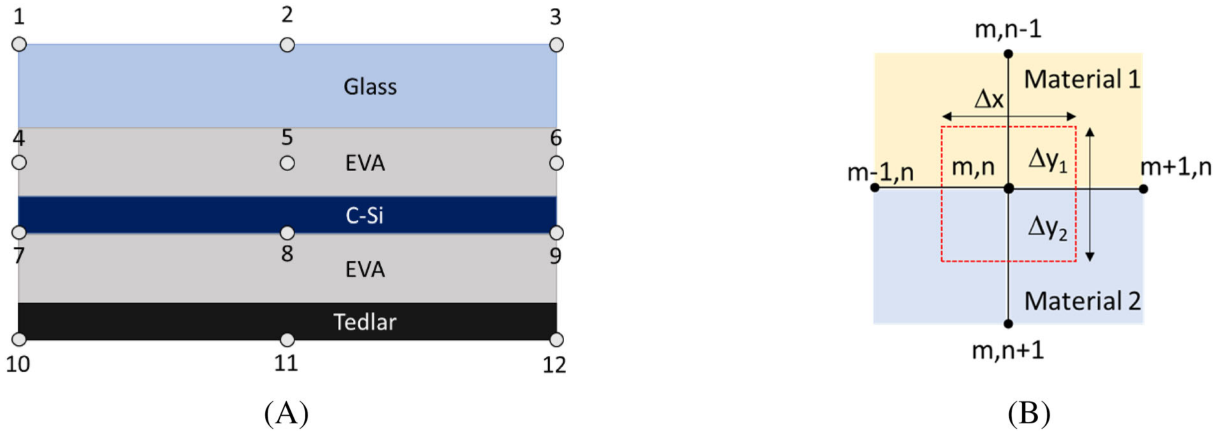

FIGURE 4 The spectral thermal model divides the photovoltaic (PV) module structure into finite volumes. Each volume is represented by a node. At each node, an energy balance is carried out depending on the heat transfer mechanisms associated with the node. The model allows the user to set the number of vertical and horizontal nodes. (A) The structure of the PV module has 12 different nodes in which the energy balance equation is unique, the remaining nodes have a similar equation to any of these 12 options. (B) Example of a central node located within two materials (see. e.g., node 8 on (A)). The energy balance for this node consists of conduction of heat from the adjacent nodes both on the vertical axis and the horizontal axis [Colour figure can be viewed at wileyonlinelibrary.com]

To quantify this, we calculate the coordinates on the Hue Saturation Value (HSV) color space of two selected combination of thicknesses: (90 nm of SiO_2, 110 nm of SiN_X) and (50 nm of SiO_2, 110 nm of SiN_X). These combinations yield a bright orange and a bright green color, respectively, when deposited on flat glass, as shown in Figure 5. Similarly, they produce a dark brown and a dark green color, respectively, when deposited on the solar cell. The conversion from RGB to HSV is relatively simple via the MATLAB® image processing tool. The values of HSV for the selected colors for each case can be found in Table 2.

Table 2 shows that a specific color filter deposited on flat glass produces higher brightness compared with deposition on a textured solar cell (denoted by the third coordinate V of the HSV values). The first coordinate (H) denotes the hue of the color. To find its position on the cylindrical coordinate of the color space, the value of H must be multiplied by 360°. The color space starts with reds (0°), and it is followed by orange, yellow, green, cyan, blue, and magenta at every 60°, respectively. The saturation value can be maximum both on dark and bright colors (coordinate S). The explanation for this is outside the scope of this paper, but more information can be found in Lumb et al..[55] The calculation of HSV helps to analyze the effect of encapsulation on a colored solar cell.

5.1.1 | Validation of the color perception model

It is important to note that colors perceived in Figure 5A can be deceiving. Since the system is an OF on glass, gray must be taken as transparent or *not perceived color* rather than an opaque gray surface. From this color matrix three colors were selected for fabrication as summarized in Figure 6. Three OFs (based on design Option 1) showing a red, yellow, and green color appearance were designed and realized on glass. The thicknesses of the layers composing the different colored OFs are indicated also in Table 3. Photographic evidence of the fabricated samples is in good agreement with colors predicted by our model as shown in Figure 6. The R spectra exhibited by the fabricated filters were measured using a spectrophotometer. They are presented in Figure 7 alongside simulated results, showing good agreement in the wavelength range between 380 and 1180 nm.

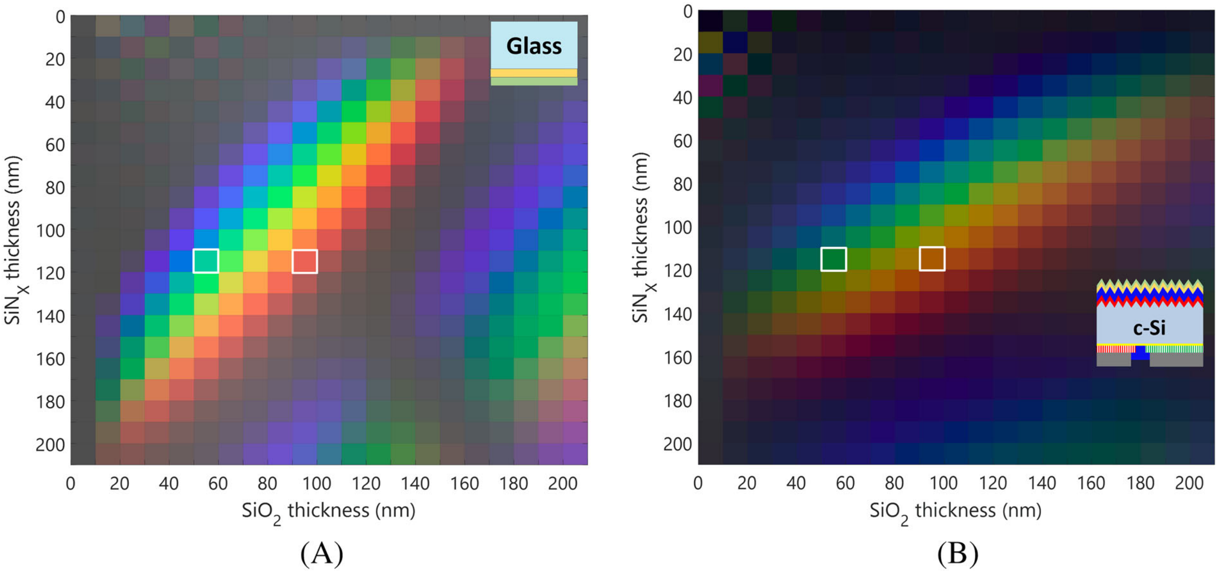

FIGURE 5 Differences in color perception according to the placement of the color filter: (A) color matrix for 10 pairs of SiO_2/SiN_X layers deposited behind the front glass, (B) color matrix for 10 pairs of SiO_2/SiN_X layers deposited directly on the c-Si solar cell. Placing the filter on the front textured surface of a solar cell produces color with a brightness lower than placing it on the flat surface of the glass. The white squares represent the selected colors used to compare the colors on the Hue Saturation Value (HSV) color space [Colour figure can be viewed at wileyonlinelibrary.com]

TABLE 2 RGB coordinates and HSV coordinates of two different color filters: one deposited on flat and another on nonencapsulated colored solar cells

Surface	SiO_2/SiN_X thickness (nm)	R-G-B color coordinate	HSV color coordinate
Flat glass	90/110	204-077-077	0.00-0.62-0.80
Textured cell	90/110	170-089-000	0.08-1.00-0.66
Flat glass	50/110	125-221-025	0.25-0.88-0.86
Textured cell	50/110	000-121-049	0.40-1.00-0.47

Abbreviations: HSV, Hue Saturation Value; RGB, Red, Green and Blue.

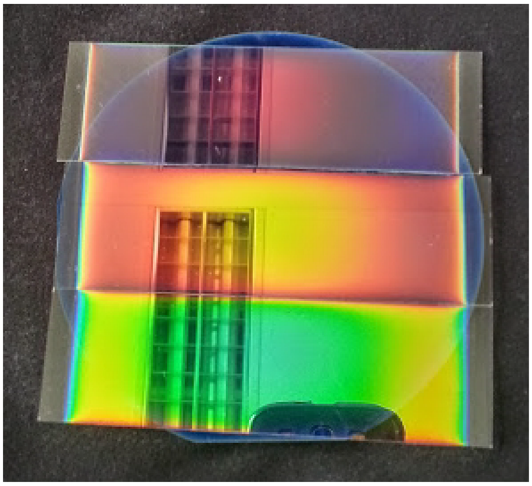

FIGURE 6 Perceived colors of the chosen optic filters (OFs). Notice that the three samples are placed above a double textured c-Si solar cell with standard antireflective coating (ARC). The colors perceived by placing the filter above a solar device are not altered by the device. Note that the deposition area of the layers is not homogeneous, so the desired thicknesses were only achieved in the middle of each glass sheet [Colour figure can be viewed at wileyonlinelibrary.com]

TABLE 3 Thicknesses and perceived color of the filters

Color	Thickness
🟥	$SiO_2 = 100$ nm $SiN_X = 100$ nm
🟨	$SiO_2 = 90$ nm $SiN_X = 100$ nm
🟩	$SiO_2 = 40$ nm $SiN_X = 110$ nm

The mean average error (MAE) and the mean bias error (MBE) of the measurements were calculated as follows:

$$MAE = \frac{\sum_{i=1}^{n} |y_i - x_i|}{n} \qquad \text{Equation (7)}$$

and

$$MBE = \frac{\sum_{i=1}^{n} (y_i - x_i)}{n} \qquad \text{Equation (8)}$$

where y_i is the predicted value, x_i is the measured value, and n represents the number of measured points. The results are presented in Table 4. Overall, the color model can accurately predict the resulting surface color once deposited on a flat glass.

The deposition of a multistack colored filter on the textured surface of a solar cell can be accurately translated from the planar model. In their work, Ingenito et al.[32] demonstrated that by increasing the deposition time on the PECVD machine by a factor of 1.7, the thickness calculated for a planar surface could be obtained on the orthogonal direction to the pyramid facet of a textured solar cell.

5.2 | Electrical model validation

The main objective of this work is to find ways to accurately model the effect of implementing a color filter on a solar cell in a simplified way. From an electrical point of view, we decided to test whether the use of a standard two-diode model could be suitable to this end. The two-diode model can be described as an analytical expression to describe the behavior of a solar cell. The model assumes (i) low injection level conditions, (ii) infinite thickness on the cell, (iii) uniform generation-rate, (iv) superposition principle, and (v) an ideal behavior on its diodes and resistances. On the other hand, TCAD Sentaurus describes the working principles of a solar cell by using the fundamental equations of a semiconductor. It makes no assumptions and uses as inputs the properties of the layers and the materials involved on the cell structure. For this reason, TCAD Sentaurus was deployed as a validation step of our approach of how to electrically model a colored cell with a two-diode model.

To monitor the impact of the color tuning OF on the η of our IBC c-Si solar cell, if the color tuning OF covers the textured front side of the device, several SiO_2/SiN_X stacks were adapted onto the reference solar cell and modeled. Like the flat case on glass, the thickness of every material was varied from 0 to 200 nm at 10-nm steps. The color matrix of the colored filters applied to our textured IBC c-Si solar cell is reported in Figure 5. As stated before, the obtained colors are less bright with the respect to those deposited on glass owing to the front texturing of the device. On the other hand, the front texturing yields lower R values at the wavelength of design and, therefore, lower optical losses. The EQE spectra obtained by placing the color tuning OF on the textured device ***before*** encapsulation of a dark green cell and a brown cell are shown in Figure 8A. The impact of the dark green and the brown OFs on the *J-V* curves is shown in Figure 8B. The EQE spectra of the colored solar cells show a slight increase at a wavelength value of 400 nm. Since Sentaurus simulations are carried on bare solar cells, the refractive indexes of the materials that compose the filter improve the optical performance of the cell's front surface. From a value of n in the ARC layer ($n = 2.4$), the tuned SiN_X ($n = 1.73$) and the SiO_2 ($n = 1.50$) can reduce light reflection at wavelengths outside the interference range. Additionally, for the case of the brown colored cell, the dip on the EQE occurs on a wavelength range in which the standard device absorbs better. Because of this, the impact of this color on the performance of the cell is greater than the effect produced by the green filter. We also observe that while the J_{SC} changes significantly for the presence of the color tuning OF, the V_{OC} and the FF remain largely color-independent, as reported in Figure 8B. This is demonstrated by the opto-electrical modeling of colored IBC c-Si solar cells

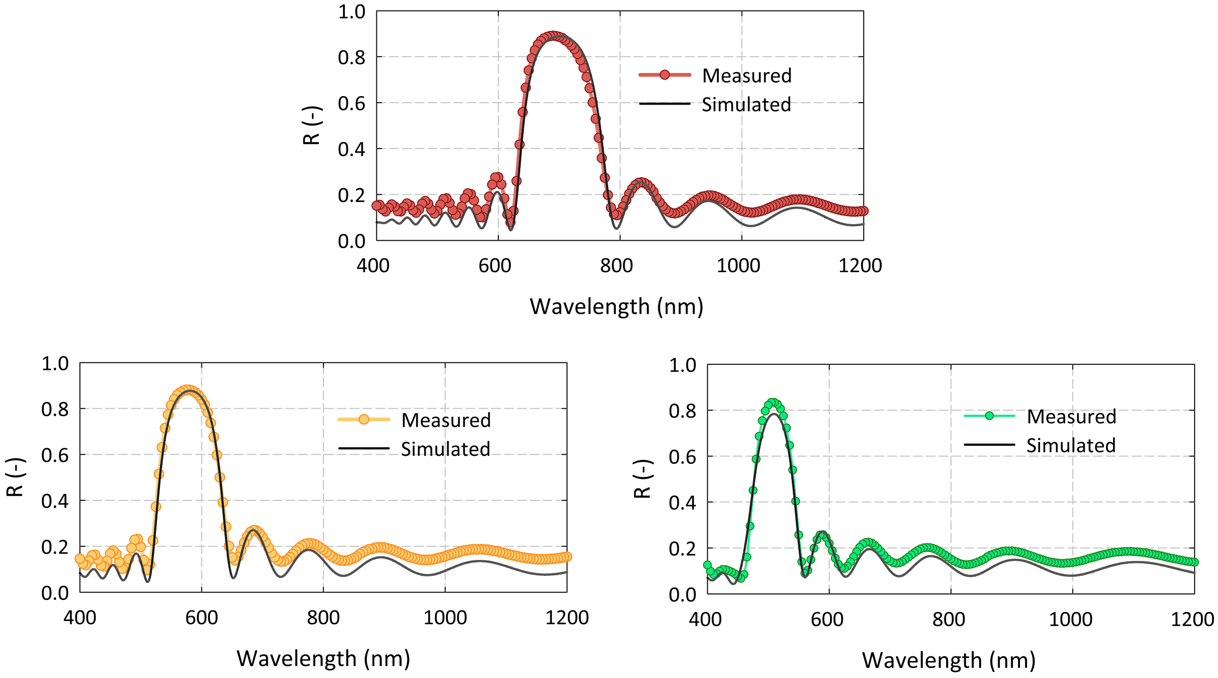

FIGURE 7 Measured and simulated reflectance spectra of the (A) red, (B) yellow, and (C) green samples. These OFs resemble the optical system in Figure 6 R spectra were measured from the glass side of the samples [Colour figure can be viewed at wileyonlinelibrary.com]

TABLE 4 Mean absolute error and mean bias error of the reflectance spectrum for each selected color

Color	Thickness
🟥	MAE = 5.10% MBE = 2.80%
🟨	MAE = 5.30% MBE = 3.92%
🟩	MAE = 4.00% MBE = 3.57%

Abbreviations: MAE, mean average error; MBE, mean bias error.

within the complete thickness space of both SiO_2 and SiN_x. From these simulations, we extracted the values of V_{OC}, FF, J_{SC}, and η. In Appendix C we report the trends of η and J_{SC}, respectively, as function of SiO_2 /SiN_x thickness pairs for the case of the filter Option 1. From the similarity of both trends, the variation in J_{SC} as function of different color tuning OF is the main driver for the variation in η. Relating to the color matrix in Figure 5, it is also noticeable that lowest J_{SC} values are obtained for colors that reflect light in wavelength ranges in which the IBC utilizes the light better. Considering the reference J_{SC} value and the values in Figure 8B, a color-specific $\Delta J_{SC} = J_{SC\text{-ref}}$ - $J_{SC\text{-color}}$ map could be generated. Such a map would help predict the impact that each color has on the η of a nonencapsulated colored IBC c-Si solar cell by derating its J_{SC} from the reference value. That is, not accounting for any potential manufacturing issues, the implementation of a color tuning OF is not expected to negatively impact on the electrical quality of the device itself.

To evaluate the effects that values of AOI larger than 0° have on V_{OC}, V_{MPP}, J_{MPP}, and FF, Sentaurus simulations were carried out to calculate these performance parameters on both the standard cell and the green and brown solar cell. The selected values were 0°, 20°, 40°, 60°, and 80°. Results from these simulations are presented by the J-V curves found in Appendix C and the numeric values shown in Table 5.

From the simulations from Sentaurus, we concluded that even at different angles of incidence, the main driver in power loss on both the colored and standard solar cells is the reduction of current generation. From Table 5, the voltage variation for all three cases remains reasonably similar. The biggest difference is found to be of 6 mV between the standard cell and the brown solar cell at an incidence angle of 80°. This voltage difference represents a deviation of less than 1%. For lower AOI values, the differences are in the order of 2 mV or less. Regarding the FF, the maximum difference is of 0.001. With these two findings, we conclude that the addition of a color filter produces negligible effects on the values of V_{OC} and FF, even at higher angles of incidence.

In their work, Balenzategui and Chenlo[56] state that the angular effect on short circuit current density can be approximated by the following cosine relation:

$$J_{SC(\theta)} = J_{SC(0^\circ)} \cdot \cos(\theta) \tag{9}$$

According to Equation 9, the ratio between the J_{SC} at any angle of incidence with respect to its value at normal incidence equals the

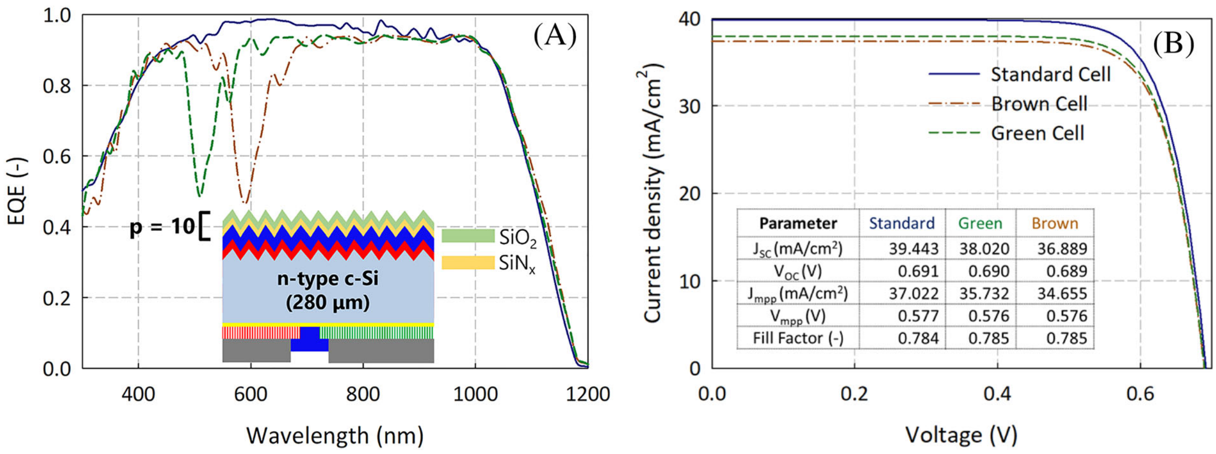

Parameter	Standard	Green	Brown
J_{SC} (mA/cm²)	39.443	38.020	36.889
V_{OC} (V)	0.691	0.690	0.689
J_{mpp} (mA/cm²)	37.022	35.732	34.655
V_{mpp} (V)	0.577	0.576	0.576
Fill Factor (-)	0.784	0.785	0.785

FIGURE 8 Simulated effect of a dark green (dashed) and brown (dash-dotted) color tuning Optic filter (OF) on (A) the external quantum efficiency (EQE) and (B) the J-V curve of a nonencapsulated interdigitated back-contacted (IBC) c-Si solar cell endowed with the color tuning OF (see inset) compared with a standard cell (blue line) [Colour figure can be viewed at wileyonlinelibrary.com]

TABLE 5 External parameters of nonencapsulated standard, dark green and brown colored IBC c-Si solar cells for different angles of incidence

Parameter	0° - Standard	40°	80°	0° - Green	40°	80°	0° - Brown	40°	80°
J_{SC} (mA/cm^2)	39.443	29.197	6.045	38.020	26.956	5.255	36.889	25.942	4.958
ΔJ_{SC} (mA/cm^2)	0.000	−10.246	−33.399	−1.423	−12.487	−34.188	−2.554	−13.501	−34.485
V_{OC} (V)	0.691	0.682	0.634	0.690	0.680	0.630	0.689	0.679	0.628
J_{mpp} (mA/cm^2)	37.022	27.480	5.686	35.732	25.316	4.948	34.655	24.378	4.661
V_{mpp} (V)	0.577	0.572	0.531	0.576	0.572	0.526	0.576	0.571	0.525
Fill factor (−)	0.784	0.789	0.787	0.785	0.790	0.787	0.785	0.790	0.786
Efficiency (%)	21.362	15.719	3.019	20.582	14.481	2.603	19.961	13.920	2.447

Abbreviation: IBC, interdigitated back-contacted.

cosine of the angle. For the case of colored cells, such approach can be inaccurate. To study this, the values of J_{SC} obtained from the simulations for all cases were used to calculate a short circuit current angular factor j_{SC}, mathematically defined as follows:

$$j_{SC(\theta)} = \frac{J_{SC(\theta)}}{J_{SC(0^\circ)}} \tag{10}$$

Notice that according to Equation 9, the value of j_{SC} always equals the cosine of the angle of incidence. The trends obtained from Equation 10 for the standard and the colored cells are shown in Figure C4. The approximation used in Equation 3 is sensible for the case of the standard solar cell, but not for the colored cells, as their angular behavior deviates significantly.

The suitability of the two-diode model was analyzed by keeping all but the light collected current density (J_L) parameters constant. The value of (J_L) was changed to the values previously found with Sentaurus. The calculated j_{SC} factors were used to modify the effective normal incidence irradiance G_{cell} as follows:

$$G_{cell(\theta)} = G_{cell(0^\circ)} \cdot j_{SC(\theta)} \tag{11}$$

The objective is to verify that, if by reducing the intensity of light without changing the angle of incidence, similar behavior is produced (see Figure 9). The j_{SC} factor used for each cell is presented in Table 6. Figure 9 shows that modeling the angular behavior of a cell by using the angular factor j_{SC} to modify the value of effective irradiance at normal incidence produces very accurate results. The prediction of the maximum power point at every angle of incidence, for a standard and a colored cell, produces very little error, as shown in Table 7.

The complete data for the case of the colored cells can be found in Appendix C.

We then assessed the suitability of using the implied photocurrent density J_{ph} obtained from GenPro4 to calculate the angular modifying factors j_{SC}. We report the validity of this approach in Appendix C (Figure C7).

5.3 | Thermal model validation

We validated the thermal model in two steps: First, by simulating the PV module working under NOCT conditions. The AM1.5 spectrum, with its DNI and DHI components (on a wavelength range from

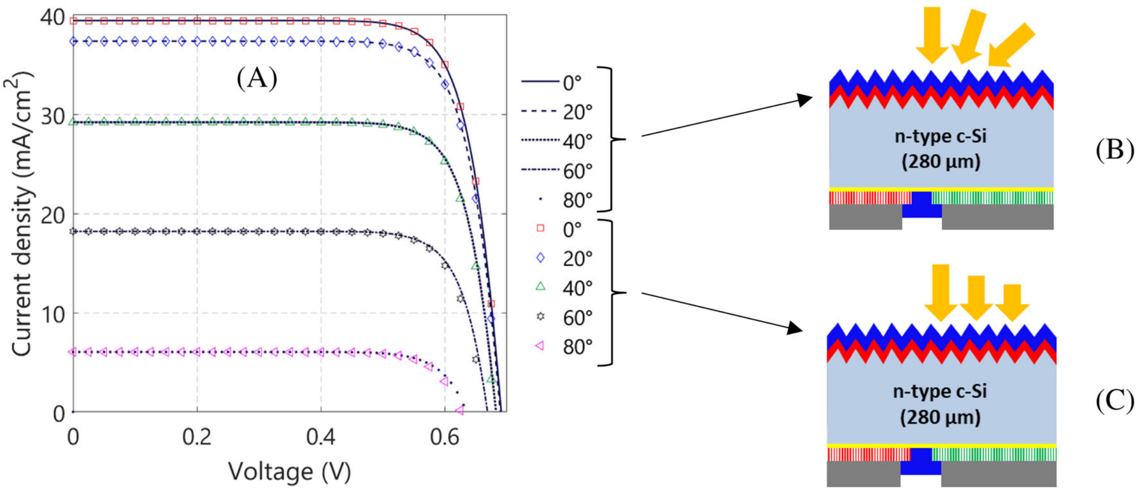

FIGURE 9 (A) Comparison between the J-V curves of a standard interdigitated back-contacted (IBC) solar cell obtained by Sentaurus simulation (lines) and those obtained by the two-diode model (markers). (B) The effect on performance for different angles of incidence of light can be modeled with great accuracy (C) by adjusting the value of irradiance at normal incidence with the angular factor j_{SC} [Colour figure can be viewed at wileyonlinelibrary.com]

TABLE 6 Values of the j_{SC} angular factors for a nonencapsulated standard, a green and a brown colored solar cell

AOI	Standard	Green	Brown
0°	1.000	1.000	1.000
20°	0.947	0.925	0.916
40°	0.740	0.709	0.703
60°	0.461	0.414	0.401
80°	0.153	0.138	0.134

Abbreviation: AOI, angle of incidence.

TABLE 7 Error on the estimation of the maximum power point (mpp) with a two-diode model compared with TCAD Sentaurus for both a standard, a green and a brown nonencapsulated solar cell at different angles of incidence of light

Error (%)			
AOI	Standard	Green	Brown
0°	−0.151	−0.086	−0.028
20°	−0.066	0.061	0.152
40°	0.329	0.445	0.525
60°	0.819	0.921	0.927
80°	1.251	1.328	1.409

Abbreviation: AOI, angle of incidence.

300 to 1800 nm) scaled down and equal to 800 W/m^2 was used as the input of the model. The remaining conditions were set according to the Standard[57]: module tilt of 45°, wind speed of 1 m/s, and ambient temperature of 20°C. The thermal properties of the module were kept as those reported in Appendix B.4.

The thermal behavior of a standard module was simulated under NOCT conditions for a duration of 1 h, calculating its temperature every 5 s. The results, shown in Figure 10, produce a temperature at quasi-steady state conditions of 47.20°C. The front glass surface presents a temperature that is almost 1°C lower than the c-Si. Likewise, the back Tedlar presents a temperature difference of 0.5°C.

These results match the findings of.[53] Using equal thermal property data, the authors calculated a temperature of the solar cell under NOCT of 48.75°C for a module that reported a NOCT temperature value of 47.5°C ± 1.5°C. This represents an error for our model of 3.1% with respect to the authors findings and of 0.6% compared with the datasheet used as benchmark. Moreover, Peter et al.[58] created a three-dimensional finite element model based on COMSOL multiphysics. In their findings, they calculated an NOCT temperature of 46.05°C for a crystalline silicon module, with a temperature difference between the solar cell and the glass of 1°C. Such results match those obtained with our model framework. This first validation process allows the analysis of the effect of the color filter on the temperature of an encapsulated cell and the assessment of its cooling potential when working under stable weather conditions.

We performed a second validation step to assess the accuracy of the thermal model when dealing with changing environmental conditions. A 250 Wp module, manufactured in our facilities, was installed on a rack that was tilted at 30° oriented towards south; further details of the set up can be found in Appendix B.4. A total of four thermocouples were installed with appropriate isolation to the backside of the module. Measurements of temperature were carried out from the 12 to 24 June 2021 with a time resolution of 1 min.

The spectrally resolved thermal model can follow the behavior of the measurements with a minutely resolution. For the entire captured data (12,630 data points) the root-mean-square error (RMSE) is 1.88°C, with an MBE of −0.76°C. Estimation of the daily values of RMSE and MBE is reported in Table C1. The daily values of both

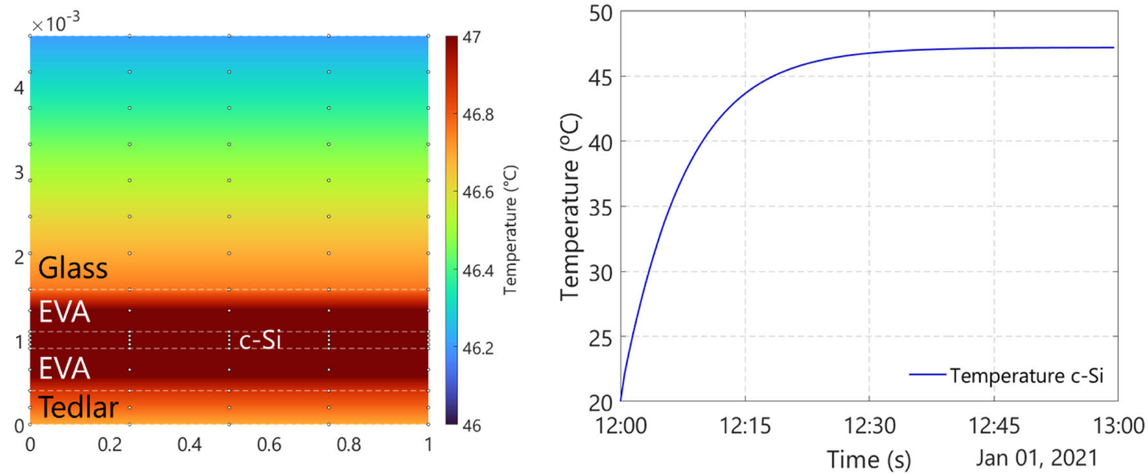

FIGURE 10 Operational temperature of a photovoltaic (PV) module under NOCT conditions. (A) Temperature profile after 1 h of simulation time of all the layers of the PV module. (B) Transient behavior of the c-Si cell inside the PV module [Colour figure can be viewed at wileyonlinelibrary.com]

TABLE 8 Effect of the encapsulation on the saturation of colored solar cells (a), when the cells are encapsulated with a flat glass layer (b), the saturation value of the bare cell drops dramatically, and when the front surface of the glass is textured (c), in some cases, the saturation value increases to high values but the hue changes

	🟫	🟩	🟪	⬛	🟩	🟦
Perceived color	**Brown**	**Green**	**Encapsulation effect**		**Front glass texturing effect**	
H-S-V coordinates	0.08-1.00-0.66	0.40-1.00-0.47	0.84-0.15-0.31	0.45-0.34-0.32	0.23-0.31-0.34	0.54-0.80-0.31
Structure	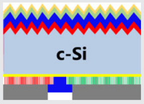 (a)		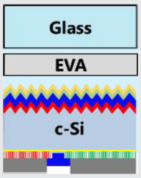 (b)		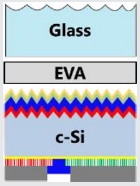 (c)	

RMSE and MBE are higher compared with those calculated the entire data set. The model itself performs well, given that the error reported on other transient models, for entire data sets, is within the range as that produced here.[59,60]

5.4 | Effect of encapsulation on color saturation and application of angular factors on module level simulations

In Figure 5 we showed that a color filter deposited on a textured solar cell could produce colors with similar saturation, but lower brightness, than when deposited on flat glass. However, the appearance of a colored cell can change significantly due to the encapsulation. We study this effect by calculating the HSV color coordinates of the brown and green solar cells ***after*** encapsulation.

Table 8 shows the effect of the encapsulation on the saturation value of a colored cell. For both the brown and the green solar cell, encapsulation with a flat glass reduces the perceived saturation of colors significantly. Moreover, the brown solar cell presents a significant change in its hue, meaning that it will not appear as brown anymore. For the case of the green solar cell, the effect on the perceived hue is lower, and the cell could still be perceived as a dark green, although with poor saturation and brightness.

Evidently, good color saturation should be an important aspect on a module with encapsulated colored solar cells. For this reason, we studied different ways of improving this aspect. One approach was to consider the front glass of the PV module with a random micro-textured pattern. These patterns can be produced via wet etching, as shown by previous studies.[61–64] On section (c) of Table 8, we present the effect produced by the texturing on the perceived color of the cell. For the case of the brown cell, neither the hue nor the saturation can be restored. There is a slight improvement on the saturation, but its value remains low. For the case of the green cell, the front texturing improves the saturation significantly, albeit with an important change on the hue. On both cases, the brightness of the color itself remains lower than for the case of the bare cell.

The calculation of the color saturation was performed for all the thickness combinations shown in Figure 5B. Considering encapsulation with a textured front glass (as shown in Table 8c), colors that presented values of the S coordinate higher than 0.5 were selected, see Figure C8B. A very small number of colors achieve a value higher than this threshold. Further ways to improve the S and V values of encapsulated colored cell involve, for example, modeling different front glass texturing. If very high color brightness is required, the best approach is to deposit the filter on glass. This last solution will be explored on a future publication.

Increasing the difference between the refractive indexes of the materials that constitute the filter has profound effects on color saturation, as shown by Equation 1. However, Equation 2 also states that the increasing this difference also affects the photonic bandgap, which can lead to greater performance losses. Still, given that the color saturation produced by a filter with a SiN_X of $n = 1.73$ (**Option 1**) is limited, we explored how changing this property can produced better color appearance. By implementing **Option 2**, the color saturation of the encapsulated cell is significantly improved. Figure C16A highlights this improvement and shows better brightness on the perceived colors as well.

The angular factors j_{SC} (as defined by Equation 10) were calculated for a range of angles of incidence from 0° to 85° with a resolution of 5° for all the colors depicted in Figure C16A). The values of the j_{SC} obtained for a standard module were then compared with other angle of incidence modifiers models developed by Martin-Ruiz[65] and Marion,[66] showing good agreement (See Appendix C).

Since these factors already consider the effect of absorptance and reflectance from the glass/EVA/Filter, the irradiance reaching an encapsulated cell at any AOI is defined as follows:

$$G_{cell(\theta)} = \tau_0 \cdot G_{POA} \cdot j_{SC(\theta)} \tag{12}$$

where G_{POA} is the irradiance on the plane of array of the module.

As explained previously and presented in Figure 8, the implementation of a color produces changes on the EQE of the cell. Even for similar peak reflectance, the brown colored cell presents a larger J_{SC} degradation compared with the green cell. This spectral behavior needs to be considered when performance calculations are done with scalar values of G_{POA}. To account for the *spectral sensitivity* of a colored cell, the following color factor (CF) is introduced:

$$CF = \frac{J_{PHcolor}}{J_{PHstd}} \tag{13}$$

CF is then defined as the ratio of the photogenerated current density of a colored cell ($J_{PHcolor}$) with respect to that of a standard device (J_{PHstd}) for the same spectrum. In this work, AM1.5 spectrum was used to calculate this factor for each color.

As the relationship between J_{PH} and Irradiance can be considered linear,[56] CF modifies Equation 12 as follows:

$$G_{cell(\theta)} = \tau_0 \cdot CF \cdot \left[j_{SC(dir,c)} \cdot (G_{dir} + G_c) + j_{SC(id,hb)} \cdot (G_{id} + G_{hb}) + j_{SC(gr)} \cdot G_{gr} \right] \tag{14}$$

with all the respective angular modifiers being considered for each component of irradiance.

6 | IMPACT OF A COLOR TUNING OF ON THE DC ENERGY YIELD OF AN ENCAPSULATED CELL

Once we validated the optical and the thermal models and demonstrated that the optical losses produced by the filter can be modeled by scaling down the plane of array irradiance by using angular and color dependent factors, we calculate the DC energy yield of a colored solar cell.

To this end, we selected five different encapsulated solar cells, one standard device, without any color filter, two colored cells with a colored filter made with SiO_2/SiN_X, for both color filter options discussed.

Two different locations were selected for this study: Delft, in the Netherlands, and Alice Springs, in Australia. The former is a location with an average annual diffuse to global (D2G) factor of 0.531.[67] This means that, on average, due to environmental conditions, the diffuse component of irradiance dominates over the direct normal component. The latter, by contrast, has an average annual D2G factor of 0.211, making it a location with a greater occurrence of clear skies. For both locations, we extracted weather data from the software Meteonorm.[51] The selected time resolution was 10 min. The modeling framework was deployed, calculating the effective irradiance reaching the silicon of the cell, estimating its temperature under the ambient conditions at the given time instant and, via iteration, calculating its power production.

6.1 | Effect on operational temperature

Given that the additional reflectance produced by the filter can imply a temperature reduction, we studied this effect under NOCT conditions, like the validation procedure. For this, we selected the case of encapsulation with a textured front glass surface.

For the standard device, the operational temperature calculated under NOCT was 47.20°C. The thermalization losses were estimated with a wavelength resolution of 10 nm. Figure 11B shows the amount of energy thermalized by the c-Si cell and the power extracted for a

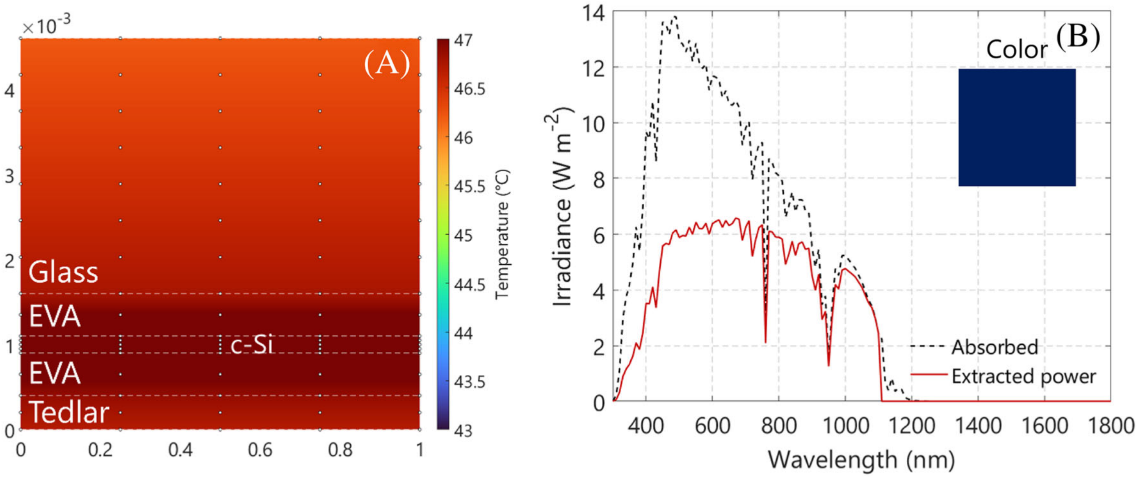

FIGURE 11 (A) Temperature profile of the encapsulated standard solar cell without color filter. (B) Representation of the thermalized power on the c-Si cell for a wavelength range from 300 to 1800 nm. For this calculation, the bandgap of the cell was assumed independent from the temperature and equal to 1100 nm [Colour figure can be viewed at wileyonlinelibrary.com]

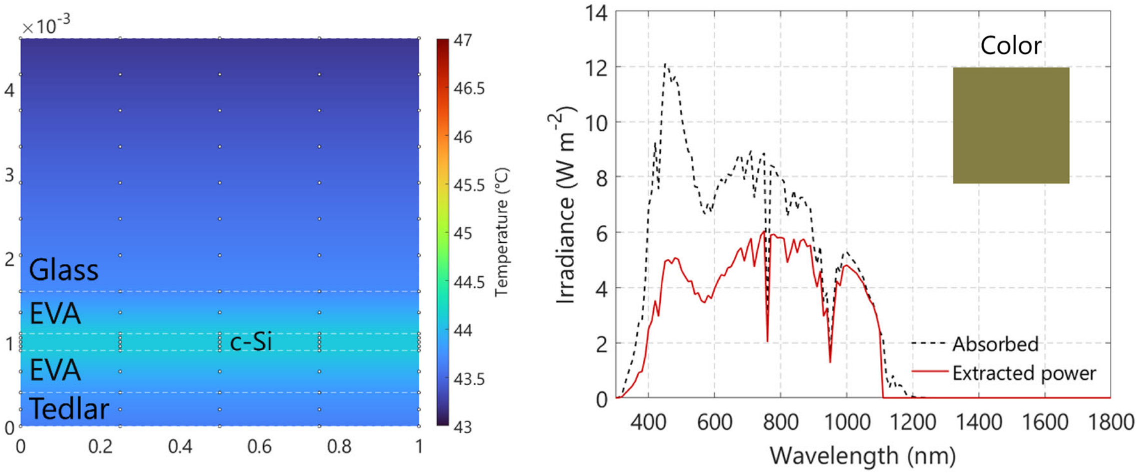

FIGURE 12 (A) Temperature profile of an encapsulated colored cell with an optic filter with 10 pairs of $SiO_2 = 110$ nm and $SiN_X = 80$ nm (option 2) under NOCT conditions. At steady state, the encapsulated cell reaches a temperature of 44.10°C, nearly 3°C lower than an encapsulated standard solar cell under the same conditions. (B) Thermalization losses are reduced due to the additional reflectance required to change the color appearance of the solar cell [Colour figure can be viewed at wileyonlinelibrary.com]

wavelength range from 300 to 1800 nm. Notice that the bandgap was considered temperature independent and equal to 1100 nm.

For the case of an encapsulated colored solar cell, we selected a color produced by the deposition of a filter based on Option 2. The thicknesses selected in this example were $SiO_2 = 110$ and $SiN_X = 80$ nm. Figure 12A shows that the colored solar cell reaches a steady state temperature under NOCT conditions of 44.10°C, which is 3.10°C lower than the standard cell under the same conditions. This temperature reduction is driven by a reduction on the thermalization losses close to 600 nm, as shown in Figure 12B. The effect also negatively affects the amount of power that can be extracted from the cell, which is translated into lower electric energy.

We then calculated the steady state temperature under NOCT conditions for all combination of thicknesses (ranging from 0–200 nm). For Option 1, we found a maximum temperature reduction of 2.5°C under NOCT conditions. Most of the colors with high saturation, however, did not present reductions beyond 2.0°C. For Option 2, the temperature reduction produced is higher, reaching a maximum of 5.2°C. Bright and saturated colors presented reductions ranging from 2.0°C to 5.0°C. The results for all color combinations can be found in Appendix D.

6.2 | Effect on DC energy yield

Finally, we calculated the DC energy yield of the five encapsulated solar cells. On all cases, the encapsulated front surface **was textured glass**. We selected this case as it is the one that yields better saturation and brightness of colors for both options of filters compared with the case of encapsulation with a flat front glass. The chosen colors from both options of color filter can be found in Table 9. Notice that the colors were selected for a high saturation as obtained with Option 2, and a comparison is made with the filter produced by Option 1 with the same thickness combination.

The installation layout assumed that the encapsulated cell is tilted 35° from the horizontal, oriented towards the optimum azimuth according to the location (i.e., South for Delft and North for Alice Springs). Also, the backside of the encapsulated cell has no forced convection on its backside (BIPV condition). All the simulation parameters can be found in Figure 13.

The simulation results for each of the selected colors and the standard devices are summarized in Table 10. For the case of the color filter with SiN_X with a value of $n = 1.73$ (Option 1), the green colored cell installed in Delft presents a relative DC yield loss of 2.25% compared with the standard cell. The dark brown color presents higher relative losses of 3.93%, despite its poor saturation. On Alice Springs, the relative energy loss for the green cell is slightly lower compared with Delft, with a value of 2.23%. Similar case is found for the dark brown cell, which on the Australian city presents a relative annual yield loss of 3.57% compared with the standard case.

Of all the colors that can be produced from this filter option, the maximum relative DC energy yield loss for Delft was of 11.3%, whereas on Alice Spring it was found to be of 10.9% (see Appendix D for the full overview of all color combinations). In Alice Springs the losses were slightly lower than Delft due to a slight better thermal performance of the colored cell.

When the refractive index of the SiN_X is increased to $n = 2.1$ (Option 2), the increase in saturation is followed by a decrease in the relative annual DC energy loss compared with a standard solar cell. For Delft, the green colored cell has an 8.15% relative DC yield loss, whereas the brown colored cell presents a relative loss of 10.95%. In Alice springs, the relative loss was 7.73% for a green colored cell, whereas the brown cell presented relative losses of 10.55%.

For Option 1, the colors that present a saturation value above 0.5 (shown in Figure 13) yield relative DC yield losses in Delft that range from 1.20% to 2.70%. However, the color with the least relative loss (1.20%) is a green color that, despite presenting a relatively high saturation color, presents a very low brightness. This is a general trend

TABLE 9 Selected colored cells for DC energy yield assessment

Filter	Thickness 1	Perceived color 1	Thickness 2	Perceived color 2
Option 1 SiO_2/SiN_X ($n = 1.73$)	110 nm/80 nm	🟩	130 nm/100 nm	🟫
Option 2 SiO_2/SiN_X ($n = 2.10$)		🟩		🟫

Note: The perceived colors account for the effect produced by the encapsulation.
Abbreviation: DC, direct current.

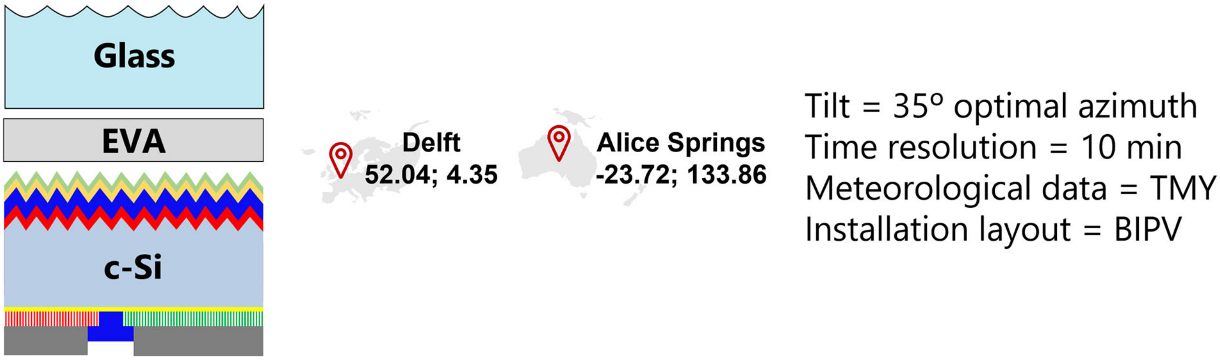

FIGURE 13 Simulation parameters for the direct current (DC) energy yield calculation. The simulated structure was an encapsulated interdigitated back-contacted (IBC) solar cell with a textured front glass. All the colors produced by the combination of the different thicknesses from each color filter were simulated by using typical meteorological year (TMY) data obtained from Meteonorm. The selected time resolution was 10 min [Colour figure can be viewed at wileyonlinelibrary.com]

TABLE 10 DC energy yield for the selected colors on the chosen locations

Colored cell	🟦	🟩	🟫	🟩	🟫
	Standard	Green Option 1	Brown Option 1	Green Option 2	Brown Option 2
RGB value		23-88-72	101-70-64	93-140-83	139-92-60
HSV value		0.46-0.74-0.34	0.02-0.37-0.40	0.30-0.41-0.55	0.07-0.57-0.55
Delft					
Energy yield (kWh/year)	3.56	3.48	3.42	3.27	3.17
Relative loss (%)	-	2.25	3.93	8.15	10.95
Max. temp. (°C)	60.3°C	60.2°C	60.1°C	57.1°C	57.0°C
Alice Springs					
Energy yield (kWh/year)	6.73	6.58	6.49	6.21	6.02
Relative loss (%)	-	2.23	3.57	7.73	10.55
Max. temp. (°C)	75.0°C	73.6°C	73.4°C	71.4°C	71.3°C

Note: The installation conditions considered were 35° of tilt, optimum orientation and a BIPV layout (no forced convection on the backside).
Abbreviation: DC, direct current.

observed on all the colors produced with this filter. Losses for Alice Springs share a similar trend with relative yield losses that range from 1.10% to 2.20%.

Option 2 offers much better results not only in terms of saturation but also in terms of brightness. For Delft, relative yield losses range from 0.50% to 12.90% for colors with saturation values above 0.5. Like Option 1, the colors with low losses lack brightness. A combination of both is desirable from an esthetics perspective. To produce such combination, losses increase in the rage from 7.00% to 12.90%; this is consistent with findings from the works of Kutter et al.[17]

Notice that a filter can produce a color with poor saturation, poor brightness, and still present high losses, which is the case of the brown color produced with Option 1 for the thickness combination shown in Table 9. This is due to a relatively high reflectance produced outside the visible spectrum, which increases losses without affecting color perception.

7 | CONCLUSIONS

We created a computational model to aid the design of a color tuning OF for PV solar cells applications. The model uses (i) the standard proposed by the International Committee of Illumination (CIE) to predict color perception and (ii) advanced models validated via TCAD software platform and experimental data that help predict the impact on the opto-electrical performance when applied on a c-Si IBC solar cell. The materials selected for the OF proposed in this work are SiO_2 and SiN_X. Such materials were chosen because of their nonabsorptive nature, their availability for industrial scale application, and their adequate refractive index values over the entire visible spectrum. Samples manufactured and measured via spectrophotometry show that the optical model accurately predicts reflectance spectra for different colored OF.

Performance wise, the opto-electrical simulations deployed on TCAD Sentaurus showed that the application of the filter is expected to not influence the electrical quality of the cell, as the values of V_{OC}, FF and V_{MPP} remain relatively unaffected. On the other hand, the OF can have a significant impact on the current generation of the device.

Sentaurus simulations were deployed to opto-electrically assess the effect of the color filter. Two selected colors, green and brown, were studied. Results showed that, for normal incidence of light, the green color reduces the efficiency of the cell by 0.78% absolute, whereas the brown presented a reduction of 1.40% absolute, mostly driven by current loss. For angles of incidence greater than 0°, the current density of the standard changes closely to a cosine relationship. Colored cells, however, have a significant deviation from this behavior. By means of a two-diode equivalent electrical circuit, the angular behavior of the cells was modeled by modifying the effective irradiance with scaling factors. These factors were equal to the ratio of photogenerated current at a given angle of incidence with respect to the value at normal incidence. The approach was proven to be very accurate, yielding absolute errors on the prediction of the maximum power point of less than 0.2% for normal incidence and less than 2% for an angle of incidence of light equal to 80°.

Since the filters operate by selectively reflecting light within the visible spectrum, a two-dimensional finite volume thermal model was developed to study the effect on the cell temperature produced by a color filter. The model considers the absorption on every layer of the module for a wavelength range from 300 to 1800 nm. Validation of the model was carried on two ways: first, by studying its behavior under NOCT conditions and second, by comparing its estimated temperature against measurements taken during 12 days. The error produced under constant environmental conditions was below 2% absolute. Compared against measurements with a resolution of 1 min, the model produced MBE and RMSE of 0.89°C and 2.10°C, respectively, when considering the entire measurement period. Daily values of MBE and RMSE are significantly higher due to the low time resolution.

With the validated optical and thermal models, we performed an analysis of the effect that encapsulation has on color saturation. The use of SiN_X with a relatively low refractive index ($n = 1.71$, Option 1) was studied first given its good results in terms of color saturation and brightness on bare solar cells. However, once the effect of encapsulation was accounted, these properties were negatively impacted. On some colors, the encapsulation eliminated almost entirely the saturation and brightness of a bare colored cell.

The use of front glass texturing and increasing the value of the refractive index of the SiN_X to $n = 2.1$ (Option 2) was shown to increase both the brightness and the saturation of color substantially. This second option was also selected to study its effects on the performance of an encapsulated cell.

Temperature calculations under NOCT conditions showed that the deposition of Option 1 could have temperature reductions of up to 2.20°C. The use of Option 2, given its better reflectance, produces significant reductions of up to 5.20°C. We discussed that this temperature reduction comes from the additional reflectance produced by the colored filter, which reduces thermalization losses.

The reduction in operational temperature, however, does not bridge the gap in electrical performance between an encapsulated colored solar cell and an encapsulated standard solar cell. It is important to highlight that this temperature reduction can have potential benefits. Research has shown that degradation rates produced by thermal cycling can significantly reduce the lifetime of PV modules, particularly on very warm climate.[68] This aspect will be studied in future works.

The model was used to study the effect of the colored filters on the energy yield of an encapsulated cell. The installation layout selected was a tilt of 35° with the optimal orientations for Delft in the Netherlands and Alice Springs in Australia.

Calculations of DC energy yield showed that using color filters can produce low relative yield losses compared with an encapsulated standard device. For selected colors with high saturation values (a value of S on the HSV color space greater than 0.5), the losses presented by using Option 1 were up to 6.40% for Delft and 5.9% for Alice Springs. Despite the high saturation, the brightness was still poor. This option of filter, however, is still a valid approach for installation looking for dark tones with minimal impact on performance.

If highly bright and highly saturated colors are desired, Option 2 is a promising alternative, but the relative DC yield losses will increase up to 13.70%. There are, however, color options that meet both high saturation and high brightness with relative losses below 7.00%.

Overall, we believe that colored filters produced by deposition of multilayer optical systems is a promising alternative to improve the esthetics of PV modules.

DATA AVAILABILITY STATEMENT

The data that support the findings of this study are available from the corresponding author upon reasonable request.

ORCID

Juan Camilo Ortiz Lizcano https://orcid.org/0000-0002-0165-5493
Paul Procel https://orcid.org/0000-0003-4997-3551
Andres Calcabrini https://orcid.org/0000-0002-1940-4705
Guangtao Yang https://orcid.org/0000-0001-8288-7394
Andrea Ingenito https://orcid.org/0000-0002-9254-6179
Rudi Santbergen https://orcid.org/0000-0001-9273-4244
Miro Zeman https://orcid.org/0000-0002-1710-360X
Olindo Isabella https://orcid.org/0000-0001-7673-0163

REFERENCES

1. United Nations. Cities and climate change: global report on human settlements. *UN Habitat*. London: Earthscan; 2011;2011:1-300. https://unhabitat.org/sites/default/files/download-manager-files/Cities%20and%20Climate%20Change%20Global%20Report%20on%20Human%20Settlements%202011.pdf
2. United Nations “World Population Prospects: The 2012 Revision. File POP/1–1: Total population (both sexes combined) by major area, region and country, annually for 1950–2100 (thousands). Medium fertility, 2010–2100”, United Nations, 2013.
3. Frei B., “World Economic Forum,” World Economic Forum, 26 01 2021. [Online]. Available: https://www.weforum.org/agenda/2021/01/here-s-how-to-decarbonize-the-eu-s-building-stock/. [Accessed 12 02 2021].
4. Architecture2030. *Roadmap to Zero Emissions*. Santa Fe, New Mexico; 2014.
5. Department of Energy. *Research and Development Needs for Builidng-Integrated Solar Technologies*. Burlington, MA: Navigant Consulting. Inc; 2014.
6. Jelle BP, Breivik C, Rokenes HD. Buil Integrated Photovoltaic Products: A state of the art review and future research opportunities. *Sol Energy Mater Sol Cells*. 2012;100:69-96.
7. EUR-Lex, “Document 32018L0844,” EU, 2020. [Online]. Available: https://eur-lex.europa.eu/legal-content/EN/TXT/?uri=uriserv%3AOJ.L_.2018.156.01.0075.01.ENG. [Accessed 12 06 2020].
8. Eder G., Perharz G., Trattnig R., Bonomo P., Saretta E., Frontini F., Polo Lopez C., Rose Wilson H., Eisenlohr J., Chivelet N., Karlsson S., Jakica N. and Zanelli A., "*Coloured BIPV: Market, Research and Development*," IEA, 2019.
9. International Energy Agency. *Potential for Building Integrated Photovoltaics*. Ursen: NET Nowak Energy & Technology Ltd; 2002.
10. NREL. *Building-Integrated Photovoltaics in the Residential Sector: An Analysis of Installed Rooftop System Prices*. Oak Ridge: U.S. Department of Energy; 2011.
11. Heinstein P, Ballife C, Perret-Aebi L-E. Building Integrated Photovoltaics (BIPV): Review, Potentials, Barriers and Myths. *Green*. 2013;3(2):125-156.
12. PV Magazine. “PV Magazine,” 1 12 2019. [Online]. Available: https://www.pv-magazine.com/2019/12/31/bipv-more-than-the-module/. [Accessed 1 3 2020].
13. Eiffert P. and I. LLC, “Non-technical barriers to the commercialization of PV power system in the built environment,” NREL, Golden, 2003.
14. Masuda T, Kudo Y, Banerje D. Visually attractive and high-power-retention solar modules by coloring with automotive paints. *Coatings*. 2018;8(282):1-7.
15. Slooff L, Van Roosmalen J, Okel L, et al. An architectural approach for improving aesthetics of PV. In: *European PV Solar Energy Conference and Exhibition EUPVSEC*. Amsterdam; 2017.

16. Kameleon Solar, “Color Blast,” Kameleon Solar, 2021. [Online]. Available: https://kameleonsolar.com/nl/colorblast/. [Accessed 12 03 2021].
17. Kutter C, Blasi B, WIlson H, et al. Decorated building integrated photovoltaic modules: Power loss, color appereance and cost analysis. In: *European PV Solar Energy Conference and Exhibition*. Brussels; 2018.
18. Neder V, Luxembourg S, Polman A. Efficient colored silicon solar modules using integrated resonant dielectric nanoscatterers. *Appl Phys Lett*. 2017;111:1-5.
19. Blasi B, Kroyer T, Hohn O, et al. Morpho butterfly inspired colored BIPV modules. In: *33rd European Photovoltaic Solar Energy Conference and Exhibition*. Amsterdam; 2017.
20. Yoshikawa K, Yoshida W, Irie T, et al. Exceeding conversion efficiency of 26% by heterojunction interdigitated back contact solar cell with thin film Si technology. *Sol Energy Mater Sol Cells*. 2017;173:37-42.
21. Haase F, Hollemann C, Schafer S, et al. Laser contact openings for local poly-Si-metal contacts enabling 26.1%-efficient POLO-IBC solar cells. *Sol Energy Mater Sol Cells*. 2018;186:184-193.
22. Cousins P, Smith D, Luan HC, et al. Generation 3: Improved performance at lower cost. *Proceedings of the 35th IEEE Photovoltaic Specialist Conference*. 2010:275-278.
23. Macleod H. *Thin Film Optical Filters*. Arizona: Institute of Physics Publishing Bristol and Philadelphia; 2001.
24. RP Photonics Consulting, “RP Photonics Encyclopedia,” RP Photonics consulting, [Online]. Available: http://www.rp-photonics.com/optical_filters.html. [Accessed 20 05 2014].
25. Griot M. 5. Optical Coatings. In: *Fundamental Optics*; 2009.
26. Isabella O. *Light Management in Thin-Film Silicon Solar Cells*. Delft: Delft University of Technology; 2013.
27. Kvavle J, Bell C, Henrie J, Schultz S, Hawkins A. Improvement to reflective dielectric film color pictures. *Optics Express*. 2004;12(23):5789-5794.
28. Schneiderlochner E, Bruckner J, Biedermann R, et al. High throughput magnetron sputtering technology at 10,000 wafers per hour cost-competitive manufacturing of transparent conductive oxides (TCO). *3rd International workshop on SHJ Solar Cells*, Online event. 2020:1-17.
29. Kelly P, Arnell R. Magnetron sputtering: A review of recent developments and applications. *Vacuum*. 2000;56(3):159-172.
30. Isabella O, Dobrovolskiy G, Zeman M. Design and application of dielectric distributed Bragg back reflector in thin-film silicon solar cells. *J Non Cryst Solids*. 2012;358(17):2295-2298.
31. Ingenito A, Isabella O, Zeman M. Experimental demonstration of 4n2 classical absorption limit in nanotextured ultrathin solar cells with dielectric omnidirectional back reflector. *ACS Photonics*. 2014;(1):270-278.
32. Ingenito A, Ortiz Lizcano J, Luxembourg S, et al. Optimized back reflectors for rear difussed c-Si solar cells. *Energy Procedia*. 2014;55:94-100.
33. Lumb M, Yoon W, Bailey CG, Scheiman D, Tischler J, Walters R. Modeling and analysis of high performance, multicolored anti-reflection coatings for solar cells. *Optical Society of America*. 2013:A585-A594.
34. Santbergen R, Meguro T, Suezaki T, Koizumi G, Yamamoto K, Zeman M. GenPro4 optical model for solar cell simulation and its application to multijunction solar cells. *IEEE J Photovolt*. 2017;7(3):919-926.
35. Yang G, Ingenito A, Hammeren NV, Isabella O, Zeman M. Design and application of ion-implanted polySi passivating contacts for interdigitated back contact c-Si solar cells. *Appl Phys Lett*. 2016;108(3):033903-1-033903-4.
36. Yang G, Ingenito A, Isabella O, Zeman M. IBC c-Si solar cells based on ion-implanted poly-silicon passivating. *Sol Energy Mater Sol Cells*. 2016;(158):84-90.
37. Procel P, Ingenito A, De Rosse R, et al. Opto-electrical modelling and optimization study of a novel IBC c-Si solar cell. *Prog Photovolt*. 2017;(25):452-469.
38. Procel P, Yang G, Isabella O, Zeman M. Numerical Simulations of IBC solar cells based on poly-Si Carrier-selective passivating contacts. *IEEE J Photovolt*. 2019;9(2):374-384.
39. Conway B. *Neural Mechanisms of Color Vision*. Norwell: Kluwer Achademic Publishers; 2002.
40. Nadenau M, Winkler S, Alleysson D, Kunt M. Human Vision Models for Perceptually Optimized Image Processing—A Review. *Proceedings of the IEEE*. 2000;32:1-15.
41. Ibraheem NA, Hasan MM, Khan RZ, Mishra PK. Understanding color models: A review. *ARPN Journal of science and technology*. 2(3):265-275.
42. Schanda J. *Colorimetry: understanding the CIE system*. John Wiley & Sons; 2007.
43. Qui K, Bittkau K, Lambertz A, et al. The impact of reflectance variation in silicon heterojunction solar cells and modules on the perception of color differences. *IEEE J Photovolt*. 2021;(11):306-311.
44. Wolf M, Noel G, Stirn R. Investigation of the double exponential in the current—voltage characteristics of silicon solar cells. *IEEE Transactions on electron Devices*. 1977;24(4):419-428.
45. Charles J, Bordure G, Khoury A, Mialhe P. Consistency of the double exponential model with physical mechanisms of conductions for solar cell under illumination. *J Phys: Appl Phys*. 1985;18(11):2261-2268.
46. SunPower, “Maxeon (TM) Gen III Solar cells,” SunPower Corporation, 2016.
47. PV Lighthouse, “PV lighthouse: Equivalent-circuit calculator,” 2020. [Online]. Available: https://www.pvlighthouse.com.au/equivalent-circuit. [Accessed 6 1 2021].
48. Vogt M, Hahn H, Holst H, et al. Measurement of the Optical Constants of Soda-Lime Glasses in Dependence of Iron Content and Modeling of Iron-Related Power Losses in Crystalline Si Solar Cell Modules. *IEEE J Photovolt*. 2016;6(1):111-118.
49. Vogt M, Holst H, Schulte-Huxel H, et al. Optical Constants of UV transparent EVA and the impact on the PV module output power under realistic irradiation. *Energy Procedia*. 2016;92:523-530.
50. Perez R, Seals R, Ineichen P, Stewart R, Menicucci D. A new simplified version of the perez diffuse irradiance model for tilted surfaces. *Solar Energy*. 1987;39(3):221-231.
51. Meteonorm, “Meteonorm - Features,” Meteotes, 2020. [Online]. Available: https://meteonorm.com/en/meteonorm-features. [Accessed 12 07 2020].
52. Gilman P, Dobos A, DiOrio N, Freeman J, Janzou S, Ryberg D. *SAM Photovoltaic Model Technical Reference Update*. National Renewable Energy Laboratory: Golden, CO.; 2018.
53. Aly Pamir S, Ahzi S, Barth N, Figgis B. Two dimensional finite difference-based modle for coupled irradiation and heat transfer in photovoltaic modules. *Sol Energy Mater Sol Cells*. 2018;(108):289-302.
54. Guyemard C., “Simple model of the atmospheric radiative transfer of sunshine, version 2 (SMARTS2): Algorithms description and performance assessment,” Florida Solar Energy Center, Report FSEC-PF-270-95, 1995.
55. Yu-Ichi Ohta TKTS. Color information for region segmentation. *Comput Graph Image Process*. 1980;13(3):222-241.
56. Balenzategui J, Chenlo F. Measurement and Analysis of angular response of bare and encapsulated silicon solar cells. *Sol Energy Mater Sol Cells*. 2005;86:53-83.
57. IEC, "IEC 61215–1:2016," IEC, Geneva, 2016.
58. Nyanor P, Kabu OE, Kudadze S, Deku A. 3D finite element method modelling and simulation of the temperature of crystalline photovoltaic module. *International Journal of Research in Engineering and Technology*. 2015;04(09):378-384.

59. Heusinge J, Broadbent A, Sailor D, Georgescu M. Introduction, evaluation and application of an energy balance model for photovoltaic modules. *Solar Energy*. 2020;195:382-395.
60. Armstrong S, Hurley WG. A thermal model for photovoltaic panel under varying atmospheric conditions. *Appl Therm Eng*. 2010;30:1448-1495.
61. Tan H, Psomadaki E, Isabella O, et al. Micro-textures for efficient light trapping and improved electrical performance in thin-film nanocrystalline silicon solar cells. *Appl Phys Lett*. 2013;103:173905-1-173905-5.
62. Yang G, Swaaij V, Rene ACMM, Tan H, Isabella O. Modulated surface textured glass as substrate for high efficiency microcrystalline silicon solar cells. *Sol Energy Mater Sol Cells*. 2015;133:156-162.
63. Yang G, Swaaij V, Rene ACMM, Isabella O, Zeman M. A novel way of texturing glass for microcrystalline silicon thin film solar cells application. *Progress in Photovoltaics*. 2015;23(10):1283-1290.
64. Loef T. *Periodic-Random Modulated Surface Textures for Efficient Light Trapping in Thin-Film Silicon Solar Cells*. Delft: Delft University of Technology; 2018.
65. Martin N, Ruiz JM. Calculation of the PV modules angular losses under field conditions by means of an analytical model. *Sol Energy Mater Sol Cells*. 2001;70(1):25-38.
66. Marion B. Numerical method for angle-of-incidence correction factors for diffuse radiation incident photovoltaic modules. *Solar Energy*. 2017;147:344-348.
67. SolarGIS, "SolarGIS Prospect," SolarGIS, 2020. [Online]. Available: https://apps.solargis.com/prospect/. [Accessed 6 1 2021].
68. Kaaya I, Koehl A, Mehilli P, de Cardona Mariano S, Weiss K. Modeling outdoor service lifetime prediction of PV modules: Effects of combined climatic stressors on PV module power degradation. *IEEE J Photovolt*. 2019;9(4):1105-1112.
69. HunterLab. *CIE Standard Observers and calculation of CIE X, Y and Z Color Values*. Reston, VA: HunterLab; 2012.
70. International Comission on Illumination, "CIE," CIE, 2013. [Online]. Available: http://www.cie.co.at/index.php/LEFTMENUE/index.php?i_ca_id=298. [Accessed 10 12 2013].
71. Image engineering, "Image Engineering," 2013. [Online]. Available: http://www.image-engineering.de/index.php?option=com_content&view=article&id=502. [Accessed 21 12 2013].
72. Hunt R, Pointer M. *Measuring Color*. Fourthed. Ltd: John Wiley & Sons; 2011.
73. Douglas A. *The CIE XYZ and xyY Color Spaces*. University of Standford; 2010.
74. Lindbloom B., "BruceLindbloom," 11 12 2011. [Online]. Available: http://www.brucelindbloom.com/index.html?Eqn_RGB_XYZ_Matrix.html. [Accessed 15 12 2013].
75. Sjerps-koomen E, Alsema E, Tukenburg W. A simple model for PV module reflection losses under field conditions. *Solar Energy*. 1996;57(6):421-432.
76. Knisely B, Janakeeraman S, Kuitche J, TamizhMani G. *Validation of Draft International Electrotechnical Commission 61853–2 Standard: Angle of incidence effect on photovoltaic modules*. Tempe: Solar American Board for Codes and Standards; 2013.
77. Duell M., Ebert M., Muller M., Li B., Koch M., Christian T., Perdichizzi R., Marion B., Kurtz S. and Doble D., "*Impact of Structured Glass on Light Transmission, Temperature and Power of PV Modules*," 2021.
78. Zhou Z, Jiang Y, Elkin-Daukes N, Keevers M, Green M. Optical and thermal emission benefits of differently textured glass for photovoltaic modules. *IEEE J Photovolt*. 2021;11:131-137.
79. Google maps, "Google maps," Google, 2021. [Online]. Available: https://tinyurl.com/2tbjmpdp

How to cite this article: Ortiz Lizcano JC, Procel P, Calcabrini A, et al. Colored optic filters on c-Si IBC solar cells for building integrated photovoltaic applications. *Prog Photovolt Res Appl*. 2021;1-35. doi:10.1002/pip.3504

APPENDIX A: MATERIALS, OPTICAL PROPERTIES, AND MANUFACTURING DETAILS

Color filter Option 1 was fabricated so that when used in a PV module it can be protected by the glass from environmental hazards. This means that during encapsulation, the filter/glass system must be rotated by 180° with respect to the fabrication position (see Figure A1). This increases the lifetime of the filter, avoiding unscheduled replacement due to scratches, or premature wear, which can produce substantial changes on the color perceived. For this reason, the material with the value of refractive index closer to that of glass (in this case n_L) is deposited as the outermost layer. Figure A2 presents the optical properties of the materials used onthis filter.

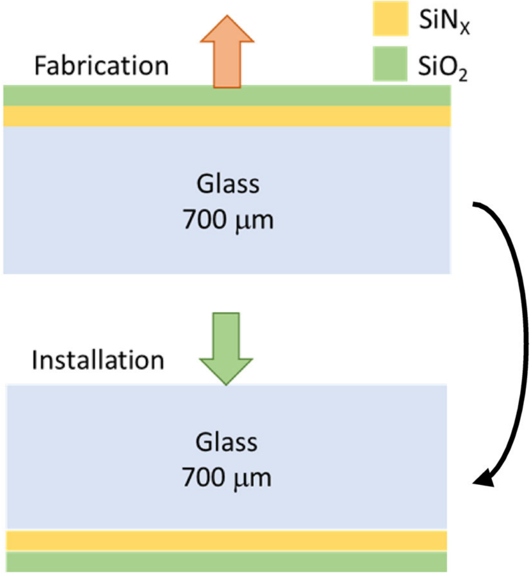

FIGURE A1 To avoid confusions in the sequence during fabrication the color tuning optic filter was designed to provide the same reflectance pattern once installed on a real device. By installing the filter as shown below, it is protected from environmental hazards [Colour figure can be viewed at wileyonlinelibrary.com]

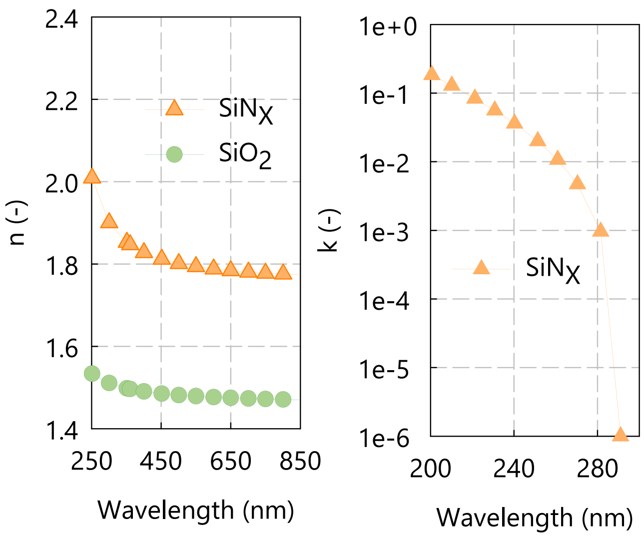

FIGURE A2 Wavelength-dependent real (n) and imaginary part (k) of the complex refractive indexes of SiN$_x$ and SiO$_2$ used in this work. Measurements were carried out with a Woollam ellipsometer; SiO$_2$ was found to be nonabsorbing ($k = 0$) in the full wavelength range of interest [Colour figure can be viewed at wileyonlinelibrary.com]

A.1 | Details on the deposition process for the colored filter Option 1—SiN$_X$ with $n = 1.73$

The substrate used for the fabrication of the color tuning OF was Corning Eagle XG glass. The necessary parameters to obtain an almost

TABLE A1 Manufacturing parameters for color filter Option 1 (SiN$_X$ with $n = 1.73$)

Parameter	SiO$_2$	SiN$_X$
Temperature (°C)	300	300
Gas 1 flow (sccm)	SiH$_4$ = 1	SiH$_4$ = 2.5
Gas 2 flow (sccm)	CO$_2$ = 55	NH$_3$ = 47.5
Pressure (mbar)	1.40	0.80
Plasma power (W)	20	4
CTune (–)	26	26
CLoad (–)	53	53
Deposition rate on glass (nm/s)	0.44	0.30

TABLE A2 Manufacturing parameters for color filter Option 2 (SiN$_X$ with $n = 2.10$)

Parameter	SiO$_2$	SiN$_X$
Temperature (°C)	300	300
Gas 1 flow (sccm)	SiH$_4$ = 8.5	SiH$_4$ = 20
Gas 2 flow (sccm)	N$_2$O = 710	NH$_3$ = 20
Pressure (mbar)	1000	650
Plasma power (W)	20	20
Deposition rate on glass (nm/s)	1.20	0.21

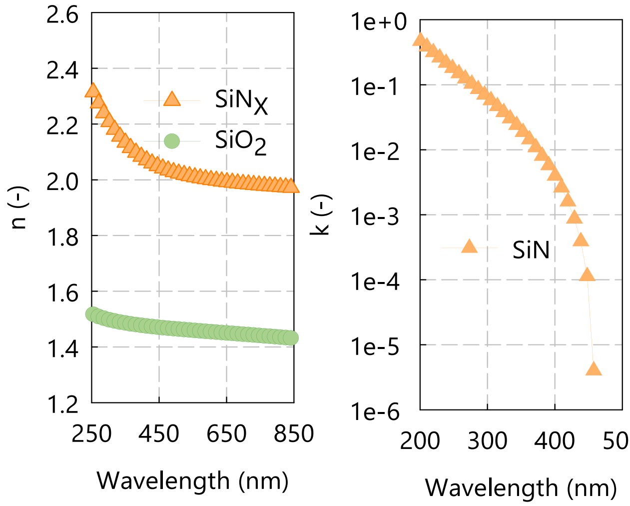

FIGURE A3 Refractive index and extinction coefficients of the materials selected for the **Option 2** filter [Colour figure can be viewed at wileyonlinelibrary.com] stoichiometric SiO_2 layer on glass and the recipe for the growth of Si_3N_4 were developed at the PVMD staff. These parameters are summarized in Table A1 below.

To ensure the same temperature between the substrate and the chamber, the glass substrate was kept for 1 h with the process gasses flowing through the chamber but without ignition of the plasma.

A.2 | Details on deposition process and optical characterization of color filter Option 2—SiN_X with $n = 2.10$

Like Option 1, the substrate used for fabrication and characterization was Corning Eagle XG glass. The parameters of the manufacturing process are shown below in Table A2.

The optical properties of the materials composing filter Option 2 are shown in Figure A3.

APPENDIX B: ADDITIONAL INFORMATION REGARDING MODELING FRAMEWORK

The complete modeling flow chart used to estimate the energy yield in this work can be found in Figure B1

B.1 | Complete modeling flow chart

B.2 | Color perception model theory

The CIE model uses a *standard observer* that is represented by three mathematical functions called *color matching functions*.[69] These functions, denoted by *x*, *y*, and *z*, are wavelength dependent. Functions $x(\lambda)$ and $z(\lambda)$ represent an approximation of the spectral response of the cones of the human eye to light, while $y(\lambda)$ models human perception of luminosity. Once each of their values is normalized with respect to $y(\lambda)_{max}$ – $\bar{x}(\lambda)$, $\bar{y}(\lambda)$, and $\bar{z}(\lambda)$, they become scaling factors called *tri-stimulus values*[69] and can be seen as mathematical constructs that depict a unique hue.[33] The CIE model also provides several theoretical light sources called *illuminants*. Each illuminant represents the spectral power distributions of a certain illumination source such as daylight, fluorescence, and incandescent lamps. They are categorized in letters and can be found elsewhere.[70] The selected illuminant for this work is called D65. This source emulates natural daylight conditions at noon, and is the standard source used in simulations to render colors on a computer's monitor.[71,72]

From the spectral power distribution of the source $S(\lambda)$, the reflectance profile of the surface $R(\lambda)$, and the color matching functions $\bar{x}(\lambda)$, $\bar{y}(\lambda)$, and $\bar{z}(\lambda)$, it is possible to calculate the following three coordinates:

$$X = \frac{1}{N}\int_{380}^{780} \bar{x}(\lambda) \times R(\lambda) \times S(\lambda) d\lambda \tag{B1}$$

$$Y = \frac{1}{N}\int_{380}^{780} \bar{y}(\lambda) \times R(\lambda) \times S(\lambda) d\lambda \tag{B2}$$

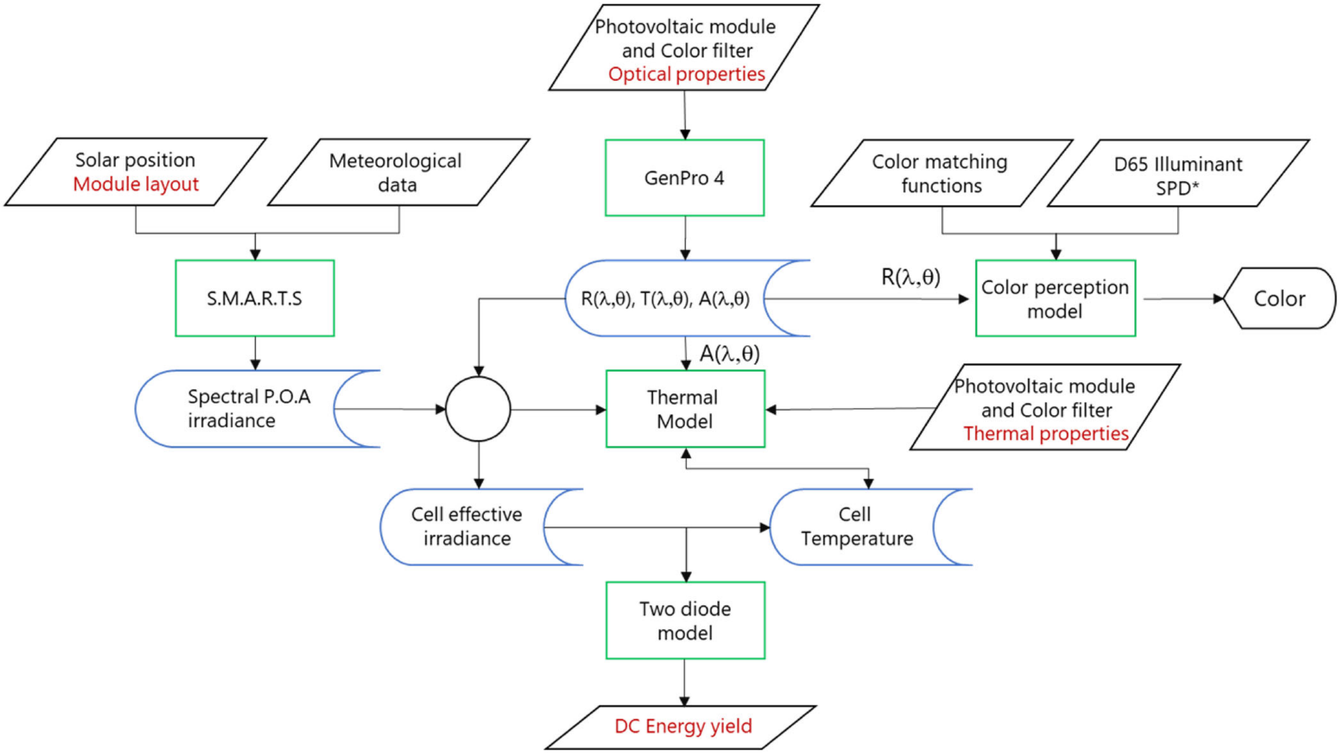

FIGURE B1 Flow chart of the modeling framework used in this research. *Denotes a selected illuminant for color perception, which can be selected by the user. D65 is the most used illuminant for color representation on standard displays. Note that the thermal model and the two-diode model have an iterative step, given their interdependency [Colour figure can be viewed at wileyonlinelibrary.com]

$$Z = \frac{1}{N}\int_{380}^{780} \bar{z}(\lambda) \times R(\lambda) \times S(\lambda) d\lambda \tag{B3}$$

where

$$N = \int_{380}^{780} \bar{y}(\lambda) \times S(\lambda) d\lambda \tag{B4}$$

Since the obtained *X*, *Y*, and *Z* values are based on models of human perception of light, they are used to produce a three-dimensional space in which every color a human perceives can be represented.[73] This space is called the *CIE XYZ* color space. To transform the *X*, *Y*, and *Z* coordinates into color coordinates used by computer monitors, a transformation matrix is needed. The values of this matrix depend on the illuminant used as reference and the color space coordinates we want to find (e.g., sRGB and AdobeRGB). These matrices can be found in Lindbloom.[74] For the D65 illuminant and sRGB color space (the one chosen for this project), the transformation matrix is as follows:

$$\begin{bmatrix} R \\ G \\ B \end{bmatrix} = \begin{bmatrix} 3.2406 & -1.5372 & -0.4986 \\ -0.9689 & 1.8758 & 0.0415 \\ 0.0557 & -0.2040 & 1.5070 \end{bmatrix} \begin{bmatrix} X \\ Y \\ Z \end{bmatrix} \tag{B5}$$

Since these *R*, *G*, and *B* values are linear, so-called *gamma correction* must be performed to increase the accuracy of color rendering. This is achieved by replacing each color coordinate into an equation of the following form:

$$R_{sRGB} = \begin{cases} 12.92R \quad if\, R \leq 0.0031308 \\ or \\ (1.005)R^{\frac{1}{2.4}} - 0.005\, if\, R > 0.0031308 \end{cases} \tag{B7}$$

Equation (B7) shows the gamma correction for the *R* coordinate; this same procedure must be performed for the *G* and *B* coordinates. With this, the color rendering on a screen that uses sRGB becomes accurate.

B.3 | Geometry of the selected solar cell

The geometry selected for the modeling of a full solar cell via the two-diode model is based on the Maxeon Generation III IBC solar cell. The geometry sketch, taken from Maxeon own datasheet,[46] is shown in Figure B2.

B.4 | Thermal model

For each different node (numbered 1 to 12 below), an energy balance is computed by using linearized equations. All the equations are then properly group into the matrix form:

$$[A]\{C\} = \{T\} \tag{B8}$$

where [*A*] is the matrix fill with the temperature dependent variables of the heat transfer mechanisms on each node at the time instant analyzed, {*C*} is the vector of the temperature independent constants, and {*T*} is the vector of the know temperatures, belonging to the previous time step. Equation (B8) can be solved via Gauss–Seidel method. The equation for each node is shown in the table below. The equation for each node is presented on Table B1

For a better understanding of the equations shown above, the schematic of each node is presented in Figure B3.

B.5 | Estimation of heat generation in the solar cells

The main mechanisms of heat generation within the solar cells are four: thermalization, absorption of photons with energy lower than the gap, recombination, and resistive losses. It is assumed that absorbed photons with energies higher than the bandgap ($E_{gap} = \frac{h \cdot c}{\lambda_{gap}}$) generate an electron–hole pair; hence, parasitic

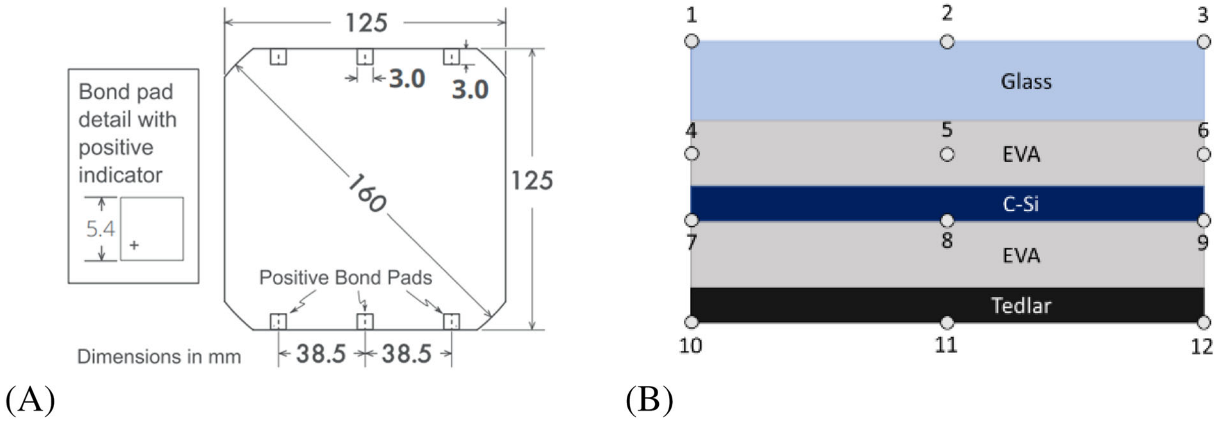

FIGURE B2 (A) Selected **area** value from a commercial IBC solar cell produced by SunPower.[46] The remaining values used for the electrical simulation are based on the JV characteristics of the cell produce on our group. (B) Sketch of the encapsulated cell used for performance calculations [Colour figure can be viewed at wileyonlinelibrary.com]

TABLE B1 Equations for each of the 12 different nodes used on the thermal model of the PV module

Node	Equation
1.	$\frac{Q_{gen}\Delta_t}{\rho C_p}+T^p_{m,n}+2Bi_cFo_yT_a+2Bi_RFo_yT_s=T^{p+1}_{m,n}(1+2Fo_y+2Fo_x+2Bi_cFo_y+2Bi_RFo_y)-2Fo_yT^{p+1}_{m,n+1}-2Fo_xT^{p+1}_{m+1,n}$
2.	$\frac{Q_{gen}\Delta_t}{\rho C_p}+T^p_{m,n}+2Bi_cFo_yT_a+2Bi_RFo_yT_s=T^{p+1}_{m,n}(1+2Fo_y+2Fo_x+2Bi_cFo_y+2Bi_RFo_y)-2Fo_yT^{p+1}_{m,n+1}-Fo_xT^{p+1}_{m+1,n}-Fo_xT^{p+1}_{m-1,n}$
3.	$\frac{Q_{gen}\Delta_t}{\rho C_p}+T^p_{m,n}+2Bi_cFo_yT_a+2Bi_RFo_yT_s=T^{p+1}_{m,n}(1+2Fo_y+2Fo_x+2Bi_cFo_y+2Bi_RFo_y)-2Fo_yT^{p+1}_{m,n+1}-2Fo_xT^{p+1}_{m-1,n}$
4.	$\frac{Q_{gen}\Delta_t}{\rho C_p}+T^p_{m,n}=T^{p+1}_{m,n}(1+2Fo_y+2Fo_x)-Fo_yT^{p+1}_{m,n+1}-Fo_yT^{p+1}_{m,n-1}-2Fo_xT^{p+1}_{m+1,n}$
5.	$\frac{Q_{gen}\Delta_t}{\rho C_p}+T^p_{m,n}=T^{p+1}_{m,n}(1+2Fo_y+2Fo_x)-Fo_yT^{p+1}_{m,n+1}-Fo_yT^{p+1}_{m,n-1}-Fo_xT^{p+1}_{m+1,n}-Fo_xT^{p+1}_{m-1,n}$
6.	$\frac{Q_{gen}\Delta_t}{\rho C_p}+T^p_{m,n}=T^{p+1}_{m,n}(1+2Fo_y+2Fo_x)-Fo_yT^{p+1}_{m,n+1}-Fo_yT^{p+1}_{m,n-1}-2Fo_xT^{p+1}_{m-1,n}$
7.	$Q_1+Q_2+T^p_{m,n}=T^{p+1}_{m,n}(1+R_1+R_2+R_3+R_4)-R_1T^{p+1}_{m,n-1}-R_2T^{p+1}_{m,n+1}-(R_3+R_4)T^{p+1}_{m+1,n}$
8.	$Q_1+Q_2+T^p_{m,n}=T^{p+1}_{m,n}(1+R_1+R_2+2R_3)-R_1T^{p+1}_{m,n-1}-R_2T^{p+1}_{m,n+1}-R_3T^{p+1}_{m+1,n}-R_3T^{p+1}_{m-1,n}$
9.	$Q_1+Q_2+T^p_{m,n}=T^{p+1}_{m,n}(1+R_1+R_2+R_3+R_4)-R_1T^{p+1}_{m,n-1}-R_2T^{p+1}_{m,n+1}-(R_3+R_4)T^{p+1}_{m-1,n}$
10.	$\frac{Q_{gen}\Delta_t}{\rho C_p}+T^p_{m,n}+2Bi_cFo_yT_a+2Bi_RFo_yT_s=T^{p+1}_{m,n}(1+2Fo_y+2Fo_x+2Bi_cFo_y+2Bi_RFo_y)-2Fo_yT^{p+1}_{m,n-1}-2Fo_xT^{p+1}_{m+1,n}$
11.	$\frac{Q_{gen}\Delta_t}{\rho C_p}+T^p_{m,n}+2Bi_cFo_yT_a+2Bi_RFo_yT_s=T^{p+1}_{m,n}(1+2Fo_y+2Fo_x+2Bi_cFo_y+2Bi_RFo_y)-2Fo_yT^{p+1}_{m,n-1}-2Fo_xT^{p+1}_{m+1,n}$
12.	$\frac{Q_{gen}\Delta_t}{\rho C_p}+T^p_{m,n}+2Bi_cFo_yT_a+2Bi_RFo_yT_s=T^{p+1}_{m,n}(1+2Fo_y+2Fo_x+2Bi_cFo_y+2Bi_RFo_y)-2Fo_yT^{p+1}_{m,n-1}-2Fo_xT^{p+1}_{m-1,n}3$

Note: For more information regarding these equations, please consult the work of Aly et al.[53]
Abbreviation: PV, photovoltaic.

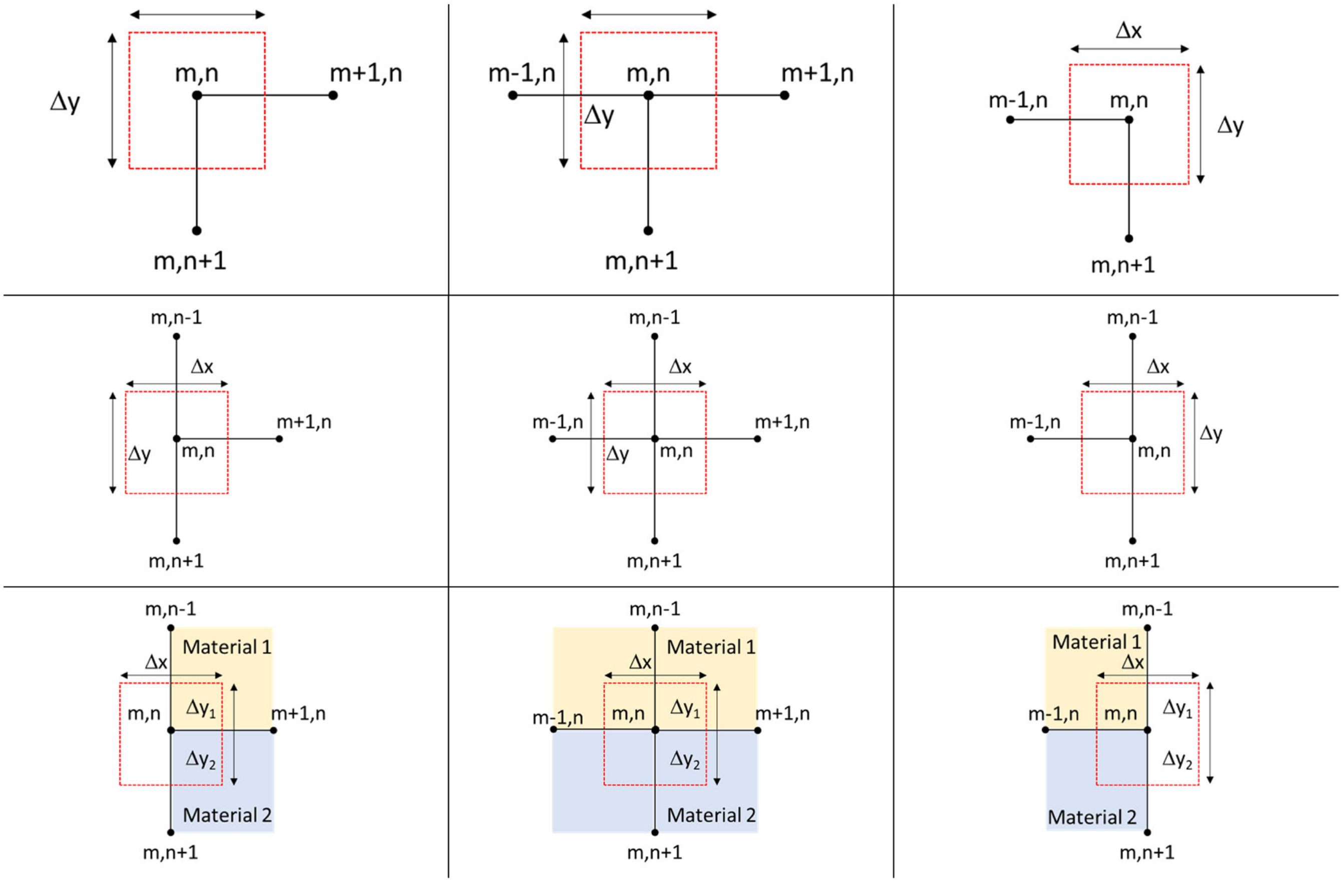

FIGURE B3 Details on the node distribution of the thermal model. Notice that on the equations above, each equation relates to a previous node either on the vertical or the horizontal axis. Full information about the meaning of all the variables presented here is available at[53] [Colour figure can be viewed at wileyonlinelibrary.com]

absorption of photons with $E \geq E_{gap}$ within the bulk is neglected. Also, radiative recombination processes are neglected since we are considering c-Si solar cells.

$P_{abs}(\lambda)$ is defined as the total spectral power density absorbed in the bulk of the solar cell (made of c-Si). Notice that $P_{abs}(\lambda)$ for $\lambda > \lambda_{gap}$ is not necessarily zero.

TABLE B2 Physical and thermal properties of each layer of the encapsulated cell

Layer	Thickness—*t* (m)	Thermal conductivity—*k* (W/m K)	Density—ρ (kg/m3)	Specific heat capacity—Cp (J/kg K)
Glass	3.2×10^{-3}	1.8	3,000	500
EVA (× 2)	580×10^{-6}	0.35	960	2090
PV cell	210×10^{-6}	148	2330	677
Back sheet	100×10^{-6}	0.2	1200	1250

Note: The physical properties are obtained from the materials used to build the module that was measured for validation (see next section). The thermal properties were obtained from.[53]

Abbreviation: PV, photovoltaic.

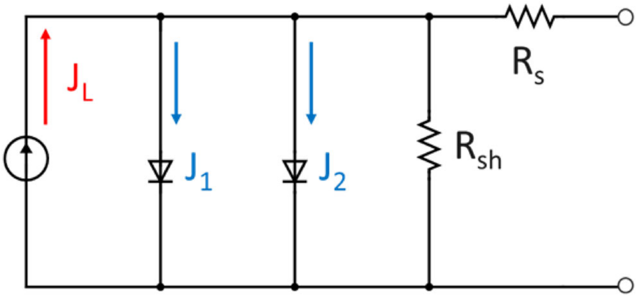

FIGURE B4 Sketch of the two-diode model used on this work [Colour figure can be viewed at wileyonlinelibrary.com]

TABLE B3 Parameters used of the two-diode model with an assumed cell temperature of 298.15 K

Parameter			Value
Light collected current	(J_L)	(mA/cm^2)	39.443
Saturation current 1	(J_1)	(pA/cm^2)	83.650
Ideality factor 1	(m_1)	(–)	1.347
Saturation current 2	(J_2)	(nA/cm^2)	0.453
Ideality factor 2	(m_2)	(–)	2
Shunt resistance	(R_{SH})	(kΩ cm^2)	23.570
Series resistance	(R_S)	(Ω cm^2)	0.424

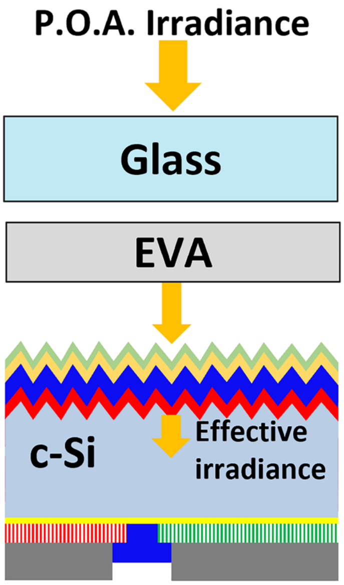

FIGURE B5 The calculation of the effective irradiance used in the two-diode model considers the losses produced by reflectance and absorptance of the different layers placed above the bulk of the c-Si solar cell. These losses are translated into a transmittance factor τ_O [Colour figure can be viewed at wileyonlinelibrary.com]

$\Phi_{abs}(\lambda) = P_{abs}(\lambda)\frac{\lambda}{h \cdot c}$ represents the spectral photon flux absorbed in the bulk.

$P_{rel}(\lambda) = \begin{cases} \Phi_{abs}(\lambda)\dfrac{h \cdot c}{\lambda_{gap}}, \text{ if } \lambda \le \lambda_{gap} \\ 0, \text{ if } \lambda > \lambda_{gap} \end{cases}$ is the spectral power density of the absorbed photons after thermalization, that is, after relaxing to E_{gap}. The heat due to thermalization and absorption beyond λ_{gap} is as follows:

$$P_1 = \int_0^{\infty} \left(P_{abs}(\lambda) - P_{rel}(\lambda)\right) \mathrm{d}\lambda.$$

The heat due to recombination and resistive losses can be calculated knowing the electrical power generated by the solar cell P_e:

$$P_2 = \int_0^{\infty} P_{abs}(\lambda)\, \mathrm{d}\lambda - P_1 - P_e.$$

At the specific irradiance and temperature conditions, P_e can be approximated in different ways; for this work, we considered that the FF of the cell was independent of the temperature. This makes the estimation of the power produced by the cell straightforward.

Lastly, we estimate the total heat generation in the solar cell as follows: $P_1 + P_2$

The physical and thermal properties of each layer of the encapsulated cell used on this work are summarized in Table B2.

B.6 | Electrical model details

The effective irradiance used in the two-diode model (Figure B4) is estimated by considering all the optical losses produced by the glass, the EVA, the color filter, and the antireflective coating used on the solar cell (Figure B5).

The J-V curve from the selected solar architecture discussed on Section 3.1 was used to extract the parameters necessary to model it by means of a two-diode model. Table B3 showcases the results.

APPENDIX C: ADDITIONAL INFORMATION REGARDING SIMULATION AND VALIDATION

C.1 | Trends for short circuit current density and efficiency of colored cells (unencapsulated cells)

The J-V curves obtained from Sentaurus for both the standard device and the colored devices are shown below (see Figure C1 for the case of a standard cell, and Figure C2 and Figure C3, for a green and a brown cell, respectively). Additionally, the trend of the angle of incidence modifying factors j_{SC} for each case is shown in Figure C4.

Additionally, TCAD Sentaurus simulations were carried for all the possible thickness combinations of filter **Option 1** SiO_2/SiN_X ($n = 1.73$) to found overall trends. In the figures below, the main effect on the efficiency (Figure C5(B) lies on the reduction of the short circuit current density due to the reflectance produced by the filter (Figure C5(A). The effects produced by the filter on the FF and open circuit voltage of the cell, for all color combinations, are negligible.

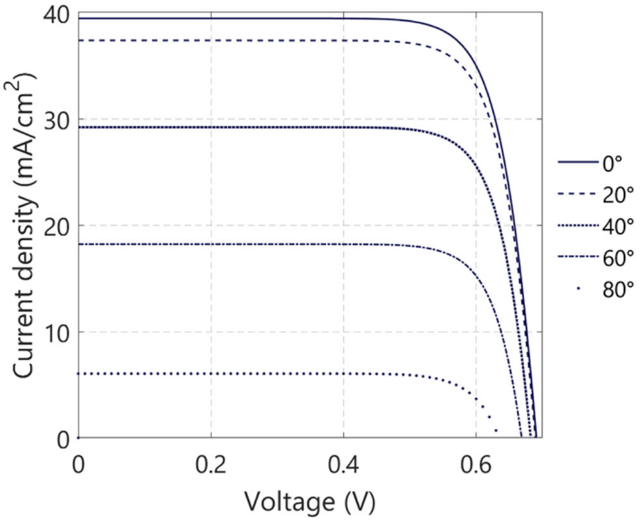

FIGURE C1 J-V curves obtained from Sentaurus simulations for a nonencapsulated standard solar cell for different angles of incidence [Colour figure can be viewed at wileyonlinelibrary.com]

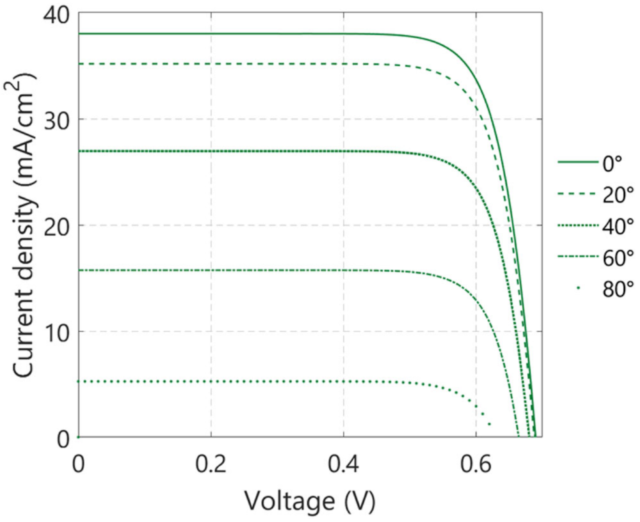

FIGURE C2 J-V curves obtained from Sentaurus simulations for a nonencapsulated green colored solar cell for different angles of incidence [Colour figure can be viewed at wileyonlinelibrary.com]

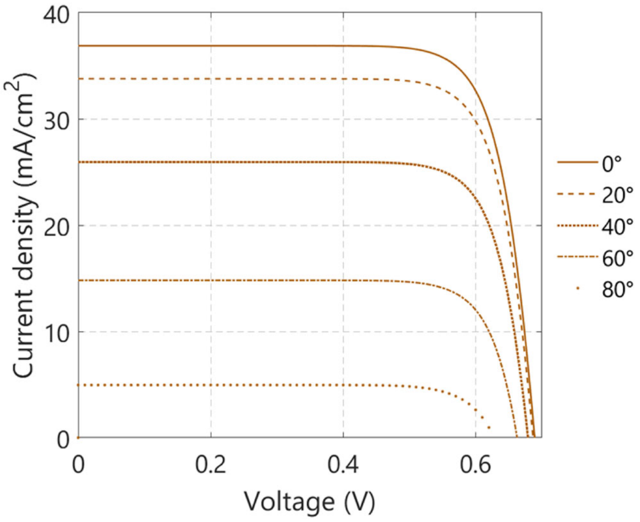

FIGURE C3 J-V curves obtained from Sentaurus simulations for a nonencapsulated brown colored solar cell for different angles of incidence [Colour figure can be viewed at wileyonlinelibrary.com]

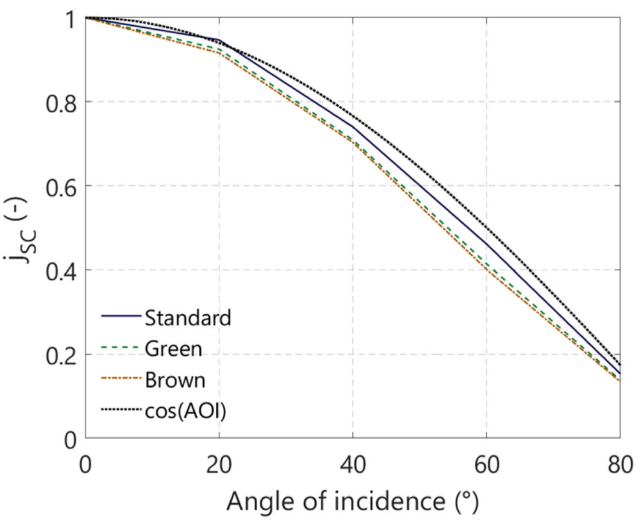

FIGURE C4 Trends of the j_{SC} factor for a standard, a green and a brown colored solar cell compared with the cosine relationship established by[56] [Colour figure can be viewed at wileyonlinelibrary.com]

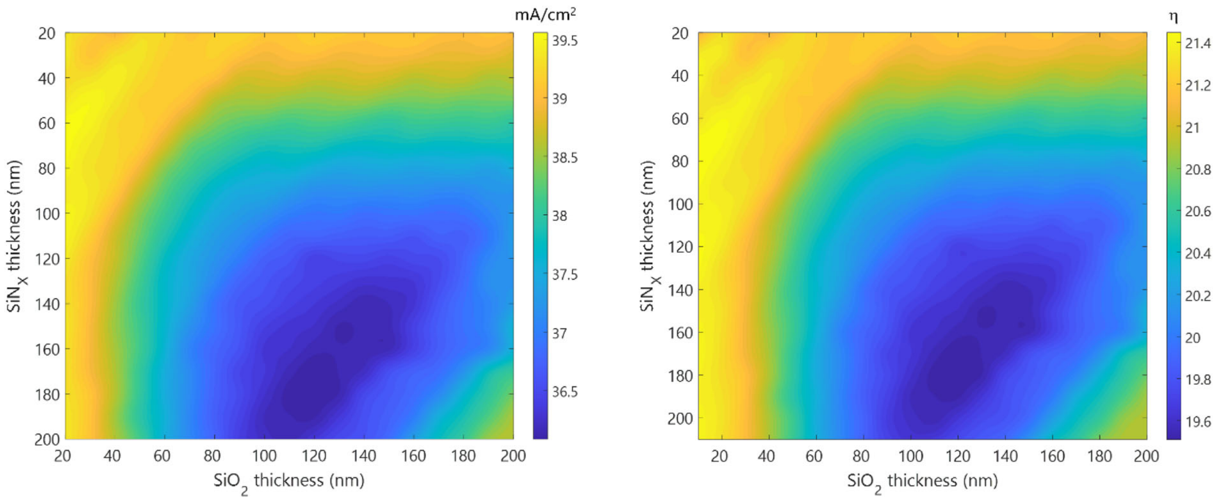

(A)

(B)

FIGURE C5 Effect of the color filter on the short circuit current density (left) and the efficiency (right) of an interdigitated back-contacted (IBC) solar cell. The loss in efficiency is driven by the additional reflectance produced by the filter, which translated in lower current generation [Colour figure can be viewed at wileyonlinelibrary.com]

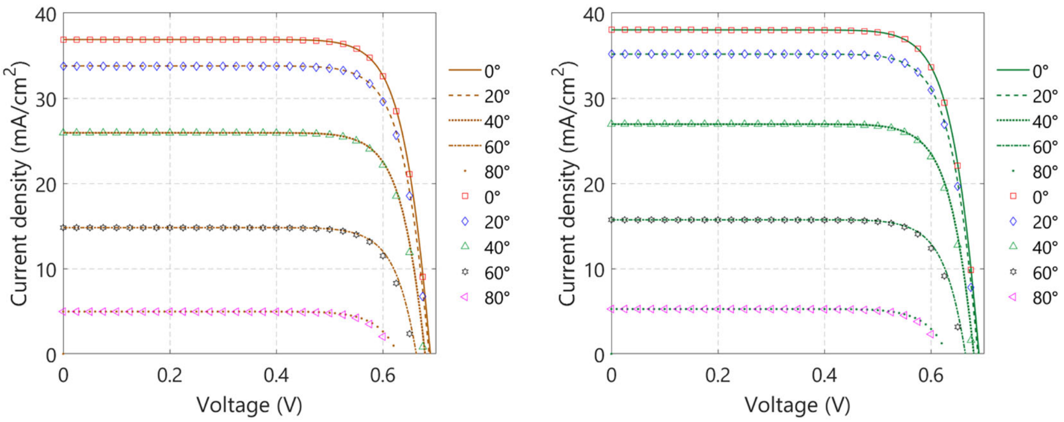

(A)

(B)

FIGURE C6 Comparison between the J-V curves of a brown (A) and a green (B) interdigitated back-contacted (IBC) solar cell obtained by Sentaurus simulation (lines) and those obtained by the two-diode model (markers) [Colour figure can be viewed at wileyonlinelibrary.com]

C.2 | Validation of the use of two-diode model for colored cells

Following the approach shown in Figure 9, we present the results for the colored cells. Figure C6(A) presents the comparison of the J-V curves produced by the two diode with respect to TCAD Sentaurus for the case of a brow cell, whereas Figure C6(B) shows this same comparison for the case of a green colored cell. The effect produced by a color filter on the performance of a solar cell can be easily modeled by scaling the POA irradiance of a standard device with color-specific factors obtained with the optical model.

We extracted the photogenerated current J_{ph} obtained with GenPro4 and calculated the angular modifying factors j_{ph} and compared them with those obtained with Sentaurus (j_{SC}). Figure C7 shows this comparison. The modeling framework, therefore, only requires the optical model to calculate the factors that will scale the effective irradiance reaching the cell and the value of operative temperature calculated via the spectral thermal model.

C.3 | Validation of the angular factor approach for encapsulated devices

Figure C8A shows that the trend of the value of j_{SC} obtained with GenPro4 closely follows those from literature for a standard module. Similar findings were observed by Sjerps-koomen et al..[75] Also, Knisely et al.[76] found that even for modules with different photovoltaic technologies, the relative optical response factor for different AOI was remarkably equal on those using flat glass as a front layer. Figure C8B shows the value of j_{SC} also for the green and brown modules. The effect of the OF is noticeable for angles of incidence ranging

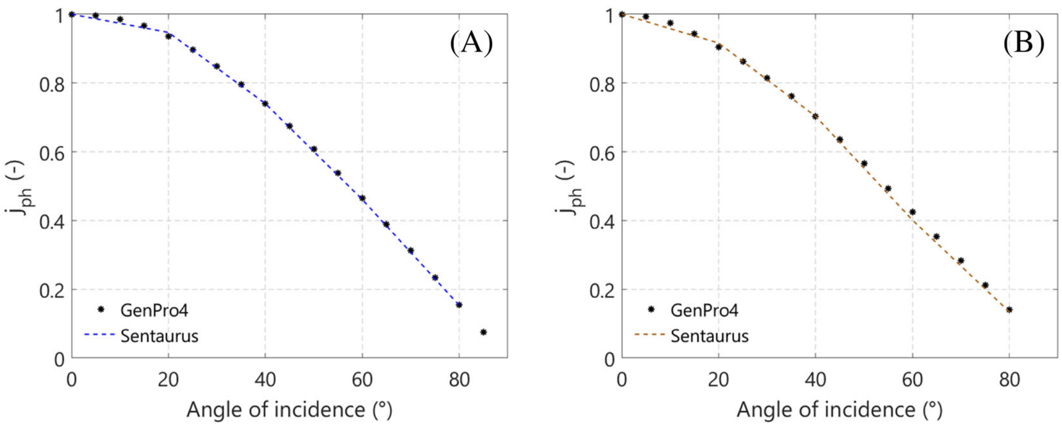

FIGURE C7 Comparison between the angular factor j_{ph}. obtained from GP4 simulations to those obtained with Sentaurus (j_{SC}) for (A) a standard solar cell and (B) a brown colored solar cell [Colour figure can be viewed at wileyonlinelibrary.com]

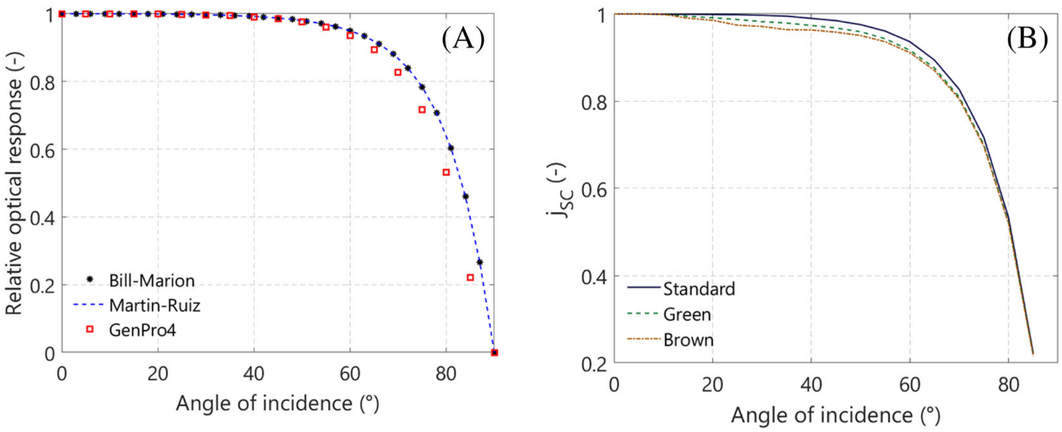

FIGURE C8 (A) Comparison of the relative optical response (a concept similar to j_{SC} used in this work) between the computational model produced in this work and the Martin-Ruiz and Bill-Marion models to account for the effect of different angles of incidence (AOI) on the performance of a standard dark blue module. (B) Change in the j_{SC} factor for 153 cm^2 wide, encapsulated standard and colored solar cells [Colour figure can be viewed at wileyonlinelibrary.com]

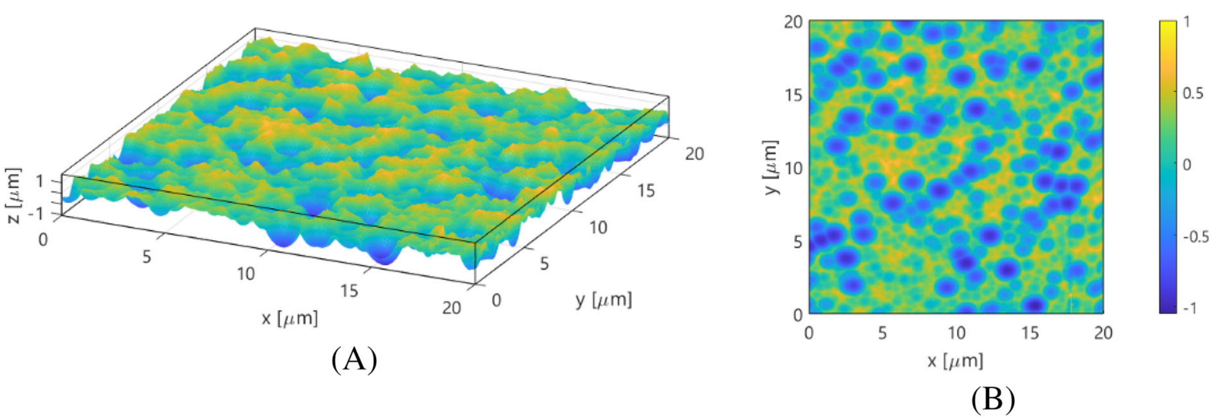

FIGURE C9 Modeled surface morphology for the randomly textured glass substrate. (A) Orthogonal projection of the 3D model, which was built based on the scan obtained by AFM. (B) Crater depths and peaks heights of the textured surface. The average crater depth on the sample was found to be of 0.7 μm. For more information, please refer to[61–64] [Colour figure can be viewed at wileyonlinelibrary.com]

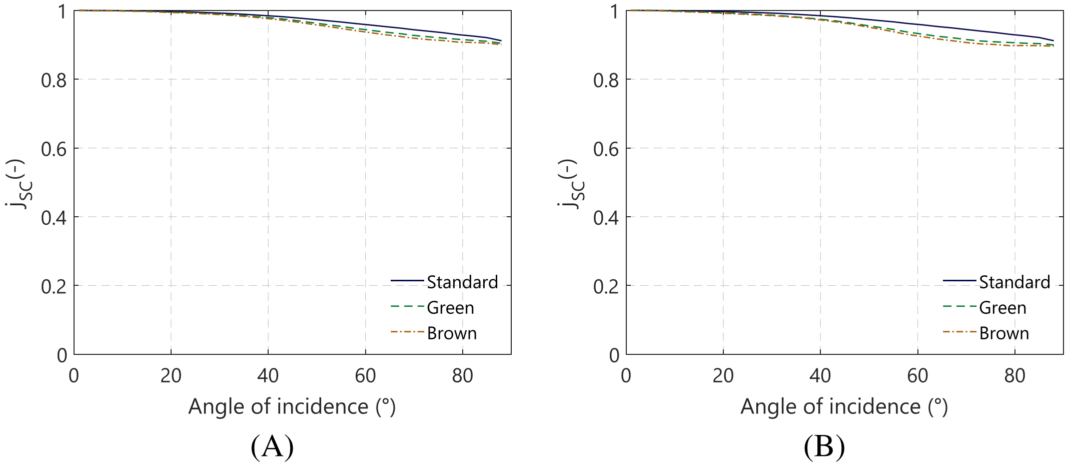

FIGURE C10 Value of the angle of incidence modifier (j_{SC}) for an encapsulated colored and standard cell with textured glass: (A) for an encapsulated colored cell using filter option 1; (B) for an encapsulated colored cell using filter Option 2. Improving saturation and color brightness increases the angular losses produced by the filter, as shown by the lower value of j_{SC} produced by the filter Option 2 [Colour figure can be viewed at wileyonlinelibrary.com]

FIGURE C11 Photograph of the set up used for the validation of the thermal model. The arrows indicate the module measured (left) and the location of the thermocouples (right) [Colour figure can be viewed at wileyonlinelibrary.com]

from 20° to 60°. At values higher than 60°, the reflectance produced by the air/glass interface dominates and the difference between the standard and the colored modules practically disappears. On a textured glass, the value of j_{SC} is different than for the case of a flat glass. The results for this case are shown in the following section.

C.4 | Front glass texture

As discussed in Section 5.4, to increase color saturation and brightness, we considered that the front glass of the module had random micro-texturing. The morphology considered is presented on Figure C9.

Color perception and angular behavior are dependent on the nature of the texturing of the front glass. Additionally, the texturing considered here does not necessarily correspond to the texturing found on commercially available glasses used on PV modules. As these textures themselves usually vary for different manufacturers, we consider that an in-depth analysis of their effects merits a detailed discussion that goes beyond the scope of this work. However, their implementation on the current framework is of relative simplicity.

C.5 | Angle of incidence modifiers with a textured surface

To increase color saturation and brightness, the addition of a textured glass surface also has a significant impact on the value of the irradiance scaling factor j_{SC} for angles of incidences greater than the normal. Furthermore, each of the options of color filter presented in this work has a unique reflectance impact. We calculated the value of j_{SC}

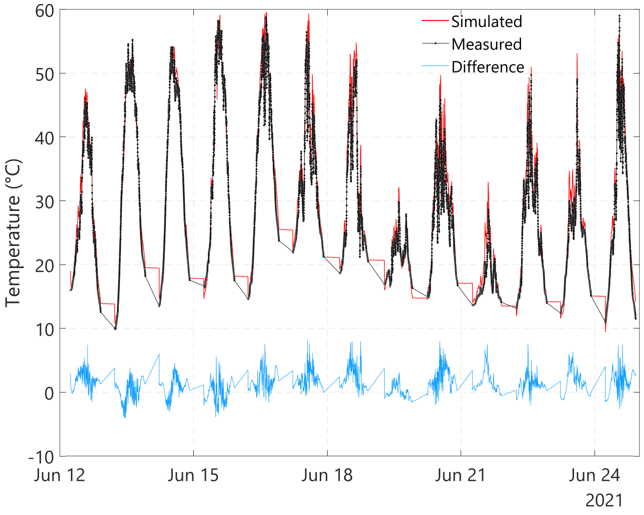

FIGURE C12 Simulated versus measured operational temperature of a 250 W_p c-Si module. The thermal model was calculated for a raw data resolution of 1 min and compared with the average value of the four thermocouples installed on the module. The model can mimic the behavior of the model even for such low time resolution [Colour figure can be viewed at wileyonlinelibrary.com]

for each filter option and for each combination of material thickness of the filter. In the figures below we show how texturing the surface of the front glass improves the angular performance of both the standard and the colored filter. The results shown on Figure C10 are consistent with the findings of Duell et al[77] and Zhou et al.[78]

C.6 | Measurement set up used for the validation of thermal model

The setup used for the temperature measurements was made up of six mini modules—each equipped with 16 Al-BSF Cells (4 × 4)—connected in series to achieve a peak power of 250 Wp (See Figure C11(A)). This cell technology was chosen due to technical availability to reach a high value of peak power in the module. The mounting of the set up closely represents a BIPV condition, with very low convection on the backside and negligible effects of the wind on the sides (See Figure C11(B)). The measurement station, located at the roof of a selected building within the Delft University of Technology campus,[79] is fully equipped with all the necessary sensors to measure irradiance components, wind speed, ambient temperature, and plane of array irradiance. The time resolution used to obtain the data was of 1 min. T-type thermocouples were attached to the back of the module (see arrows in Figure C11(B)) and connected to a PicoLog TC-08 data logger. Averaged values of temperature were taken every minute and used for validation of the model presented in this work.

The comparison between the temperature values obtained by the thermal model and those measured directly on the module is shown in Figure C12. For simplicity of viewing, all the data for a measured irradiance below 10 W/m^2 were omitted; hence, the simulated temperature value at the end of the day was used as the first iteration value for the following day (notice the straight lines). Table C1 shows the calculated daily MBE and RMSE values for the prediction of operational temperature.

TABLE C1 Daily MBE and RMSE for the minutely resolution data

Day	MBE (°C)	RMSE (°C)
June 12	−1.11	1.49
June 13	0.58	2.00
June 14	−0.25	1.74
June 15	0.58	1.64
June 16	−0.96	1.83
June 17	−1.56	2.10
June 18	−1.82	2.50
June 19	0.30	0.91
June 20	−1.67	2.44
June 21	−1.36	1.96
June 22	−0.78	1.51
June 23	−0.93	1.89
June 24	−0.95	1.93

Abbreviations: MBE, mean bias error; RMSE, root-mean-square error.

C.7 | Effect of viewing angle on color perception

The effect of how the perceived color of the device change for different AOI is depicted in Figure C13 for the abovementioned dark green and brown solar cells, respectively. The change in color appearance of these colored cells with respect to the AOI is much smaller than the case of color tuning OF deposited on glass. It is found that only for incident angles larger than 50° the OFs will exhibit a noticeable change in the color perception (= change in both hue and saturation of the color). As the angle of incidence of light increases, the photocurrent of the cell decreases due to the shift and growth of the Δ_g. Besides, it is worth mentioning that the EQE spectra exhibit larger broadband oscillations as the AOI increases, despite the color tuning OF coating a textured interface. These effects are considerable and are in accord with the trend previously shown in Figure 2B in case of nonflat color tuning OF.

For the case of an encapsulated cell with front textured glass, the effect of the viewing angle on color perception is shown in Figure C14.

C.8 | Saturation matrices for textured glass surfaces for filters Option 1 and Option 2

As discussed in Section 5.4, we estimated the color saturation of both filter options after encapsulation and selected those that presented a saturation value of 0.5 (in the HSV color space). Figure C15 presents the results obtained for filter **Option 1**. Figure C16 presents these results for filter **Option 2**.

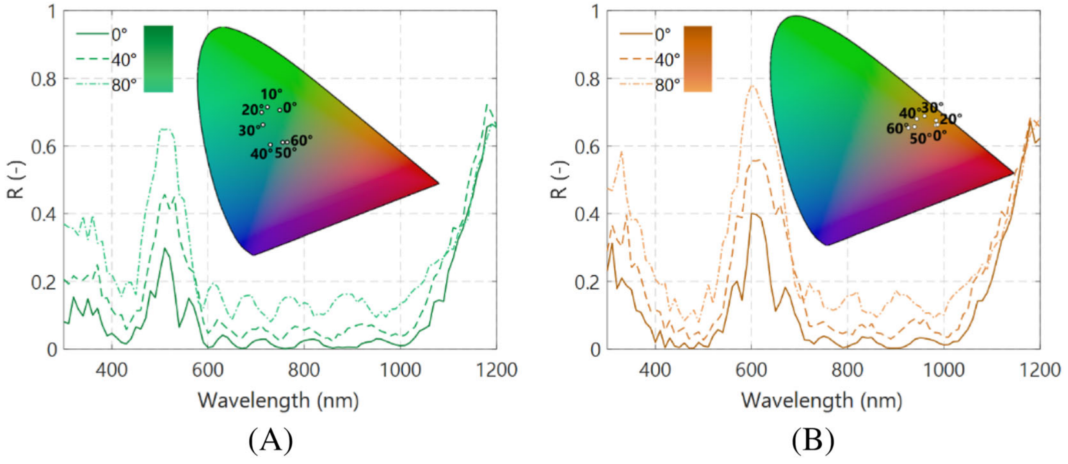

FIGURE C13 Reflectance spectra of front textured nonencapsulated (A) dark green and (B) brown solar cells for three different angles of incidence of light. In the insets, the color perception from a viewer's incident angle of the colored cells is shown: (left) the hue-bound color change (next to the legend) and (B) the same color change represented on the CIE 1931 chromaticity diagram[73] [Colour figure can be viewed at wileyonlinelibrary.com]

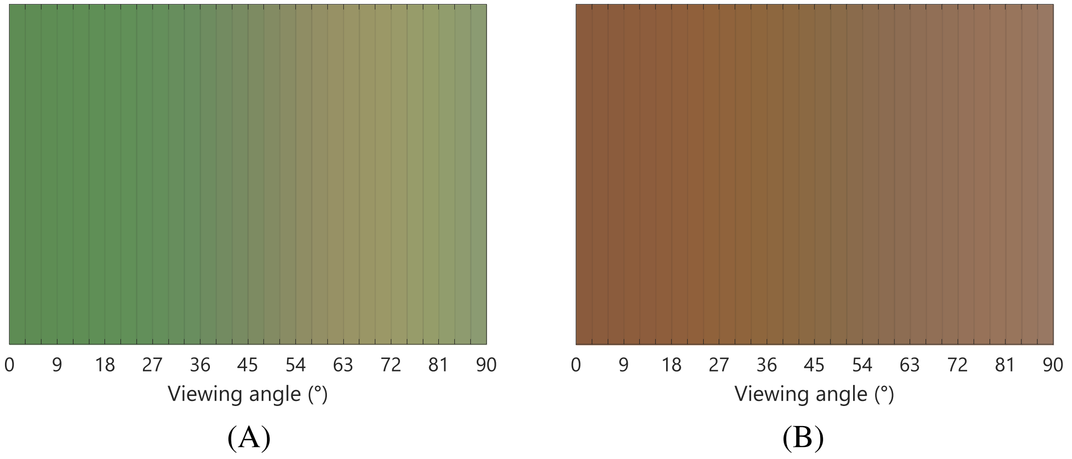

FIGURE C14 Effect of the viewing angle of an encapsulated colored solar cell. For this case, filter Option 2 was studied for the case of the textured glass. On the left, for the case of a green ($SiO_2 = 110$ nm and $SiN_X = 80$ nm) encapsulated cell, and on the right, for the case of a brown encapsulated cell ($SiO_2 = 130$ nm and $SiN_X = 110$ nm) [Colour figure can be viewed at wileyonlinelibrary.com]

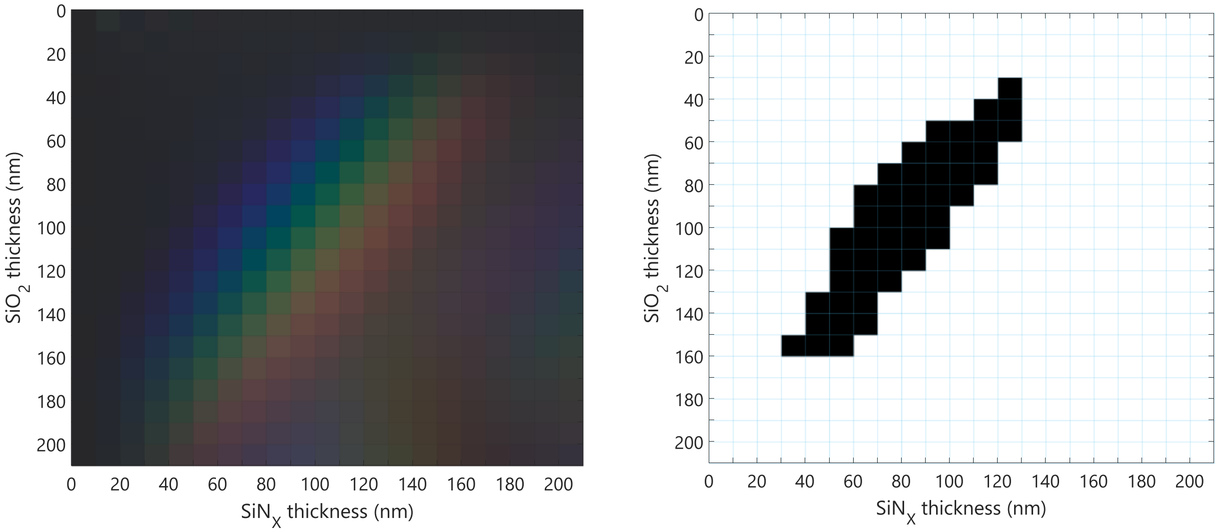

FIGURE C15 (A) Effect of encapsulating colored solar cells with a **textured front glass**. The overall effect is that of low saturation and low brightness. (B) Encapsulated colored cell that still achieves a saturation value higher than 0.5 in the Hue Saturation Value (HSV) color space [Colour figure can be viewed at wileyonlinelibrary.com]

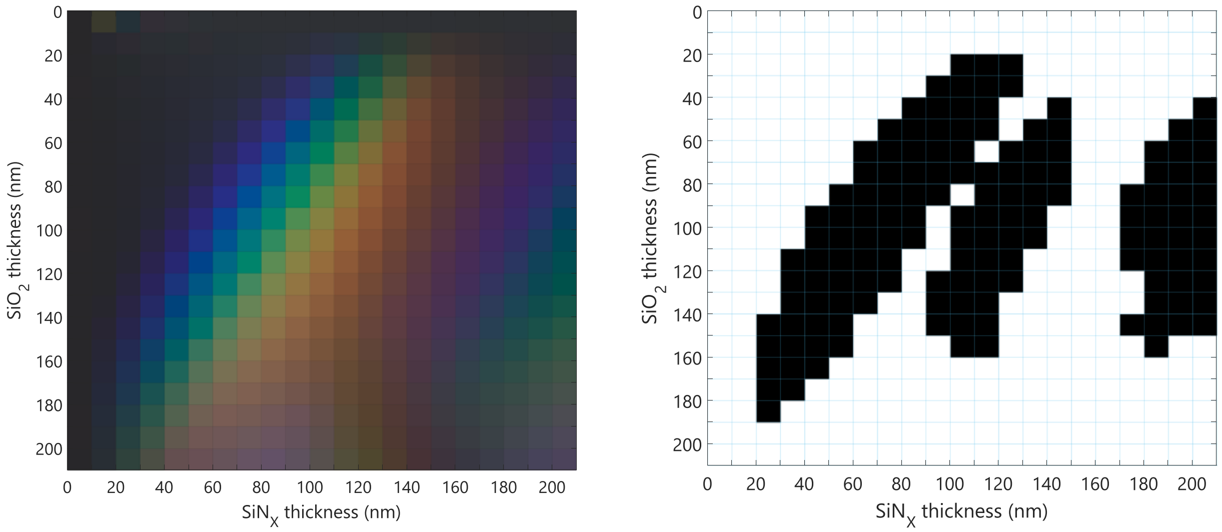

FIGURE C16 (A) Color matrix produced by deposition of 10 periods of SiO_2/SiN_X ($n = 2.1$) on a solar cell (encapsulation with front textured glass is considered). The color saturation is substantially improved. (B) The number of colors whose saturation value is above 0.5 increases substantially when compared with a filter with SiN_X with a value of $n = 1.73$ [Colour figure can be viewed at wileyonlinelibrary.com]

APPENDIX D: EFFECT ON TEMPERATURE AND ENERGY YIELD FOR ALL THICKNESS COMBINATIONS OF FILTERS OPTION 1 AND OPTION 2

D.1 | Effect of the color filter on the temperature of the module at NOCT conditions

Figure D1 presents the steady state temperature under NOCT conditions for an encapsulated color cell manufactured with filter **Option 1**. The results for a colored cell made with filter **Option 2** are shown in Figure D2.

D.2 | Effect on the annual DC energy yield: Delft

Figure D3 presents the relative DC energy yield losses for encapsulated colored cells (for filter **Option 1**) for Delft, NL.

Figure D4 presents the relative DC energy yield losses for encapsulated colored cells (for filter **Option 2**) for Delft, NL.

D.3 | Effect on the annual DC energy yield: Alice Springs

Figure D5 presents the relative DC energy yield losses for encapsulated colored cells (for filter **Option 1**) for Alice Springs, AU.

Figure D6 presents the relative DC energy yield losses for encapsulated colored cells (for filter Option 2) for AliceSprings, AU.

FIGURE D1 Steady state temperature under NOCT conditions for colored encapsulated cells based on the filter **Option 1**. Some colored cells present a maximum reduction in operational temperature compared with a standard cell of 2.1°C [Colour figure can be viewed at wileyonlinelibrary.com]

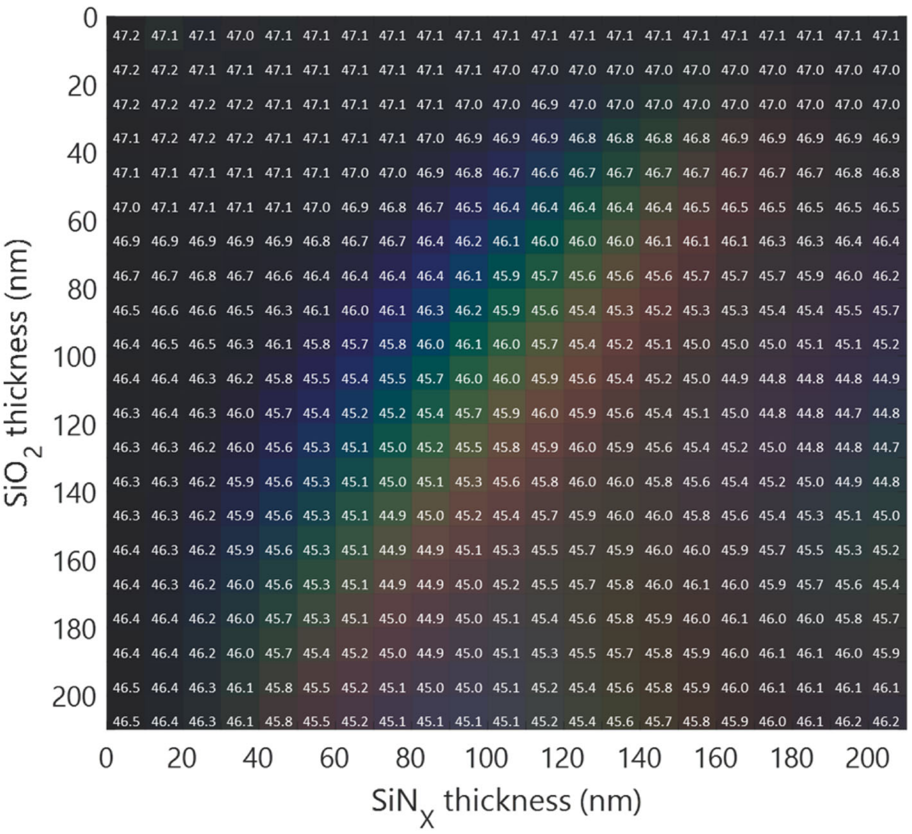

47.2	47.1	47.1	47.0	47.1	47.1	47.1	47.1	47.1	47.1	47.1	47.1	47.1	47.1	47.1	47.1	47.1	47.1	47.1	47.1	47.1
47.2	47.2	47.1	47.1	47.1	47.1	47.1	47.1	47.1	47.1	47.0	47.0	47.0	47.0	47.0	47.0	47.0	47.0	47.0	47.0	47.0
47.2	47.2	47.2	47.2	47.1	47.1	47.1	47.1	47.1	47.0	47.0	46.9	47.0	47.0	47.0	47.0	47.0	47.0	47.0	47.0	47.0
47.1	47.2	47.2	47.2	47.1	47.1	47.1	47.1	47.0	46.9	46.9	46.9	46.8	46.8	46.8	46.8	46.9	46.9	46.9	46.9	46.9
47.1	47.1	47.1	47.1	47.1	47.1	47.0	47.0	46.9	46.8	46.7	46.6	46.7	46.7	46.7	46.7	46.7	46.7	46.7	46.8	46.8
47.0	47.1	47.1	47.1	47.1	47.0	46.9	46.8	46.7	46.5	46.4	46.4	46.4	46.4	46.4	46.5	46.5	46.5	46.5	46.5	46.5
46.9	46.9	46.9	46.9	46.9	46.8	46.7	46.7	46.4	46.2	46.1	46.0	46.0	46.0	46.1	46.1	46.1	46.3	46.3	46.4	46.4
46.7	46.7	46.8	46.7	46.6	46.4	46.4	46.4	46.4	46.1	45.9	45.7	45.6	45.6	45.6	45.7	45.7	45.7	45.9	46.0	46.2
46.5	46.6	46.6	46.5	46.3	46.1	46.0	46.1	46.3	46.2	45.9	45.6	45.4	45.3	45.2	45.3	45.3	45.4	45.4	45.5	45.7
46.4	46.5	46.5	46.3	46.1	45.8	45.7	45.8	46.0	46.1	46.0	45.7	45.4	45.2	45.1	45.0	45.0	45.0	45.1	45.1	45.2
46.4	46.4	46.3	46.2	45.8	45.5	45.4	45.5	45.7	46.0	46.0	45.9	45.6	45.4	45.2	45.0	44.9	44.8	44.8	44.8	44.9
46.3	46.4	46.3	46.0	45.7	45.4	45.2	45.2	45.4	45.7	45.9	46.0	45.9	45.6	45.4	45.1	45.0	44.8	44.8	44.7	44.8
46.3	46.3	46.2	46.0	45.6	45.3	45.1	45.0	45.2	45.5	45.8	45.9	46.0	45.9	45.6	45.4	45.2	45.0	44.8	44.8	44.7
46.3	46.3	46.2	45.9	45.6	45.3	45.1	45.0	45.1	45.3	45.6	45.8	46.0	46.0	45.8	45.6	45.4	45.2	45.0	44.9	44.8
46.3	46.3	46.2	45.9	45.6	45.3	45.1	44.9	45.0	45.2	45.4	45.7	45.9	46.0	46.0	45.8	45.6	45.4	45.3	45.1	45.0
46.4	46.3	46.2	45.9	45.6	45.3	45.1	44.9	44.9	45.1	45.3	45.5	45.7	45.9	46.0	46.0	45.9	45.7	45.5	45.3	45.2
46.4	46.3	46.2	46.0	45.6	45.3	45.1	44.9	44.9	45.0	45.2	45.5	45.7	45.8	46.0	46.1	46.0	45.9	45.7	45.6	45.4
46.4	46.4	46.2	46.0	45.7	45.3	45.1	45.0	44.9	45.0	45.1	45.4	45.6	45.8	45.9	46.0	46.1	46.0	46.0	45.8	45.7
46.4	46.4	46.2	46.0	45.7	45.4	45.2	45.0	44.9	45.0	45.1	45.3	45.5	45.7	45.8	45.9	46.0	46.1	46.1	46.0	45.9
46.5	46.4	46.3	46.1	45.8	45.5	45.2	45.1	45.0	45.0	45.1	45.2	45.4	45.6	45.8	45.9	46.0	46.1	46.1	46.1	46.1
46.5	46.4	46.3	46.1	45.8	45.5	45.2	45.1	45.1	45.1	45.1	45.2	45.4	45.6	45.7	45.8	45.9	46.0	46.1	46.2	46.2

FIGURE D2 Steady state temperature under NOCT conditions for colored encapsulated cells based on the filter **Option 2**. Some colored cells present a maximum reduction in operational temperature compared with a standard cell of 5.2°C [Colour figure can be viewed at wileyonlinelibrary.com]

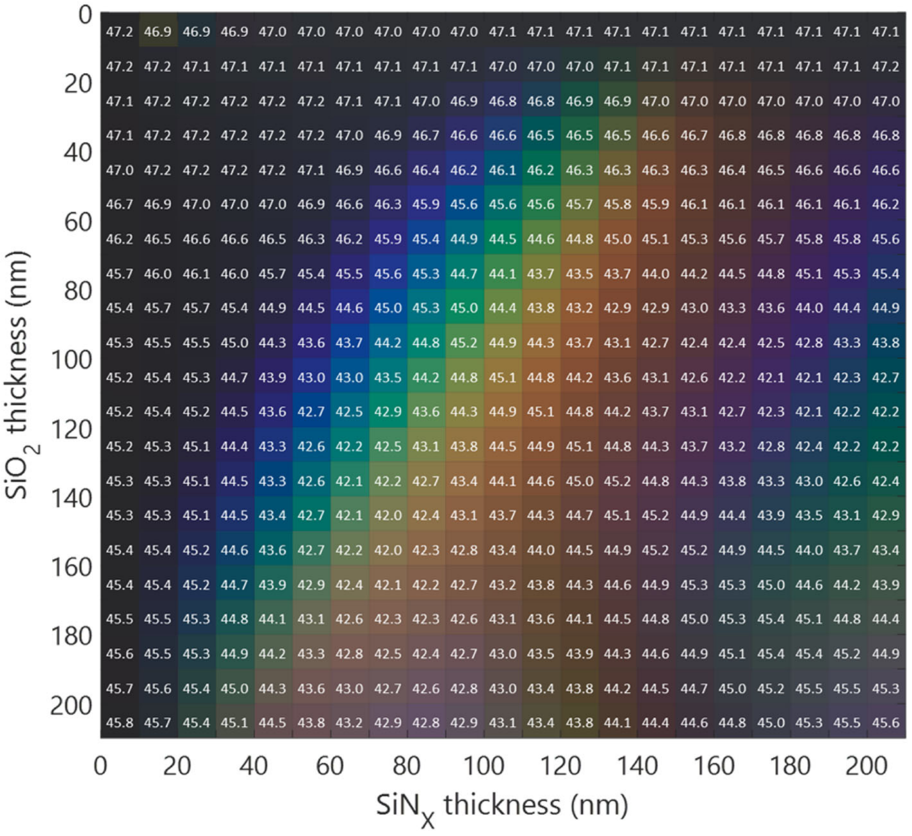

47.2	46.9	46.9	46.9	47.0	47.0	47.0	47.0	47.0	47.0	47.1	47.1	47.1	47.1	47.1	47.1	47.1	47.1	47.1	47.1	47.1
47.2	47.2	47.1	47.1	47.1	47.1	47.1	47.1	47.1	47.1	47.0	47.0	47.0	47.1	47.1	47.1	47.1	47.1	47.1	47.1	47.2
47.1	47.2	47.2	47.2	47.2	47.2	47.1	47.1	47.0	46.9	46.8	46.8	46.9	46.9	47.0	47.0	47.0	47.0	47.0	47.0	47.0
47.1	47.2	47.2	47.2	47.2	47.2	47.0	46.9	46.7	46.6	46.6	46.5	46.5	46.5	46.6	46.7	46.8	46.8	46.8	46.8	46.8
47.0	47.2	47.2	47.2	47.2	47.1	46.9	46.6	46.4	46.2	46.1	46.2	46.3	46.3	46.3	46.3	46.4	46.5	46.6	46.6	46.6
46.7	46.9	47.0	47.0	47.0	46.9	46.6	46.3	45.9	45.6	45.6	45.6	45.7	45.8	45.9	46.1	46.1	46.1	46.1	46.1	46.2
46.2	46.5	46.6	46.6	46.5	46.3	46.2	45.9	45.4	44.9	44.5	44.6	44.8	45.0	45.1	45.3	45.6	45.7	45.8	45.8	45.6
45.7	46.0	46.1	46.0	45.7	45.4	45.5	45.6	45.3	44.7	44.1	43.7	43.5	43.7	44.0	44.2	44.5	44.8	45.1	45.3	45.4
45.4	45.7	45.7	45.4	44.9	44.5	44.6	45.0	45.3	45.0	44.4	43.8	43.2	42.9	42.9	43.0	43.3	43.6	44.0	44.4	44.9
45.3	45.5	45.5	45.0	44.3	43.6	43.7	44.2	44.8	45.2	44.9	44.3	43.7	43.1	42.7	42.4	42.4	42.5	42.8	43.3	43.8
45.2	45.4	45.3	44.7	43.9	43.0	43.0	43.5	44.2	44.8	45.1	44.8	44.2	43.6	43.1	42.6	42.2	42.1	42.1	42.3	42.7
45.2	45.4	45.2	44.5	43.6	42.7	42.5	42.9	43.6	44.3	44.9	45.1	44.8	44.2	43.7	43.1	42.7	42.3	42.1	42.2	42.2
45.2	45.3	45.1	44.4	43.3	42.6	42.2	42.5	43.1	43.8	44.5	44.9	45.1	44.8	44.3	43.7	43.2	42.8	42.4	42.2	42.2
45.3	45.3	45.1	44.5	43.3	42.6	42.1	42.2	42.7	43.4	44.1	44.6	45.0	45.2	44.8	44.3	43.8	43.3	43.0	42.6	42.4
45.3	45.3	45.1	44.5	43.4	42.7	42.1	42.0	42.4	43.1	43.7	44.3	44.7	45.1	45.2	44.9	44.4	43.9	43.5	43.1	42.9
45.4	45.4	45.2	44.6	43.6	42.7	42.2	42.0	42.3	42.8	43.4	44.0	44.5	44.9	45.2	45.2	44.9	44.5	44.0	43.7	43.4
45.4	45.4	45.2	44.7	43.9	42.9	42.4	42.1	42.2	42.7	43.2	43.8	44.3	44.6	44.9	45.3	45.3	45.0	44.6	44.2	43.9
45.5	45.5	45.3	44.8	44.1	43.1	42.6	42.3	42.3	42.6	43.1	43.6	44.1	44.5	44.8	45.0	45.3	45.4	45.1	44.8	44.4
45.6	45.5	45.3	44.9	44.2	43.3	42.8	42.5	42.4	42.7	43.0	43.5	43.9	44.3	44.6	44.9	45.1	45.4	45.4	45.2	44.9
45.7	45.6	45.4	45.0	44.3	43.6	43.0	42.7	42.6	42.8	43.0	43.4	43.8	44.2	44.5	44.7	45.0	45.2	45.5	45.5	45.3
45.8	45.7	45.4	45.1	44.5	43.8	43.2	42.9	42.8	42.9	43.1	43.4	43.8	44.1	44.4	44.6	44.8	45.0	45.3	45.5	45.6

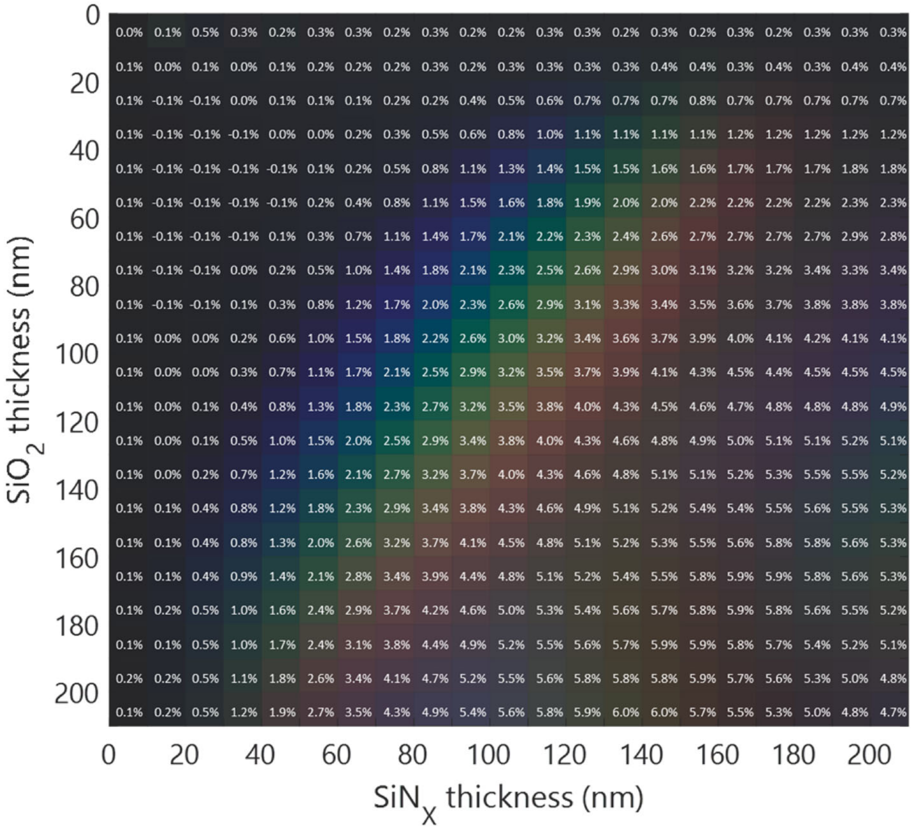

0.0%	0.1%	0.5%	0.3%	0.2%	0.3%	0.3%	0.2%	0.3%	0.2%	0.2%	0.3%	0.3%	0.2%	0.3%	0.2%	0.3%	0.2%	0.3%	0.3%	0.3%
0.1%	0.0%	0.1%	0.0%	0.1%	0.2%	0.2%	0.2%	0.3%	0.2%	0.3%	0.3%	0.3%	0.3%	0.4%	0.4%	0.3%	0.4%	0.3%	0.4%	0.4%
0.1%	-0.1%	-0.1%	0.0%	0.1%	0.1%	0.1%	0.2%	0.2%	0.4%	0.5%	0.6%	0.7%	0.7%	0.7%	0.8%	0.7%	0.7%	0.7%	0.7%	0.7%
0.1%	-0.1%	-0.1%	-0.1%	0.0%	0.0%	0.2%	0.3%	0.5%	0.6%	0.8%	1.0%	1.1%	1.1%	1.1%	1.1%	1.2%	1.2%	1.2%	1.2%	1.2%
0.1%	-0.1%	-0.1%	-0.1%	-0.1%	0.1%	0.2%	0.5%	0.8%	1.1%	1.3%	1.4%	1.5%	1.5%	1.6%	1.6%	1.7%	1.7%	1.7%	1.8%	1.8%
0.1%	-0.1%	-0.1%	-0.1%	-0.1%	0.2%	0.4%	0.8%	1.1%	1.5%	1.6%	1.8%	1.9%	2.0%	2.0%	2.2%	2.2%	2.2%	2.2%	2.3%	2.3%
0.1%	-0.1%	-0.1%	-0.1%	0.1%	0.3%	0.7%	1.1%	1.4%	1.7%	2.1%	2.2%	2.3%	2.4%	2.6%	2.7%	2.7%	2.7%	2.7%	2.9%	2.8%
0.1%	-0.1%	-0.1%	0.0%	0.2%	0.5%	1.0%	1.4%	1.8%	2.1%	2.3%	2.5%	2.6%	2.9%	3.0%	3.1%	3.2%	3.2%	3.4%	3.3%	3.4%
0.1%	-0.1%	-0.1%	0.1%	0.3%	0.8%	1.2%	1.7%	2.0%	2.3%	2.6%	2.9%	3.1%	3.3%	3.4%	3.5%	3.6%	3.7%	3.8%	3.8%	3.8%
0.1%	0.0%	0.0%	0.2%	0.6%	1.0%	1.5%	1.8%	2.2%	2.6%	3.0%	3.2%	3.4%	3.6%	3.7%	3.9%	4.0%	4.1%	4.2%	4.1%	4.1%
0.1%	0.0%	0.0%	0.3%	0.7%	1.1%	1.7%	2.1%	2.5%	2.9%	3.2%	3.5%	3.7%	3.9%	4.1%	4.3%	4.5%	4.4%	4.5%	4.5%	4.5%
0.1%	0.0%	0.1%	0.4%	0.8%	1.3%	1.8%	2.3%	2.7%	3.2%	3.5%	3.8%	4.0%	4.3%	4.5%	4.6%	4.7%	4.8%	4.8%	4.8%	4.9%
0.1%	0.0%	0.1%	0.5%	1.0%	1.5%	2.0%	2.5%	2.9%	3.4%	3.8%	4.0%	4.3%	4.6%	4.8%	4.9%	5.0%	5.1%	5.1%	5.2%	5.1%
0.1%	0.0%	0.2%	0.7%	1.2%	1.6%	2.1%	2.7%	3.2%	3.7%	4.0%	4.3%	4.6%	4.8%	5.1%	5.1%	5.2%	5.3%	5.5%	5.5%	5.2%
0.1%	0.1%	0.4%	0.8%	1.2%	1.8%	2.3%	2.9%	3.4%	3.8%	4.3%	4.6%	4.9%	5.1%	5.2%	5.4%	5.4%	5.5%	5.6%	5.5%	5.3%
0.1%	0.1%	0.4%	0.8%	1.3%	2.0%	2.6%	3.2%	3.7%	4.1%	4.5%	4.8%	5.1%	5.2%	5.3%	5.5%	5.6%	5.8%	5.8%	5.6%	5.3%
0.1%	0.1%	0.4%	0.9%	1.4%	2.1%	2.8%	3.4%	3.9%	4.4%	4.8%	5.1%	5.2%	5.4%	5.5%	5.8%	5.9%	5.9%	5.8%	5.6%	5.3%
0.1%	0.2%	0.5%	1.0%	1.6%	2.4%	2.9%	3.7%	4.2%	4.6%	5.0%	5.3%	5.4%	5.6%	5.7%	5.8%	5.9%	5.8%	5.6%	5.5%	5.2%
0.1%	0.1%	0.5%	1.0%	1.7%	2.4%	3.1%	3.8%	4.4%	4.9%	5.2%	5.5%	5.6%	5.7%	5.9%	5.9%	5.8%	5.7%	5.4%	5.2%	5.1%
0.2%	0.2%	0.5%	1.1%	1.8%	2.6%	3.4%	4.1%	4.7%	5.2%	5.5%	5.6%	5.8%	5.8%	5.8%	5.9%	5.7%	5.6%	5.3%	5.0%	4.8%
0.1%	0.2%	0.5%	1.2%	1.9%	2.7%	3.5%	4.3%	4.9%	5.4%	5.6%	5.8%	5.9%	6.0%	6.0%	5.7%	5.5%	5.3%	5.0%	4.8%	4.7%

FIGURE D3 Relative losses on the direct current (DC) annual energy yield of an encapsulated color solar cell (with the filter **Option 1**) for a tilt angle of 35° and azimuth towards south located in Delft, NL [Colour figure can be viewed at wileyonlinelibrary.com]

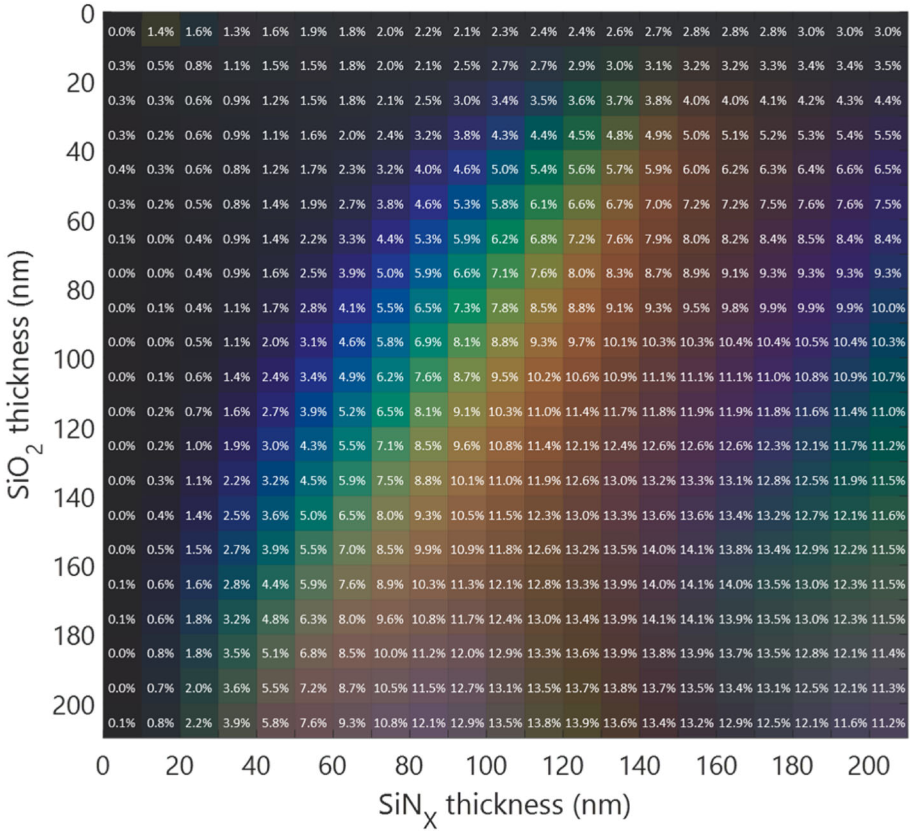

0.0%	1.4%	1.6%	1.3%	1.6%	1.9%	1.8%	2.0%	2.2%	2.1%	2.3%	2.4%	2.4%	2.6%	2.7%	2.8%	2.8%	2.8%	3.0%	3.0%	3.0%
0.3%	0.5%	0.8%	1.1%	1.5%	1.5%	1.8%	2.0%	2.1%	2.5%	2.7%	2.7%	2.9%	3.0%	3.1%	3.2%	3.2%	3.3%	3.4%	3.4%	3.5%
0.3%	0.3%	0.6%	0.9%	1.2%	1.5%	1.8%	2.1%	2.5%	3.0%	3.4%	3.5%	3.6%	3.7%	3.8%	4.0%	4.0%	4.1%	4.2%	4.3%	4.4%
0.3%	0.2%	0.6%	0.9%	1.1%	1.6%	2.0%	2.4%	3.2%	3.8%	4.3%	4.4%	4.5%	4.8%	4.9%	5.0%	5.1%	5.2%	5.3%	5.4%	5.5%
0.4%	0.3%	0.6%	0.8%	1.2%	1.7%	2.3%	3.2%	4.0%	4.6%	5.0%	5.4%	5.6%	5.7%	5.9%	6.0%	6.2%	6.3%	6.4%	6.6%	6.5%
0.3%	0.2%	0.5%	0.8%	1.4%	1.9%	2.7%	3.8%	4.6%	5.3%	5.8%	6.1%	6.6%	6.7%	7.0%	7.2%	7.2%	7.5%	7.6%	7.6%	7.5%
0.1%	0.0%	0.4%	0.9%	1.4%	2.2%	3.3%	4.4%	5.3%	5.9%	6.2%	6.8%	7.2%	7.6%	7.9%	8.0%	8.2%	8.4%	8.5%	8.4%	8.4%
0.0%	0.0%	0.4%	0.9%	1.6%	2.5%	3.9%	5.0%	5.9%	6.6%	7.1%	7.6%	8.0%	8.3%	8.7%	8.9%	9.1%	9.3%	9.3%	9.3%	9.3%
0.0%	0.1%	0.4%	1.1%	1.7%	2.8%	4.1%	5.5%	6.5%	7.3%	7.8%	8.5%	8.8%	9.1%	9.3%	9.5%	9.8%	9.9%	9.9%	9.9%	10.0%
0.0%	0.0%	0.5%	1.1%	2.0%	3.1%	4.6%	5.8%	6.9%	8.1%	8.8%	9.3%	9.7%	10.1%	10.3%	10.3%	10.4%	10.4%	10.5%	10.4%	10.3%
0.0%	0.1%	0.6%	1.4%	2.4%	3.4%	4.9%	6.2%	7.6%	8.7%	9.5%	10.2%	10.6%	10.9%	11.1%	11.1%	11.1%	11.0%	10.8%	10.9%	10.7%
0.0%	0.2%	0.7%	1.6%	2.7%	3.9%	5.2%	6.5%	8.1%	9.1%	10.3%	11.0%	11.4%	11.7%	11.8%	11.9%	11.9%	11.8%	11.6%	11.4%	11.0%
0.0%	0.2%	1.0%	1.9%	3.0%	4.3%	5.5%	7.1%	8.5%	9.6%	10.8%	11.4%	12.1%	12.4%	12.6%	12.6%	12.6%	12.3%	12.1%	11.7%	11.2%
0.0%	0.3%	1.1%	2.2%	3.2%	4.5%	5.9%	7.5%	8.8%	10.1%	11.0%	11.9%	12.6%	13.0%	13.2%	13.3%	13.1%	12.8%	12.5%	11.9%	11.5%
0.0%	0.4%	1.4%	2.5%	3.6%	5.0%	6.5%	8.0%	9.3%	10.5%	11.5%	12.3%	13.0%	13.3%	13.6%	13.6%	13.4%	13.2%	12.7%	12.1%	11.6%
0.0%	0.5%	1.5%	2.7%	3.9%	5.5%	7.0%	8.5%	9.9%	10.9%	11.8%	12.6%	13.2%	13.5%	14.0%	14.1%	13.8%	13.4%	12.9%	12.2%	11.5%
0.1%	0.6%	1.6%	2.8%	4.4%	5.9%	7.6%	8.9%	10.3%	11.3%	12.1%	12.8%	13.3%	13.9%	14.0%	14.1%	14.0%	13.5%	13.0%	12.3%	11.5%
0.1%	0.6%	1.8%	3.2%	4.8%	6.3%	8.0%	9.6%	10.8%	11.7%	12.4%	13.0%	13.4%	13.9%	14.1%	14.1%	13.9%	13.5%	13.0%	12.3%	11.5%
0.0%	0.8%	1.8%	3.5%	5.1%	6.8%	8.5%	10.0%	11.2%	12.0%	12.9%	13.3%	13.6%	13.9%	13.8%	13.9%	13.7%	13.5%	12.8%	12.1%	11.4%
0.0%	0.7%	2.0%	3.6%	5.5%	7.2%	8.7%	10.5%	11.5%	12.7%	13.1%	13.5%	13.7%	13.8%	13.7%	13.5%	13.4%	13.1%	12.5%	12.1%	11.3%
0.1%	0.8%	2.2%	3.9%	5.8%	7.6%	9.3%	10.8%	12.1%	12.9%	13.5%	13.8%	13.9%	13.6%	13.4%	13.2%	12.9%	12.5%	12.1%	11.6%	11.2%

FIGURE D4 Relative losses on the direct current (DC) annual energy yield of an encapsulated color solar cell (with the filter **Option 2**) for a tilt angle of 35° and azimuth towards south located in Delft, NL [Colour figure can be viewed at wileyonlinelibrary.com]

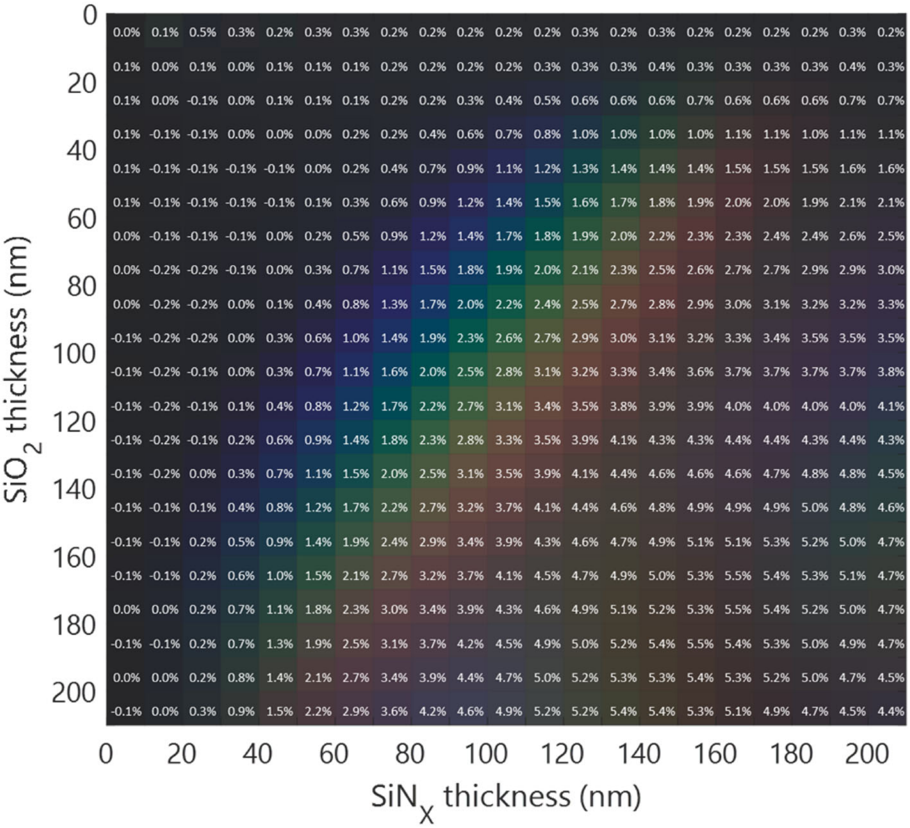

FIGURE D5 Relative losses on the direct current (DC) annual energy yield of an encapsulated color solar cell (with the filter **Option 1**) for a tilt angle of 35° and azimuth towards north located in Alice Springs, AU [Colour figure can be viewed at wileyonlinelibrary.com]

	0		20		40		60		80		100		120		140		160		180		200
0	0.0%	0.1%	0.5%	0.3%	0.2%	0.3%	0.3%	0.2%	0.2%	0.2%	0.2%	0.2%	0.3%	0.2%	0.3%	0.2%	0.2%	0.2%	0.2%	0.3%	0.2%
	0.1%	0.0%	0.1%	0.0%	0.1%	0.1%	0.1%	0.2%	0.2%	0.2%	0.2%	0.3%	0.3%	0.3%	0.4%	0.3%	0.3%	0.3%	0.3%	0.4%	0.3%
20	0.1%	0.0%	-0.1%	0.0%	0.1%	0.1%	0.1%	0.2%	0.2%	0.3%	0.4%	0.5%	0.6%	0.6%	0.6%	0.7%	0.6%	0.6%	0.6%	0.7%	0.7%
	0.1%	-0.1%	-0.1%	0.0%	0.0%	0.0%	0.2%	0.2%	0.4%	0.6%	0.7%	0.8%	1.0%	1.0%	1.0%	1.0%	1.1%	1.1%	1.0%	1.1%	1.1%
40	0.1%	-0.1%	-0.1%	-0.1%	-0.1%	0.0%	0.2%	0.4%	0.7%	0.9%	1.1%	1.2%	1.3%	1.4%	1.4%	1.4%	1.5%	1.5%	1.5%	1.6%	1.6%
	0.1%	-0.1%	-0.1%	-0.1%	-0.1%	0.1%	0.3%	0.6%	0.9%	1.2%	1.4%	1.5%	1.6%	1.7%	1.8%	1.9%	2.0%	2.0%	1.9%	2.1%	2.1%
60	0.0%	-0.1%	-0.1%	-0.1%	0.0%	0.2%	0.5%	0.9%	1.2%	1.4%	1.7%	1.8%	1.9%	2.0%	2.2%	2.3%	2.3%	2.4%	2.4%	2.6%	2.5%
	0.0%	-0.2%	-0.2%	-0.1%	0.0%	0.3%	0.7%	1.1%	1.5%	1.8%	1.9%	2.0%	2.1%	2.3%	2.5%	2.6%	2.7%	2.7%	2.9%	2.9%	3.0%
80	0.0%	-0.2%	-0.2%	0.0%	0.1%	0.4%	0.8%	1.3%	1.7%	2.0%	2.2%	2.4%	2.5%	2.7%	2.8%	2.9%	3.0%	3.1%	3.2%	3.2%	3.3%
	-0.1%	-0.2%	-0.2%	0.0%	0.3%	0.6%	1.0%	1.4%	1.9%	2.3%	2.6%	2.7%	2.9%	3.0%	3.1%	3.2%	3.3%	3.4%	3.5%	3.5%	3.5%
100	-0.1%	-0.2%	-0.1%	0.0%	0.3%	0.7%	1.1%	1.6%	2.0%	2.5%	2.8%	3.1%	3.2%	3.3%	3.4%	3.6%	3.7%	3.7%	3.7%	3.7%	3.8%
	-0.1%	-0.2%	-0.1%	0.1%	0.4%	0.8%	1.2%	1.7%	2.2%	2.7%	3.1%	3.4%	3.5%	3.8%	3.9%	3.9%	4.0%	4.0%	4.0%	4.0%	4.1%
120	-0.1%	-0.2%	-0.1%	0.2%	0.6%	0.9%	1.4%	1.8%	2.3%	2.8%	3.3%	3.5%	3.9%	4.1%	4.3%	4.3%	4.4%	4.4%	4.3%	4.4%	4.3%
	-0.1%	-0.2%	0.0%	0.3%	0.7%	1.1%	1.5%	2.0%	2.5%	3.1%	3.5%	3.9%	4.1%	4.4%	4.6%	4.6%	4.6%	4.7%	4.8%	4.8%	4.5%
140	-0.1%	-0.1%	0.1%	0.4%	0.8%	1.2%	1.7%	2.2%	2.7%	3.2%	3.7%	4.1%	4.4%	4.6%	4.8%	4.9%	4.9%	4.9%	5.0%	4.8%	4.6%
	-0.1%	-0.1%	0.2%	0.5%	0.9%	1.4%	1.9%	2.4%	2.9%	3.4%	3.9%	4.3%	4.6%	4.7%	4.9%	5.1%	5.1%	5.3%	5.2%	5.0%	4.7%
160	-0.1%	-0.1%	0.2%	0.6%	1.0%	1.5%	2.1%	2.7%	3.2%	3.7%	4.1%	4.5%	4.7%	4.9%	5.0%	5.3%	5.5%	5.4%	5.3%	5.1%	4.7%
	0.0%	0.0%	0.2%	0.7%	1.1%	1.8%	2.3%	3.0%	3.4%	3.9%	4.3%	4.6%	4.9%	5.1%	5.2%	5.3%	5.5%	5.4%	5.2%	5.0%	4.7%
180	-0.1%	-0.1%	0.2%	0.7%	1.3%	1.9%	2.5%	3.1%	3.7%	4.2%	4.5%	4.9%	5.0%	5.2%	5.4%	5.5%	5.4%	5.3%	5.0%	4.9%	4.7%
	0.0%	0.0%	0.2%	0.8%	1.4%	2.1%	2.7%	3.4%	3.9%	4.4%	4.7%	5.0%	5.2%	5.3%	5.3%	5.4%	5.3%	5.2%	5.0%	4.7%	4.5%
200	-0.1%	0.0%	0.3%	0.9%	1.5%	2.2%	2.9%	3.6%	4.2%	4.6%	4.9%	5.2%	5.2%	5.4%	5.4%	5.3%	5.1%	4.9%	4.7%	4.5%	4.4%

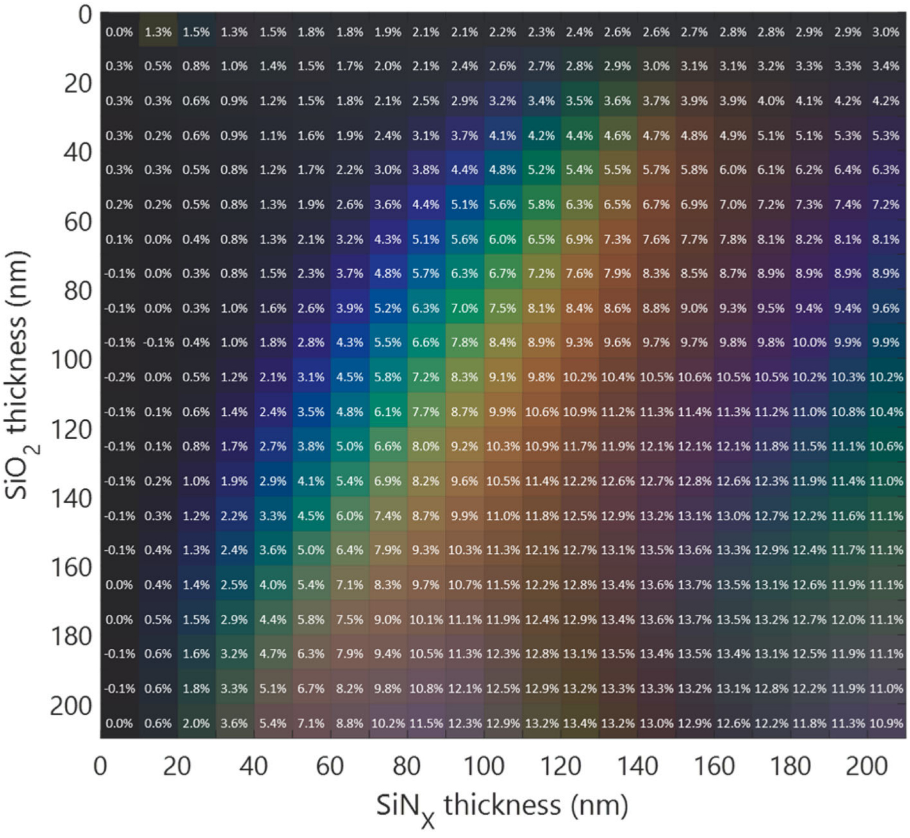

FIGURE D6 Relative losses on the direct current (DC) annual energy yield of an encapsulated color solar cell (with the filter **Option 2**) for a tilt angle of 35° and azimuth towards north located in Alice Springs, AU [Colour figure can be viewed at wileyonlinelibrary.com]

	0		20		40		60		80		100		120		140		160		180		200
0	0.0%	1.3%	1.5%	1.3%	1.5%	1.8%	1.8%	1.9%	2.1%	2.1%	2.2%	2.3%	2.4%	2.6%	2.6%	2.7%	2.8%	2.8%	2.9%	2.9%	3.0%
	0.3%	0.5%	0.8%	1.0%	1.4%	1.5%	1.7%	2.0%	2.1%	2.4%	2.6%	2.7%	2.8%	2.9%	3.0%	3.1%	3.1%	3.2%	3.3%	3.3%	3.4%
20	0.3%	0.3%	0.6%	0.9%	1.2%	1.5%	1.8%	2.1%	2.5%	2.9%	3.2%	3.4%	3.5%	3.6%	3.7%	3.9%	3.9%	4.0%	4.1%	4.2%	4.2%
	0.3%	0.2%	0.6%	0.9%	1.1%	1.6%	1.9%	2.4%	3.1%	3.7%	4.1%	4.2%	4.4%	4.6%	4.7%	4.8%	4.9%	5.1%	5.1%	5.3%	5.3%
40	0.3%	0.3%	0.5%	0.8%	1.2%	1.7%	2.2%	3.0%	3.8%	4.4%	4.8%	5.2%	5.4%	5.5%	5.7%	5.8%	6.0%	6.1%	6.2%	6.4%	6.3%
	0.2%	0.2%	0.5%	0.8%	1.3%	1.9%	2.6%	3.6%	4.4%	5.1%	5.6%	5.8%	6.3%	6.5%	6.7%	6.9%	7.0%	7.2%	7.3%	7.4%	7.2%
60	0.1%	0.0%	0.4%	0.8%	1.3%	2.1%	3.2%	4.3%	5.1%	5.6%	6.0%	6.5%	6.9%	7.3%	7.6%	7.7%	7.8%	8.1%	8.2%	8.1%	8.1%
	-0.1%	0.0%	0.3%	0.8%	1.5%	2.3%	3.7%	4.8%	5.7%	6.3%	6.7%	7.2%	7.6%	7.9%	8.3%	8.5%	8.7%	8.9%	8.9%	8.9%	8.9%
80	-0.1%	0.0%	0.3%	1.0%	1.6%	2.6%	3.9%	5.2%	6.3%	7.0%	7.5%	8.1%	8.4%	8.6%	8.8%	9.0%	9.3%	9.5%	9.4%	9.4%	9.6%
	-0.1%	-0.1%	0.4%	1.0%	1.8%	2.8%	4.3%	5.5%	6.6%	7.8%	8.4%	8.9%	9.3%	9.6%	9.7%	9.7%	9.8%	9.8%	10.0%	9.9%	9.9%
100	-0.2%	0.0%	0.5%	1.2%	2.1%	3.1%	4.5%	5.8%	7.2%	8.3%	9.1%	9.8%	10.2%	10.4%	10.5%	10.6%	10.5%	10.5%	10.2%	10.3%	10.2%
	-0.1%	0.1%	0.6%	1.4%	2.4%	3.5%	4.8%	6.1%	7.7%	8.7%	9.9%	10.6%	10.9%	11.2%	11.3%	11.4%	11.3%	11.2%	11.0%	10.8%	10.4%
120	-0.1%	0.1%	0.8%	1.7%	2.7%	3.8%	5.0%	6.6%	8.0%	9.2%	10.3%	10.9%	11.7%	11.9%	12.1%	12.1%	12.1%	11.8%	11.5%	11.1%	10.6%
	-0.1%	0.2%	1.0%	1.9%	2.9%	4.1%	5.4%	6.9%	8.2%	9.6%	10.5%	11.4%	12.2%	12.6%	12.7%	12.8%	12.6%	12.3%	11.9%	11.4%	11.0%
140	-0.1%	0.3%	1.2%	2.2%	3.3%	4.5%	6.0%	7.4%	8.7%	9.9%	11.0%	11.8%	12.5%	12.9%	13.2%	13.1%	13.0%	12.7%	12.2%	11.6%	11.1%
	-0.1%	0.4%	1.3%	2.4%	3.6%	5.0%	6.4%	7.9%	9.3%	10.3%	11.3%	12.1%	12.7%	13.1%	13.5%	13.6%	13.3%	12.9%	12.4%	11.7%	11.1%
160	0.0%	0.4%	1.4%	2.5%	4.0%	5.4%	7.1%	8.3%	9.7%	10.7%	11.5%	12.2%	12.8%	13.4%	13.6%	13.7%	13.5%	13.1%	12.6%	11.9%	11.1%
	0.0%	0.5%	1.5%	2.9%	4.4%	5.8%	7.5%	9.0%	10.1%	11.1%	11.9%	12.4%	12.9%	13.4%	13.6%	13.7%	13.5%	13.2%	12.7%	12.0%	11.1%
180	-0.1%	0.6%	1.6%	3.2%	4.7%	6.3%	7.9%	9.4%	10.5%	11.3%	12.3%	12.8%	13.1%	13.5%	13.4%	13.5%	13.4%	13.1%	12.5%	11.9%	11.1%
	-0.1%	0.6%	1.8%	3.3%	5.1%	6.7%	8.2%	9.8%	10.8%	12.1%	12.5%	12.9%	13.2%	13.3%	13.3%	13.2%	13.1%	12.8%	12.2%	11.9%	11.0%
200	0.0%	0.6%	2.0%	3.6%	5.4%	7.1%	8.8%	10.2%	11.5%	12.3%	12.9%	13.2%	13.4%	13.2%	13.0%	12.9%	12.6%	12.2%	11.8%	11.3%	10.9%